An interdisciplinary approach for developing novel methods to study silks

Yue Jin Oh
Exeter College, Oxford

A thesis submitted for the degree of

Doctor of Philosophy

Trinity Term 2021

Supervised by

Prof. Fritz Vollrath

Prof. Ben. Davis

Thesis Abstract

Silks remain objects of eternal fascination to mankind; their remarkable material properties and visual lustre attracting decades of commercial and research attention. Though much research has been conducted in the past to attempt to understand the structure of silks – as well as the highly intricate protein dynamics that occur during the spinning process – many gaps in our knowledge remain. Silks are unique in that order and hierarchy exist right from the molecular scale (primary structure of silk proteins), through to the nanoscale (secondary and tertiary silk protein structures), and right up to the microscale (microscale solid fibre). Therefore, an interdisciplinary approach must be used to understand the many facets of silk. In my thesis, I combine chemical and spectroscopic techniques, material testing techniques, and couple them with a core understanding of evolution and biology in an attempt to understand the structure-protein dynamic-mechanical property relationships of silk. I utilise unnatural amino acid incorporation to endow silks with probes for further structural and dynamic studies. I also use various fluorescence microscopy techniques to study silk structure, using silks' natural fluorescent motifs as well as incorporated fluorophores as contrast agents. Finally, I offer a perspective piece on the highly contentious subject of nanoparticle incorporation in silks as I believe that it is important to validate various claims floating about as they are likely to guide the way for future studies, and they also have important implications in understanding how nanoparticles travel through the bodies of organisms.

Acknowledgements

It's been a long journey riddled with many challenges; from the Tinbergen building shutdown, multiple lab moves and the Covid-19 pandemic the duration of my DPhil certainly has been an interesting one. Fortunately, I've had help and support from so many people who have contributed to the completion of this thesis.

Firstly, a huge thank you to my two supervisors – Fritz Vollrath and Ben Davis – for their expertise in silks and protein chemistry, constant support, patience, connecting me to my collaborators and never-ending supply of ideas and discussions.

Speaking of which, a massive thank you to all my collaborators. Simon Nadal and Satoshi Kishigami from the BGD group; Jonathan Brewer from the University of Southern Denmark; Jeremiah Woodcock, Shawn Chen and Jeff Gilman from NIST. The approach to a lot of the work in this thesis is highly multidisciplinary and without your expertise in your respective fields, much of this work would not have been possible.

A big thank you to members of the Oxford Silk Group and the BGD group, current and past. There are so many people in this regard who have helped me but I have to mention several names. Alex Greenhalgh, Martin Frydrych, Arsham Khayatapoor, Tom Mulder, Thomas Miller and Nick Hawkins for help, support, and company during my time in the Silk Group. Simon and Satoshi as mentioned before for help on my UAA chapter. Jitka Riedl and Yiqun Geng for providing much guidance during my time in the chemistry labs while I was performing rather scary organic synthesis schemes.

For funding, I thank the BBSRC for funding the research, Khazanah and the Department of Zoology, Oxford for funding my living costs.

Thank you very much to my family for their unconditional love and support. Thank you to my friends – many of which have and are going through the same journey that I am – for your friendship, advice, support and company. In particular: Chris Thomas, Cecilia Karlsson, Matishalin Patel, Aimee Ross, Marie Wong, Hele Francis, Blane Scott, Alice Lightowlers, and the D&D gang. Thanks also to my two gerbils Horace and Galahad for making much of the lockdown and WFH writing period less lonely and much more entertaining.

Last but not least, thank you to the spiders and silkworms!

Table of Contents

List of Figures and Tables

Chapter 1: Introduction

Chapter 2: Unnatural Amino Acid (UAA) Incorporation into spider silks

Chapter 3: Incorporation of fluorophore dyes into spider and silkworm silks

Chapter 4: SHG/FLIM imaging as a novel spatially-resolved method for investigating the structure of silks

Chapter 5: An investigation into the feasibility of incorporating nanoparticles into spider silks via direct feeding

Chapter 1: Introduction

1.1 General introduction to silks

Silks are fibrous protein polymers that are produced by a variety of Arthropods for various functional reasons and have evolved in these taxa over millions of years [1]. Of interest are silks produced by spiders and silkworms. Spiders and their silks have been evolving for approximately 380 million years [2], yielding 40 000 species of known extant spiders – with an estimated 40 000 – 100 000 uncharacterised spiders – all of which produce at least one type of silk. Consequently, certain species of spiders produce some of the strongest and toughest silks known to mankind. On the other hand, silkworms – more specifically the domesticated silkworm, *Bombyx mori* – have the ability to produce copious amounts of silks, having been domesticated for that purpose for several millennia in order to satisfy the demand for silk in the textile industry [3] .

There are several characteristics that distinguish silks from other protein polymers such as hair, feathers or collagen. Crucially, silks are spun into solid fibres from a liquid crystalline precursor for use outside of the body[4,5]. This is in stark contrast to other protein polymers which tend to be grown over time and may have functional purposes *in vivo.* Silk proteins – termed spidroins for spider silks and fibroins for silkworm silks – are produced and stored in the animals in specialised glands in a gel-like or liquid crystalline state. At this stage, the protein monomers are surrounded by a hydration shell as water is closely bound to the hydrophilic regions of the silk protein [6,7]. As the silk proteins travel down the silk glands, they undergo a stress-induced phase transition due to the tapering of the silk glands from the middle section to the anterior section of the gland, before finally exiting the spinneret as a solid fibre. During this transition, it is theorised that the protein monomers lose their

hydration shell, allowing a polymerisation process to occur whereby amide-amide hydrogen bonds between monomers are formed [8], in turn allowing secondary and tertiary structures (such as ordered beta-sheets) to form within and between silk proteins[9–11]. The exact details governing this transition from a liquid gel to a solid fibre remains a mystery, although factors such as pH [12,13], shearing [7,14], presence of certain ions [15], and post-draw [16] have been suggested to play a role in silk fibre production. Rheological studies have provided some insight into the effects of shear forces on the silk protein gel, however it has not been possible to measure the effects of the aforementioned factors quantitatively and controllably, as it has not been possible to conduct such studies or observations *in vivo*.

Silks aren't unique to spiders and silkworms; many animals within the Arthropoda phylum utilize silks for a variety of functions, including a variety of insects and several crustacea[1,17,18]. Interestingly, silks have evolved at least 23 times convergently in insects[17], implying that silks are Nature's very efficient and multi-functional solution to producing and utilizing fibres. Remarkably, despite having evolved from separate lineages, there are several parallels that can be seen when comparing the main protein monomers of spider silks and silkworm silks. The secondary structures or motifs formed within the two proteins, fundamental molecular composition and flow characteristics of the proteins share similarities to some extent [3,5,10,17,19,20] .This in turn means that knowledge gained from one system may provide insight for the other. It is also a testament to how silks are well-suited for a variety of ecological and functional purposes for the animals that produce them. However, while insects tend to produce one type of silk at only one stage of their life cycle, spiders can produce multiple types of silks (up to 7 or 8 in the case of orb-weaving spiders, as alluded to in Figure 1.1) and they do so throughout their lifetime[21]. These silks have evolved under different ecological constraints and selection pressures. Thus, caution and consideration of the

different selection pressures that silks have evolved under must be taken when extending conclusions or observations from one system to another.

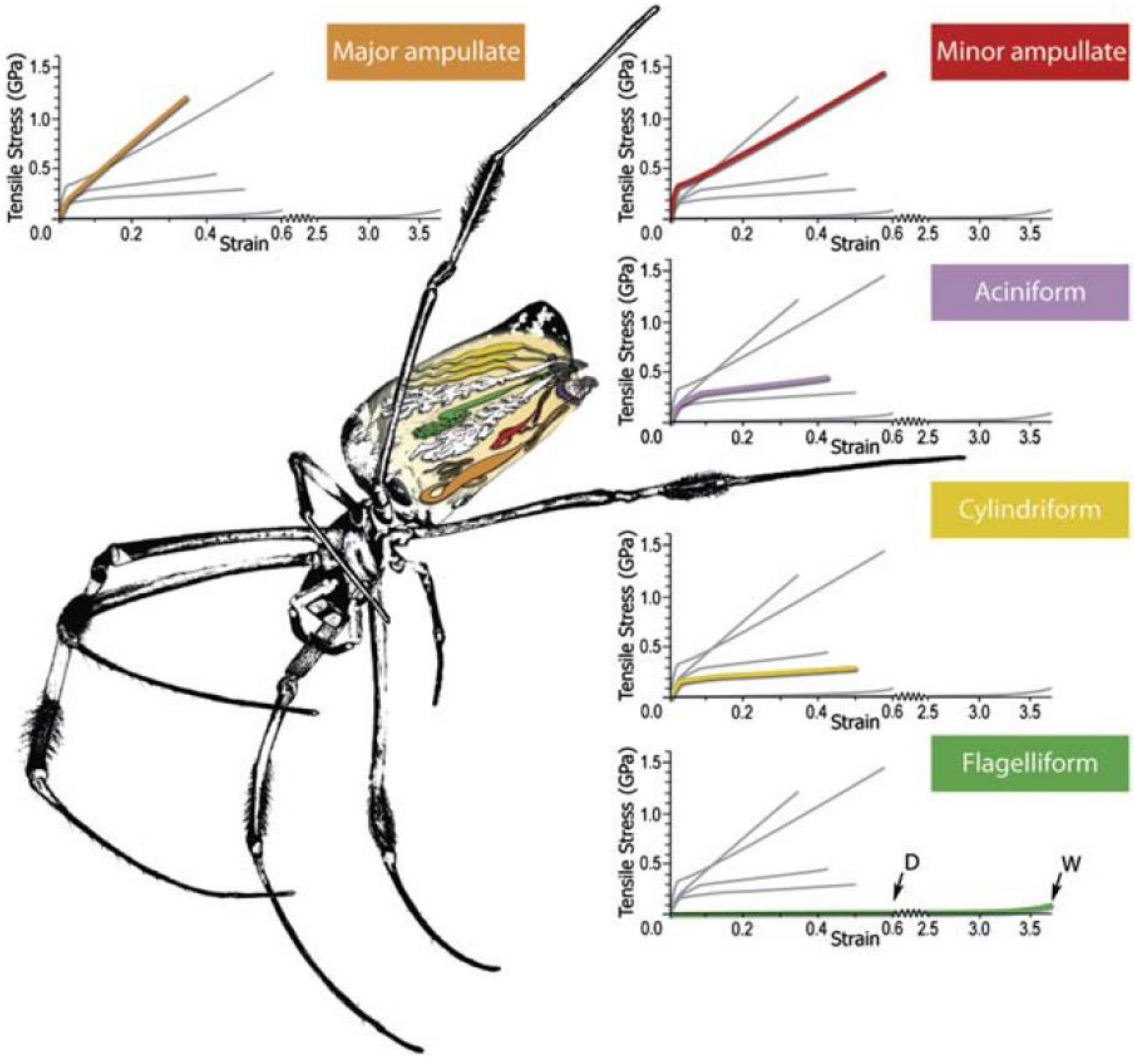

Figure 1.1: A depiction of the diversity of spider silks from a singular orb-weaving spider. Note that each silk type has distinct mechanical properties. Adapted with permission from [22]

The remainder of this chapter will focus mainly on Major Ampullate Silk (MAS), Minor Ampullate Silk (MiS), and *Bombyx mori* silks as these have garnered the most research attention and are also the silks I will be working with during my thesis.

1.2 From gene to macromolecular structure

Each type of spider and silkworm silk seem to consist of multiple types of spidroins and fibroins, as opposed to a single silk gene coding for a single silk protein[23–27]. In general, each spidroin or fibroin gene consists of highly conserved N- and C-termini, with repetitive motifs or spacer regions in between[28–30]. The N- and C- termini have been postulated to play important roles for stabilizing the proteins whilst stored in the lumen of the gland, for signaling purposes, and facilitating the fibrillation and assembly process of silk fibres during the spinning stage[31–34]. On the other hand, the repetitive motifs are glycine and alanine rich – small sized amino acids that are able to sterically pack closely together – and tend to consist of repetitive amino acid sequences such as GPGXX, $(GA)_n/(A)_n$, and GGX sequences which form β-spirals, β-sheet structures, and 3_{10}-Helices respectively[28,29,35].

Major ampullate silks seem to consist of two spidroins – MaSp1 and MaSp2 – and it has been shown that these spidroins themselves contain multiple isoforms[36,37]. MaSp1 spidroins do not contain proline, whereas MaSp2 do[24]. This is important as proline is hypothesized to be the reason for the ability of MA silks to supercontract, a phenomenon displayed only by MA silks whereby they are able to contract up to 30% its initial length on top of the 13% contraction due to the relaxation following a change in glass transition temperature [35]. Supercontraction is made possible by proline because it acts as a beta-sheet breaker, which may prevent neighbouring, more ordered motifs – which are likely glycine-rich – from crystallising, making them vulnerable to attack from water molecules [38], which in turn causes these regions to condense into a sphere or into alpha-helixes or 3_{10}-helix forms [35]. The amino acid sequences and composition – in particular the proline composition of the spidroins – of MAS spidroins also tend to vary considerably between spider species[38].

Minor ampullate silks (MiS) also consist of two separate spidroins – MiSp1 and MiSp2. However, unlike MAS silks, MiS spidroins do not contain proline and thus do not display supercontration[38]. Additionally, MiS spidroins contain serine rich spacer regions, another feature not seen in MAS spidroins[25]. Interestingly, MA and Mi silks have strong similarities in their values of crystallinity, nanocrystal orientation and nanocrystal size, yet their mechanical properties differ significantly suggesting that there are other unknown critical microstructural factors – such as the hydrophilicity of the lateral groups or the large scale organisation of the sequences [39] – that play a role in governing their mechanical behaviour and the variability between the properties of the two forms of ampullate silks.

Silks spun by *B. mori* silkworms are primarily a product of three different gene products: a large (350 kDa), insoluble protein termed the "Heavy-chain fibroin" (Fhc), a smaller (26 kDa) protein termed the "Light-chain fibroin" (Flc), and P25 which is a glycoprotein of approximately 30 kDa[26,40]. Fhc and Flc are linked by disulphide bonds, and P25 associates to the linked fibroins via non-covalent inteactions in order to form an elementary unit with a Fhc:Flc:P25 ratio of 6:6:126. It is postulated that the P25 glycoprotein is crucial for the assembly of this complex and the subsequent formation of silk fibres, though the exact mechanism in which P25 mediates this through remains unknown. In addition, the silks are coated with a serine-rich proteinaceous glue called sericin, which also consist of multiple gene products[40]. Sericin is responsible for gluing the fibres together during cocoon formation.

The silk proteins from either spiders or silkworms aggregate to form nanofibrils which themselves then interact to form microfibrils and subsequently form the final fibre, which ranges from 0.01μm to 5μm in diameter for spider silks, and generally around 10μm in diameter for silkworm silks. The fibres are postulated to consist of ordered motifs surrounded

by less-ordered regions[41–46]. Though the identity and structure of the crystalline motifs have been well studied over the years, ambiguity remains regarding the spatial distributions of these motifs. Additionally, very little is known regarding the structure and distribution of the less-ordered regions of silks, as well as the role of water within the structure of silks. This is crucial information for understanding the link between the structure of silks to their outstanding – and in some cases, bizarre – mechanical properties.

1.3 Of Isotopes and unnatural amino acids (UAAs)

Nuclear Magnetic Resonance (NMR) spectroscopy is undoubtedly an incredibly powerful tool for deducing the structure of small molecules and protein and does so by measuring the interaction of nuclear spins when aligned in a magnetic field[47]. Thus, it is not surprising that the technique has also been applied to study silks. Various studies exist whereby NMR has been employed to study the structure of silk proteins within the silk glands, as well as the structure of the proteins in solid fibre form[30,48–54]. However, the quality of the obtained spectra is highly-dependent on the concentration of the isotopes present. As a result, experiments often involve enriching silks with isotopes (often ^{13}C via ^{13}C-labelled amino acids or ^{13}C-labelled D-Glucose) simply by feeding them to the spider or silkworm[30,48,49,54–65]. These isotopes have been found to enter the silks via ingestion and – coupled with higher resolution techniques such as magic angle spinning methods – allowed for the acquisition of high-resolution spectra, enabling scientists to further refine their models of how silk proteins are arranged within the silk fibre or within the glands, thus provide understanding of silk structure in those two states. Researchers can discern such structures due to the conformational dependence of the ^{13}C isotropic chemical shift[47] . However, these enrichments tend to be non-specific as ^{13}C-labelled amino acids of one kind tended to be

converted to other forms within the spider, which limited the ability of scientists to probe specific sites of the silk surrounding an amino acid of interest[48].

Whilst isotopic modifications to amino acids in silks has been ongoing for several decades, the incorporation of unnatural amino acids (UAAs) into silks as a method for functionalizing and studying silks has only very recently taken the stage. Some of the more useful UAAs contain azides or alkynes, which allow for biorthogonal reactions to take place. Studies involving UAA incorporation have been ongoing in other organisms for several years[66], and the methods used for achieving said incorporation have been advancing as time passes. There are two principal methods for achieving UAA incorporation in organisms: residue-specific incorporation and site-specific incorporation[66]. Site-specific incorporation involves the genetic modification of the target organism to include an orthogonal tRNA - aminoacyl-tRNA synthetase (aaRS) system which can incorporate a UAA at a target codon – often the amber stop codon (UAG). Residue-specific incorporation on the other hand requires no genetic modification. Instead, the method relies on the target UAA being a close enough analog to a natural amino acid, and that the UAA will be incorporated in place of the natural amino acid, often simply through ingestion using an auxotrophic diet[67,68]. The most common and successful UAAs used for this regard are Azidohomoalanine (AHA) and Homopropargylglycine (Hpg)[68–70], both of which are analogs of Methionine. There are advantages and disadvantages to the two methods. Site-specific incorporation can often be targeted to specific proteins by limiting the expression of the orthogonal system via promoters[71], thus allowing point substitutions in proteins of interest with often minimal perturbation to the function and structure of the target. However, the process of designing an orthogonal tRNA - aaRS system and stably expressing it in the organism of interest is often non-trivial, and good knowledge of the genetics of the organism of interest is a prerequisite.

On the other hand, residue-specific incorporation requires little to no genetic knowledge of the organism, and certainly no genetic modification. However, the unnatural amino acid will be incorporated globally within the organism, which may lead to detrimental effects for the organism of interest, or the protein of interest. The repertoire of UAAs available for this method is also limited as they must be close enough analogs to their natural forms for the method to work.

Unnatural amino acid incorporation allows for the functionalization of the target protein through click-chemistry, often through copper-catalysed azide-alkyne cycloadditions (CuAAC)[70,72,73] or through strain-promoted azide-alkyne cycloaddition[74,75]. This has been utilized in various ways for studying proteins and sensory systems of interest. For example, it has been used to identify newly synthesized proteins (NSPs)[76–80], often when the organism is presented with some form of stimuli. It has also been used to study protein structure and dynamics[81,82], and quantitating proteome dynamics[83]. Examples of organisms where such studies have been successfully carried out include *E. coli*[84], *C. elegans*[85], *Xenopus*[78], Zebrafish[86], lab mice[77,87], and *Bombyx mori*[71,88–90]. With the exception of the silkworm however, UAA incorporation has not been used to generate novel natural materials, or used to study natural materials of interest, which I believe is a great avenue for research as there are many natural materials with remarkable properties, and UAA incorporation will be a very beneficial tool to scientists for further probing the chemical structure of these materials, as well as serve as a way for modifying these materials to our benefit.

Another form of UAA that has been receiving interest for its potential for imaging biological systems are UAAs that contain ^{19}F. There are several appealing features of fluorinated UAAs, especially for the application of NMR techniques in biological systems and materials. The

absence of ^{19}F in biological systems, high gyromagnetic ratio and a chemical shift that is very sensitive to its chemical environment make it an ideal probe for investigating the structure and dynamics of biological proteins and systems[91–93]. A recent example of such a study involves the specific integration of fluorinated Methionine into Virus Like Particles (VLPs) to monitor their disassembly[94].

1.4 Of fluorophores, Second-harmonic generation and nanoparticles

Both spider silks and silkworm silks are known to fluoresce intrinsically[95]. The source of this fluorescence likely originates from amino acids such as tryptophan, tyrosine, and phenylalanine; with tryptophan being the most responsive[96]. Apart from one study[97], this phenomenon has not been investigated in detail and is currently not used for characterising the structure of silks. This is perhaps unsurprising since it can be difficult to get good signal-to-noise ratios for the generated fluorescence, and that fluorescence intensity alone may not be informative of the structure of silks. However, it may be possible to derive more information about the fluorescing motifs via fluorescence lifetime imaging (FLIM). Fluorescence lifetime represents the amount of time in which a fluorophore remains in its excited state. The lifetime of a fluorophore is sensitive to not only the identity of the fluorophore, but also to the chemical environment around it[98]. Additionally, FLIM is independent of fluorescence intensity, thus negating the need for special ratiometric fluorophores[98]. The combination of these features in FLIM should theoretically be ideal for probing the chemical structure and environment of non-crystalline regions of silks.

Additionally, virtually no study to date exists whereby fluorophores were used to dye silks in order to study their structure; two studies have shown that Rhodamines are able to enter the silks of silkworms via ingestion leading to even labelling of the fibroins, but they did not use the phenomenon to investigate the structure of silks[99,100].

Second Harmonic Generation (SHG) is a nonlinear optical process that occurs when two lower energy photons up-convert to exactly twice the incident frequency[101]. The first reported use of SHG imaging in a biological context was in 1986 where it was used to investigate the polarity of collagen fibres in rat tail tendon[102]. Since then, SHG in a biological context has been applied largely for studying tissues; in particular for visualising collagen fibres in connective tissues and internal organs[102–108]. There are several features that SHG have over other imaging techniques that make it appealing for biological and biophysical imaging. Firstly, the signal source for SHG arises purely from induced polarisation – as opposed to absorption – thus leading to reduced photobleaching and phototoxicity[101]. Secondly, the typical fundamental wavelengths for the lasers used to induce SHG tend to be in the infrared spectral range; allowing high resolution imaging to depths of several hundreds of microns to be attained[109]. However, the most important feature – and one of particular interest to me – is that the SHG signals are very sensitive to the physical structure of the imaged target. A detailed calculation as to why this is the case can be found in Campagnola and Dong's review article on SHG[101] but in short, the strongest SHG signals arise from well-aligned molecules that assemble into fibrils or sheets, such as β-sheets. Indeed, SHG imaging has been used to successfully identify β-sheet structures in both spider and silkworm silks[110,111].

In recent years, there has been increasing interest in producing composite materials with the addition or doping of nanoparticles into another stock material of choice. Some groups have claimed to produced silk doped with nanoparticles that display improved mechanical properties[112–114]. However, this remains a highly contentious claim as it is debated as to whether nanoparticles can penetrate the various biological barriers found within the organism

to enter the silk gland, and the possibility of cross-contamination from external sources cannot be eliminated. Furthermore, closer inspection of the data from one of the papers[114] reveals cherry-picking of data, therefore any change in mechanical property cannot be directly attributed to the presence of nanoparticles in silks. This is not to say that nanoparticles do not enter silks and subsequently alter their mechanical properties, but simply that as of now those claims remain to be validated.

1.5 Research scope

The work in this thesis focuses on using novel techniques and approaches to study silks which as mentioned is a highly complicated biomaterial that requires a highly multi-disciplinary approach to study. This work will provide insight on how to approach investigating and/or modifying silks by either modifying the silk backbone itself using UAAs (Chapter 2), or by inserting molecular reporters such as fluorophores (Chapter 3). We also develop a multi-spectral technique with the capability of spatially resolving crystalline and non-crystalline motifs in silks (Chapter 4). One chapter of my work also aims to investigate the validity of inserting nanoparticles into silks via ingestion (Chapter 5); a field that has gained much hype over the past decade and is based off – in my opinion – unsatisfactorily controlled experiments.

1.6 Chapter introductions

1.6.1 Chapter 2: Unnatural Amino Acid (UAA) Incorporation into spider silks

UAAs are increasingly used for studying NSPs, protein dynamics, protein structure, etc. Inserting UAAs would allow us to functionalise silks for further studies or for practical/industrial applications. In this chapter, I explore the viability of inserting UAAs into the silk backbone and explore methods for verifying their incorporation.

1.6.2 Chapter 3: Incorporation of fluorophore dyes into spider and silkworm silks

Inclusion of fluorophores into silks might enable us to use novel techniques for studying the structure of spider silks. Any changes in the mechanical properties of spider silks due to their inclusion might also help us infer the structure of silks depending on what the dye structures are and how they are interacting. Here, I explore the effects of inserting fluorophore dyes into silks on both the behaviour of the animal ingesting the dye, the mechanical properties of the silks containing such modifications, and the spectral properties of the dyed silk fibre.

1.6.3 Chapter 4: SHG/FLIM imaging as a novel spatially-resolved method for investigating the structure of silks

Spatially resolved techniques are attracting increasing amounts of interest as researchers realise that the arrangement of structural motifs within silks is just as important as the identity of the motifs themselves in trying to understand silk as a material. The SHG/FLIM technique makes use of naturally occurring motifs and fluorescence in silks to discern their structure. We perform the imaging experiments on silks reeled at different speeds which theoretically should have different proportions of crystalline vs non-crystalline motifs, and corroborate the SHG/FLIM data with mechanical data obtained from stress-strain testing and DMTA.

1.6.4 Chapter 5: An investigation into the feasibility of incorporating nanoparticles into spider silks via direct feeding

In the past decade or so, there have been many claims of successfully incorporating nanoparticles into spider silks, and that the resultant silks display enhanced mechanical properties. Most of this research started as a result of one research group (Pugno et. al)[114]

claiming to enhance spider silks with nanoparticles. However, upon closer inspection of their data and methodology, it seems that the mechanical data was cherry picked and the method in which they fed the spiders NPs (via spraying a NP solution) coupled with the silk collection technique (collecting web samples as opposed to direct reeling) meant that there was a very high chance of surface-contamination by the sprayed NP. This is an attempt to repeat the experiment in a controlled manner.

1.6.5 Chapter 6: Further thoughts and future work

This chapter contains further discussions on the findings and conclusions obtained from the data chapters in the thesis, as well as my thoughts on the implications of these findings for silk research in the future.

Chapter 2: Unnatural Amino Acid (UAA) Incorporation into spider silks

1. Introduction

Spider silks are Nature's solution for multi-functional high-performing fibres suited for a variety of purposes. Through the process of natural selection – for a period of over 300 million years – spider silks have evolved to possess a combination of strength, toughness and flexibility that current man-made materials fail to achieve. Naturally, these silks have attracted a large amount of research attention aimed at analysing their structure and protein dynamics during formation[21,22,115]. However, one key challenge that researchers face is the lack of easily traceable or identifiable markers within silk proteins, in turn making it difficult to study specific aspects or regions of interest within silks. Researchers have attempted to circumvent this complication by feeding unnatural amino acids (UAAs) with isotopic changes, thus allowing silks to be studied with techniques such as Nuclear Magnetic Resonance (NMR). This is done by simply feeding spiders with unnatural amino acids or D-glucose containing these isotopic changes, the change often being an inclusion of ^{13}C within the molecules. Whilst this is a good start, the lack of specificity in where the ^{13}C labels attach themselves within silks, as well as the presence of natural ^{13}C in biological systems, limits the applicability of this technique[47–49].

In the past decade, there has been interest in synthesizing UAAs which contain ^{19}F. In theory, incorporating UAAs containing ^{19}F confers many advantages, especially for the application of NMR techniques in biological systems. The absence of ^{19}F in biological systems, high gyromagnetic ratio and a chemical shift that is very sensitive to its chemical environment make it an ideal probe for investigating the structure and dynamics of biological proteins and systems[91–93]. A recent example of such a study involves the specific integration of fluorinated

Methionine into Virus Like Particles (VLPs) to monitor their disassembly[94]. Despite their theoretical advantages, there aren't many examples of the integration of ^{19}F-UAAs into biological systems; certainly – at the time of writing – there aren't any works related to integration such UAAs into biomaterials such as silks.

UAAs may also contain structural changes as opposed to just isotopic changes. Some of these UAAs contain azides or alkynes, which allow for biorthogonal reactions to take place[73,75,116–118]. Studies involving UAA incorporation containing azides or alkynes have been ongoing in other organisms for several years[66]. There are two principal methods for achieving UAA incorporation in organisms: residue-specific incorporation and site-specific incorporation. Further details can be found in Chapter 1, Section 1.3.

The incorporation of UAAs containing structural changes into silks is a relatively recent field. Examples of such studies include the incorporation of Azidohomoalanines into genetically modified silkworms[88,90], the incorporation of other methionine analogues into silkworm silks via residue-specific incorporation[71], incorporation of azido-UAAs into spidroin-inspired proteins expressed by bacteria[119], and the synthesis of spidroin-inspired proteins with azide moieties attached to the N-terminals via EDC/NHS coupling[120]. To date, there have been no studies that involve incorporation such UAAs into native spider silks. The insertion of azide-bearing UAAs or fluorinated UAAs in specific locations within spidroins may open up many more avenues to study specific motifs that contain these UAAs.

In this chapter, I will feed spiders the following amino acids: AHA, $^{12}CF_3$-Met and $^{13}CF_3$-Met. These amino acids were chosen with several considerations in mind. Firstly, methionine is primarily found in the N- and C- terminals of spidroins, which are highly conserved and postulated to play important roles for the stabilisation of spidroins in the glands as well as potentially facilitate the fibrillation process during silk spinning[31,33,37,121,122]. Secondly,

literature suggests that when it comes to inserting UAAs into native systems, the aaRS system responsible for methionine incorporation shows the most flexibility, thus it is likely that we will achieve a higher success rate by using methionine analogues compared to other amino acid analogues[69,85,123,124]. I will employ an array of spectroscopic and chemical techniques to try and determine the presence of these UAAs within silks collected from spiders fed with these UAAs. Thirdly, the lack of natural abundance of any of these UAAs in silks should afford a high signal-to-noise ratios for spectroscopic techniques used to detect these UAAs. In particular, the high sensitivity and broad chemical shift range of ^{19}F in F-NMR in combination with the specific binding of F-UAAs to targeted sites may allow us to employ new techniques for studying the structure of silk motifs containing methionine.

2. Materials and Methods

2.1 Chemicals

Boc-Gln-OH (98%) was purchased from Sigma-Aldrich and used without further purification. $^{12}CF_3$-Methionine and $^{13}CF_3$-Methionine was synthesized and provided by Satoshi Kishigami from the BGD group. Details of the procedure used – the Shibata method[125] – can be found in the Supporting Information (S2.1).

2.2 Synthesis of Azidohomoalanine (AHA)

The synthesis scheme for AHA is based off Andruszkiewicz et. al. and Link et. al.'s synthesis schemes[70,126], as depicted in Scheme 1.

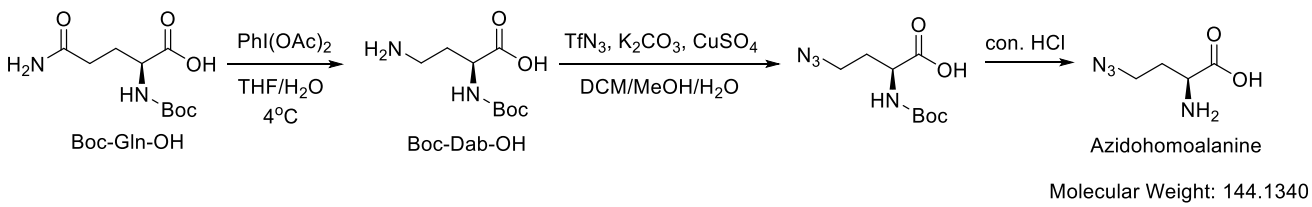

Scheme 1: Synthesis of AHA

2.2.1 (S)-4-Amino-2-(tert-butoxycarbonylamino)butanoic acid (Boc-Dab-OH)

A solution of N-tert-butoxycarbonyl-(S)-glutamine (7.38g, 30mmol) in THF (72ml) and water (18 ml) was treated with PIDA (11.386g, 35.4mmol) and stirred using a magnetic stirrer at 4 ± 2°C for 6 hr. After 6 hr, the mixture was evaporated to dryness using a rotavap, then the residue was dissolved in water (40ml) and extracted with ethyl acetate (3 x 40ml). The organic layer was discarded and the aqueous layer was evaporated to dryness with the aid of toluene. The crude solid was washed with cold chloroform several times then dried in vacuo overnight. The product was a white powder (3.9g, 59.6%).

^{1}H NMR (400 MHz, D_2O): δ = 1.35 (s, 9H, C(CH_3)$_3$), 1.83 - 1.93 (m, 1H, CH_2CH), 2.03-2.06 (m, 1H, CH_2CH), 2.97 - 3.01 (t, 2H, NH_2CH_2), 3.88 – 3.92 (m, 1H, C*H*COOH)

^{13}C NMR (100mHz, D_2O): δ = 27.60 (C(CH_3)$_3$), 29.80 (CH_2CH), 36.81 (NH_2CH_2), 53.52 (*C*HCOOH), 157.54, 177.92

ESIMS: m/z: Found 219.2 ($M-H^+$). $C_9H_{18}N_2O_4$ requires 218.1.

2.2.2 Azidohomoalanine

1. Sodium Azide (11.64g, 179.11mmol) was placed into a 250ml round bottom flask and distilled water (28.7ml) was added to it. The flask was placed in an ice bath.

2. Tf_2O (5.98ml, 35.44mmol) was added dropwise to the flask. The flask was then removed and left to stir at room temperature (24°C) for 2 hr.

3. During this period, a mixture of distilled water (57.5ml) and methanol (114.9ml) was made in a 500ml round bottom flask with a stirrer bar in. To this flask, Boc-Dab-OH (3.91g, 17.89mmol), K_2CO_3 (3.71g, 26.9mmol), and $CuSO_4.5H_2O$ (44.2mg, 0.177mmol) was added. The flask was set aside until the triflic azide was made.

4. At the conclusion of step 2, the reaction mixture was transferred to a separatory funnel and extracted twice with 18ml DCM. The DCM layers were collected.

5. DCM layers were combined and washed in a separatory funnel with 80ml of saturated Na_2CO_3. DCM layers were collected once more.

6. Triflic azide was added dropwise to the flask from step 3 and left to stir at room temperature overnight.

7. On the following day, the volatile solvents were evaporated, leaving behind an aqueous solution.

8. 6N HCl was added dropwise until the pH of the solution reached pH 6.

9. The solution was the diluted in 220ml of phosphate buffer (0.25M KH_2PO_4 + 0.25M K_2HPO_4, pH adjusted to 6.3 by HCl). The pH of the entire solution was adjusted to pH 3 by dropwise addition of 6N HCl.

10. The solution was extracted twice with 220ml of ethyl acetate.

11. The solution was washed with 110ml of saturated NaCl solution. The ethyl acetate layers were collected and dried with 11g of $MgSO_4$ for at least 30 min. The ethyl acetate was removed using a rotavap. The resulting oil was left in a high vac overnight.

12. 22ml of concentrated HCl (~37%) was added to the oil in step 11. The solution was stirred for 1 hr.

13. The solution was diluted with 200ml of distilled water.

14. The solution was then added to a column containing 55g of Dowex that had been conditioned beforehand. The flowthrough was collected and passed over the column once more.

15. The amino acid was eluted with 800ml of 1N NH_4OH.

16. The ammonia was evaporated away using a rotavap until a wet solid was left behind. The solid was then dried in a lyophiliser until a dry white powder remained.

Obtained a white powder (0.911g, 35.34% yield)

^1H NMR (400 MHz, D_2O): δ = 2.01 – 2.15 (m, 2H), 3.52 – 3.55 (m, 2H), 3.76 – 3.79 (m, 1H)

ESIMS: m/z: Found 145.0 (M^+). Calculated: 144.1 ($C_4H_8N_4O_2$)

2.3 Spider handling and silk collection

Adult *Nephila edulis* spiders were used as the candidate spider for the experiments. Individual spiders were kept in dedicated frames to keep them separate from the main population.

Spiders were fed UAA solutions which also contained 0.5% sucrose using a Gilson P20 pipette. The UAA solutions were kept in a fridge and in the dark at 4°C for up to 20 days. NMR experiments done on AHA solutions in D_2O that were kept under similar conditions indicate that there was no significant degradation of AHA when kept for this period (refer to appendix for spectra).

Throughout the 20 day experimental duration, spiders were not fed any additional food. This is to prevent competition from dietary methionine from interfering with the incorporation of the UAAs.

Spiders were silked for 1 hour at a reeling speed of 20mm s^{-1} (or equivalent in terms of amount e.g. 30 min @ 40mm s^{-1}) per silk type (MA and Mi silks were collected) before feeding (designated as day 0), to act as collect control samples as well as to empty the contents of their

silk glands. Spiders were then fed the UAA solution daily and samples collected at a reeling speed of 20mm s^{-1} for 1 hour (or equivalent) per silk type.

The weights of the silks were obtained on a Mettler Toledo XPR2 Microbalance.

Previous studies where AHA was successfully incorporated into proteins of various organisms suggested a concentration of 4mM – 8mM AHA solutions[77,79,80,127]. However, these studies involve incubating cells in the AHA solutions, rather than feeding a controlled amount to the organism. Furthermore, it has been postulated that spiders are able to consume high concentrations of amino acid solutions without deleterious effects[128]. As such, a range of doses with the aim of feeding as much AHA as possible without observing detrimental effects on the spider were trialled, as shown in Table 2.1.

2.4 Fourier-Transformed Infrared Spectroscopy

2.4.1 ATR-FTIR

FTIR spectra of AHA powder was obtained using an ATR-FTIR set-up to identify the azide peak within the spectrum. The spectrum of L-Met is also obtained as a control since AHA is an analog of L-Met. 0.22µg of silks from each treatment obtained from a spider fed with AHA (N1_AHA) were tested using a Bruker Vertex 80 with an ATR-FTIR set up. The silk was bundled in a way such that it covered the surface of the diamond.

2.4.2 KBr-FTIR

Analytical grade KBR was left in an oven at 120℃ to dry overnight. 200mg of KBr was used per sample which was ground with the silk samples in an agate pestle and mortar for approximately 3 minutes to attempt to evenly distribute the silk throughout the KBr. There is a possibility that this process introduces thermal and mechanical energy which may influence the structure of the silks by dehydrating the sample and increasing sample crystallinity. However, this is not the point of this specific IR experiment so I am not too worried about the

result of such alteration. The mixture was then pressed in a 13mm KBr die under a pressure of 10 tons for 30 seconds. The pellet was then placed in the detector and left to equilibrate for 5 minutes before measurements were taken. A blank KBr disc was also prepared in the same way before measurement of actual samples for use as a background. Details of the samples that were tested are shown in Table 2.1.

Spider	Silktype	Wg/mg
Std MAS	MAS	0.278
N0_AHA	MAS	0.226
Std MAS 2	MAS	0.224
N1_AHA	MAS 5d	0.215
N1_AHA	MAS 5d	0.223
N1_AHA	MAS 15d	0.228
N1_AHA	MiS 15d	0.223

Table 2.1: Details of the samples that were tested using the KBr-FTIR technique. N0_AHA: Spider 0 fed with AHA. Std MAS: Standard Major Ampullate Silks. N1_AHA: Spider 1, fed with AHA. MAS 5d: MAS collected 5 days after the feeding regime. MAS 15d: MAS collected 15 days after the feeding regime. MiS 15d: MiS collected 15 days after the feeding regime.

2.5 Raman Spectroscopy

Samples were either AHA powder, or silk bundles collected 5-15 days from N2_AHA and N3_AHA that were mounted onto cardboard frames which had an aperture of 10.4mm x 5mm. The samples were dry mounted onto a CaF_2 coated glass slide, before being placed in a Horiba LabRam ARAMIS Raman Spectrometer. A HeNe-632.8nm laser was used for testing the samples.

2.6 Mass Spectrometry and Proteomics

The samples used were Major Ampullate Silks (MAS) and Minor Ampullate Silks (MiS) from N1_AHA that were collected 15 days after feeding.

45µg of MAS silk sample or 36µg of MiS silk sample were denatured in 6M guanidinium-HCl in 100mM TEAB followed by incubation for 1 h at 37°C. MAS samples dissolved very well using this procedure, however MiS samples only partially dissolved leaving behind a cloud.

This was followed by subsequent reduction with 10mM TCEP for 30 min at room temperature (r.t.) and alkylation with 50mM 2-iodoacetamide for 30 min at r.t. in the dark.

AspN/Chymotrypsin/trypsin digest: Samples were diluted to 2M guanidinium-HCl with 50mM TEAB and digestion was performed with AspN (1:100 w/w) for 4h at 37°C, followed by Chymotrypsin (1:20 w/w) O/N at 37°C and trypsin (1:40 w/w) for 4h at 37°C. Samples were desalted and concentrated by C18 (Oasis HLB 10mg) and dried for 4h in a speed-vac before being resuspended in 5% FA 5% DMSO.

Resulting tryptic peptides were analyzed on an EASY-nLC 1000 UHPLC system (Proxeon) connected to a Q Exactive mass spectrometer (Thermo Fischer Scientific) possessing an EASY-Spray nanoelectrospray ion source (Thermo Fischer Scientific). The peptides were trapped on an in-house packed guard column (75µm i.d. x 20mm, reprosil C18, 3µm, 120 Å) using solvent A (0.1% Formic Acid, 5 % DMSO in water) at a pressure of 500 bar. The peptides were separated on an in-house packed C18 analytical column (75µm i.d. × 500mm, RSLC C18, 2µm, 100 Å) using a linear gradient (length: 58 minutes, 8% to 30% solvent B (0.1% formic acid, 5% DMSO in acetonitrile, flow rate: 200nL/min). The separated peptides were electrosprayed directly into the mass spectrometer operating in a data-dependent mode. Full scan MS spectra (scan range 350-1500m/z, resolution 30000, AGC target 1e6, maximum injection time 250ms) and subsequent HCD MS/MS spectra (resolution 15000, AGC target 3e4, maximum injection time 500ms) of 5 most intense peaks were acquired in the Orbitrap. HCD fragmentation was performed at 30% of normalized collision energy and the signal intensity threshold was kept at 500 counts.

Searches were performed with Peaks 8.5 for identification and *de-novo* analysis. The raw MS file was searched against or the Uniprot database entries for all *Nephila* species

(www.uniprot.org, on 1st September 2017, MaxQuant and PEAKS). Precursor mass tolerance was set to 15ppm. Fragment mass tolerances for HCD was set to 0.05Da. Trypsin with [D|P] were selected as the protease with a maximum number of 3 missed cleavages. Carbamidomethylation (Cysteine) was set as fixed modification, Oxidation (Methionine), Deamination (Asparagine, Glutamine), carbamylation (lysine, peptide N-term) and azidohomoalanine (Methionine, -4.9863) as variable modifications.

2.7 Amino Acid Analysis

Silk samples were sent to Creative Proteomics for AAA with the purpose of identifying the presence of AHA and Methionine within the samples. Samples were blinded to prevent any form of bias on their end. Table 2.2 contains details of the silk samples sent.

Sample name	Spider	SilkType	Weight/µg
S1	N4_AHA	MAS 0d (Control)	320
S2	N2_AHA	MAS 15d	300
S3	N4_AHA	MAS 15d	350
S4	N4_AHA	MAS 20d	340

Table 2.2: Details of the silk samples sent to Creative Proteomics for analysis.

Details of the procedure used for the analysis by Creative Proteomics is detailed in the Supplementary information (S2.2)

2.8 Click-chemistry

MAS samples were used from 3 adult *Nephila edulis* spiders (N1_AHA, N2_AHA and N3_AHA). The details of samples used can be found in Table 2.3.

Spider	Silk Type	Treatment	Weight (mg)
N1_AHA	MAS	0d	0.074
N1_AHA	MAS	15d	0.093
N2_AHA	MAS	0d	0.127
N2_AHA	MAS	15d	0.166
N3_AHA	MAS	0d	0.116
N3_AHA	MAS	10d	0.091

Table 2.3: Details of the samples used for the click-reaction. MAS: Major Ampullate Silk, 0d: initial (control) silks, 15d: Silks collected 15 days after daily feeding with an AHA solution, 10d: Silks collected 10 days after daily feeding with an AHA solution.

The following are the final concentrations of the reagents used for the click-reaction:

- $CuSO_4$: 0.10mM
- THPTA: 0.50mM
- Na-Ascorbate: 5mM
- Aminoguanidine-HCl: 5mM
- Sulfo-Cy3-Alkyne: 20mM
- Phosphate Buffer: 100mM, pH 7

a) Silks were placed in 2mL Eppendorf tubes. 433.3µL phosphate buffer pH 7 was added to each tube.

b) 10µL of Cargo-alkyne (Sulfo-Cy3-Alkyne) was added to each tube.

c) A premixed solution of $CuSO_4$ (2.5µL) and THTPA (5.0µL) was added to each tube.

d) 25µL of aminoguanidine followed by 25µL of Na-ascorbate was added.

e) Tubes were closed to prevent additional oxygen from entering the system. Tubes were inverted several times to mix the solution. Tubes were then left overnight in a test tube rack covered with aluminium foil to prevent light from reaching the tubes.

f) The following day, the silks were washed 3 times in 15mL of distilled H_2O, then left to soak in 2mL of deionized water for 2hr 15min.

g) Silks were rinsed once more with deionized water then dried in a dessicator that was covered in aluminium foil.

2.9 ^{19}F solid-state NMR measurement on spider silk samples

^{19}F-NMR experiments were performed on MAS samples collected from spiders fed with trifluorinated-methionine. The purpose of the experiment was to determine if the fluorinated UAAs that were fed to the spiders managed to get incorporated into silk proteins via ingestion.

Solid-state NMR experiments were performed on a Bruker HFX spectrometer (in the Chemistry Research Laboratory, Oxford) running the TOPSPIN software. The magnet was operating at a magnetic field of 9.4 Tesla, corresponding to Larmor frequencies of 400MHz for ^{1}H, 375MHz for ^{19}F. A 1.9mm HFX MAS probe with a maximum MAS frequency of 30kHz was used.

Spectra were recorded at magic angle spinning (MAS) frequencies of 15kHz and 30kHz. The sweep width was adjusted to the region of interest, where we expect the ^{19}F chemical shift of organic fluorides. For the measurements, heteronuclear decoupling for ^{19}F and ^{1}H was applied to reduce the background noise.

3. Results

3.1 Spider response to the UAA solutions

The tolerance of spiders to the UAAs incorporated into their diet was assessed by feeding them using solutions with distinct concentrations of the target UAA. A table with the dosage of AHA fed, the condition of the spider and the silks collected from the spiders is shown in Table 2.4.

Spider	Daily dosage	Survival	Samples collected
N1test_AHA, N2test_AHA	346mM AHA, 20µL	<1d	n/a
N3test_AHA, N4test_AHA	34.6mM AHA, 20µL	~4d	0d
N0_AHA	1mM AHA, 20µL	>20d	0d, 1d, 5d, 10d, 15d
N1_AHA	2mM AHA, 20µL	>20d	0d, 5d, 10d, 15d, 20d
N2_AHA	8mM AHA, 40µL	>20d	0d, 5d, 10d, 15d
N3_AHA	8mM AHA, 40µL	>20d	0d, 5d, 10d
N4_AHA	12mM AHA, 40µL	>20d	0d, 15d, 20d
N5_AHA	12mM AHA, 40µL	14d	0d
N6_AHA	12mM AHA, 40µL	8d	0d
N0_CF_3	20mM $^{12}CF_3$, 40µL	14d	0d
N1_CF_3	20mM $^{12}CF_3$, 40µL	>20d	0d, 15d
N2_CF_3	20mM $^{12}CF_3$, 40µL	>20d	0d, 15d
N3_CF_3	20mM $^{13}CF_3$, 40µL	>20d	0d, 20d
N4_CF_3	20mM $^{13}CF_3$, 40µL	>20d	0d, 20d

Table 2.4: List of spiders and corresponding AHA and CF_3 solutions fed, as well as their survivability.

Despite spiders' reputation for being able to uptake concentrated amino acid solutions without detrimental consequences[128], the results show that a high concentration and dosage of the AHA solution led to early mortality in the spiders. Behaviourally, the spiders also displayed reduced activity and responses to external stimuli such as vibrations and handling by humans. This perhaps isn't surprising since the AHA that has been ingested is likely to incorporate non-specifically in any protein containing methionine, this interrupting their

normal function. Thus, a balance between maintaining spider longevity and maximising the incorporation of AHA into silks had to be struck. I found a feeding regime of 40µL daily with a concentration of 8mM AHA to be most suitable.

In contrast, the spiders were able to uptake a much higher concentration and dosage of the CF_3-Met solution. This is likely because the chemical change due to the replacement of hydrogens by fluorine had a lesser effect on the natural properties of standard methionine, as opposed to a complete replacement of the R-moiety of methionine by the azide structure in AHA.

3.2 FTIR Spectroscopy

3.2.1 ATR-FTIR spectra of AHA vs L-Methionine

Once the feeding regime was established, and initial attempt at the detection of incorporated AHA into spider silks was done using infrared spectroscopy as it allowed the detection of distinct chemical moieties. This is because distinct chemical moieties have specific resonance frequencies – known as an IR fingerprint – which result in distinct peaks being shown in the IR spectra[129].

FTIR spectra of AHA powder was obtained using an ATR-FTIR set-up to identify the azide peak within the spectrum (12 scans, resolution of 0.1cm^{-1}). The azide-moiety in AHA is expected to display a peak at around 2100cm^{-1}, which is obtained as shown below. The spectrum of L-Met is also obtained as a control since AHA is an analog of L-Met. Figures 2.1 and 2.2 display the FTIR spectra for AHA and Met respectively.

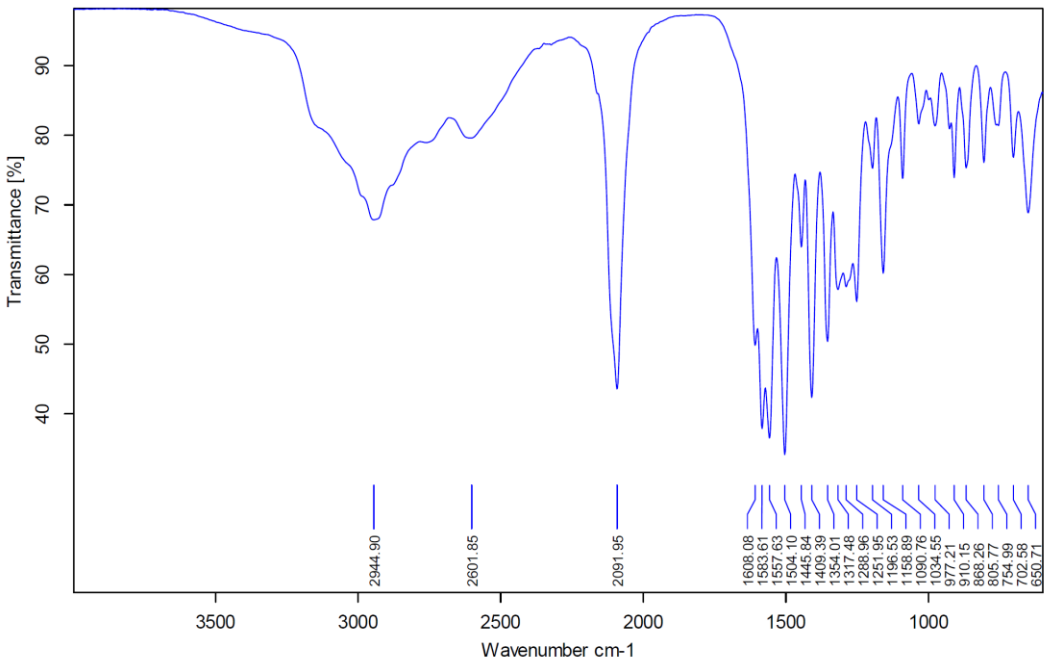

Figure 2.1: FTIR spectra of AHA. The azide peak is distinctly seen at 2091.95cm^{-1}.

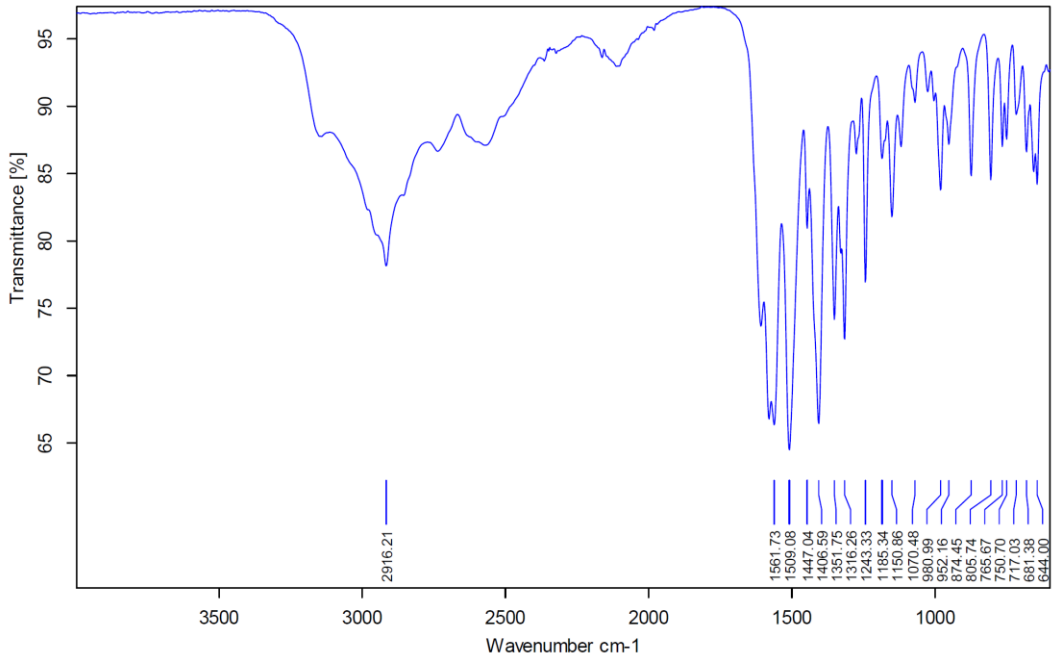

Figure 2.2: FTIR spectra of L-Met. Note the absence of a peak around 2100cm^{-1}.

Although the diamond used for the ATR-FTIR set up attenuates the signal from between 1800-2300cm^{-1} (Dr. Robert Jacobs, *Personal comm.*), there seemed to be sufficient signal-to-noise in pure AHA to overcome this barrier. The results above suggest that should AHA be incorporated in spider silks, we should expect a peak to appear around 2100cm^{-1}, although the peak may be broadened or shifted slightly in the protein itself.

3.2.2 ATR-FTIR spectra of silks

0.22µg of silks from each treatment obtained from N1_AHA were tested using a Bruker Vertex 80 with an ATR-FTIR set up. The silk was bundled in a way such that it covered the surface of the diamond.

Results yielded good signals for the amide band region from the protein backbone with good signal-to-noise ratio. However, no discernable signal could be obtained from the region

between 1800-2300cm^{-1} as expected, due to both the attenuation from the diamond as well as the (highly probable) low concentration of AHA in the silk samples. Therefore, with respect to detecting azides, no difference could be seen between the control samples and the treated samples. In addition, this confirms that the ATR-FTIR method for detecting azides in silks is not viable.

Consequently, techniques with higher sensitivity were tried to enable low-level incorporation.

3.2.3 KBr-FTIR spectra of silks

The same silks used for the ATR-FTIR tests (0.22µg of silks per treatment) were prepared for KBr-FTIR (24 scans, resolution of 0.1cm^{-1}).

The spectra for the region between 1800-2300cm^{-1} was less noisy compared to the ATR-FTIR spectra shown in Figure 2.2. However, there seems to be no discernible azide peak from the treated silks vs the control silks. Figure 2.3 depicts the results of the KBr-FTIR tests using representative spectra.

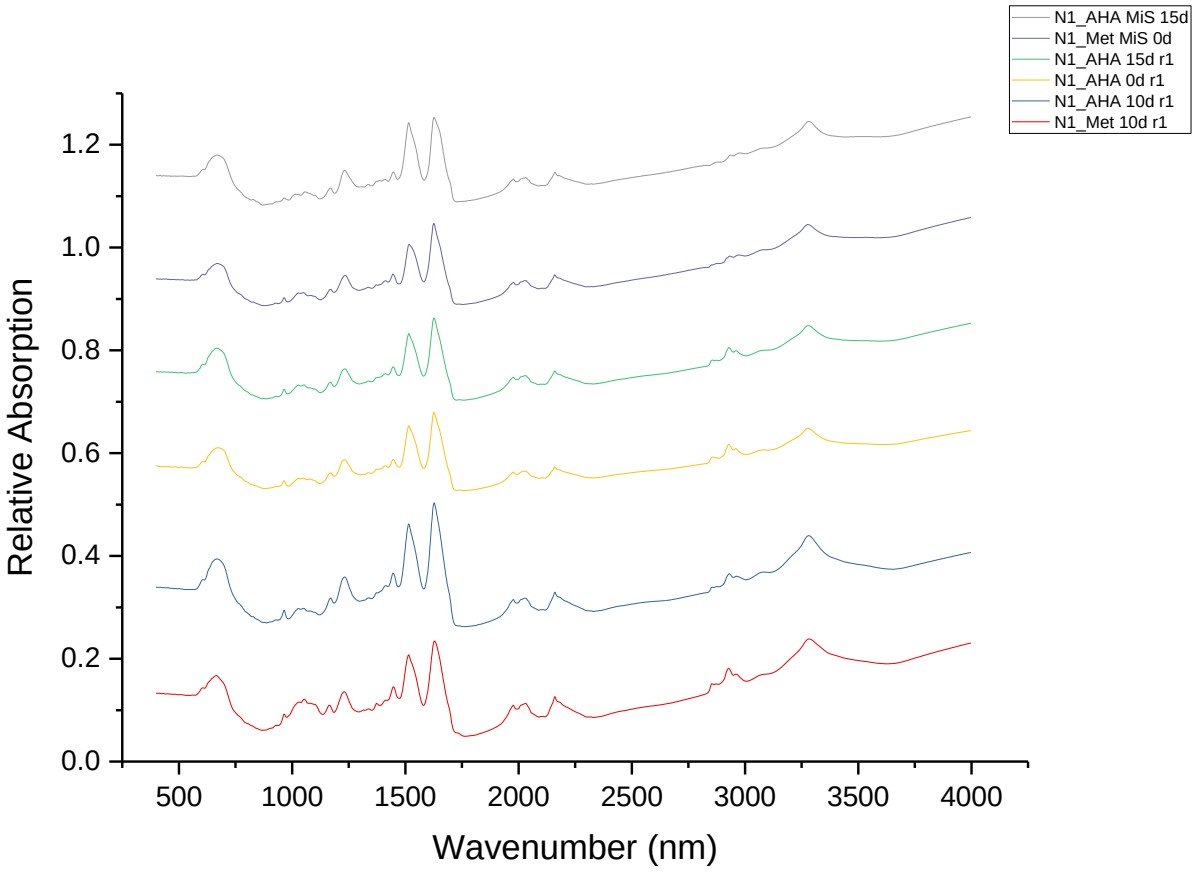

Figure 2.3: KBr-FTIR spectra of silk samples taken from N1_AHA and N1_Met. 0d: control samples. 10d: Silks collected 10d after the feeding regime. 15d: silks collected 15d after feeding. R1: run one.

3.3 Raman Spectroscopy

In a further attempt to try another spectroscopic method for detecting azides within silks, Raman spectroscopy was used on silks obtained from spiders fed with the AHA solution.

Figure 2.4 depicts the Raman spectra obtained from AHA powder. The azide peak is seen at ~2095cm^{-1} which is the expected region. However, despite the sample being pure AHA powder, the peak is of a low intensity, which is to be expected since molecules that display strong peaks in IR-spectra tend to display weak peaks in Raman-spectra130.

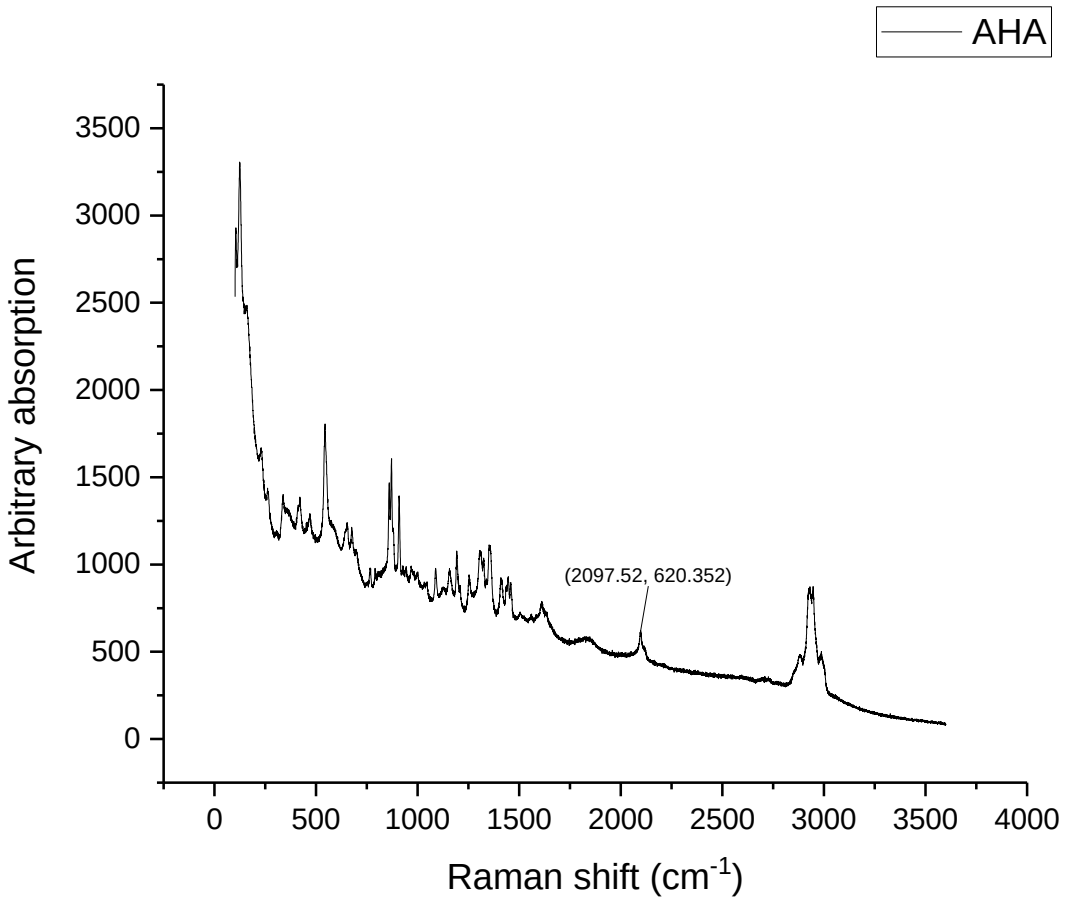

Figure 2.4: Raman spectra for pure AHA crystals. The peak at ~2097cm^{-1} corresponds to the azide peak. Note that it is much smaller than in the FTIR spectra in Section 7.2.4. Acq t: 8s. Acq. number: 10.

Given the spectral window where azide peaks can be expected, as well as some preliminary screening on silk samples, I restricted the spectral window to 1600-2400cm^{-1} to save

experimental time. Figure 2.5 displays representative Raman spectra for samples collected from N2 and N3_AHA, compared to the Raman spectra of pure AHA.

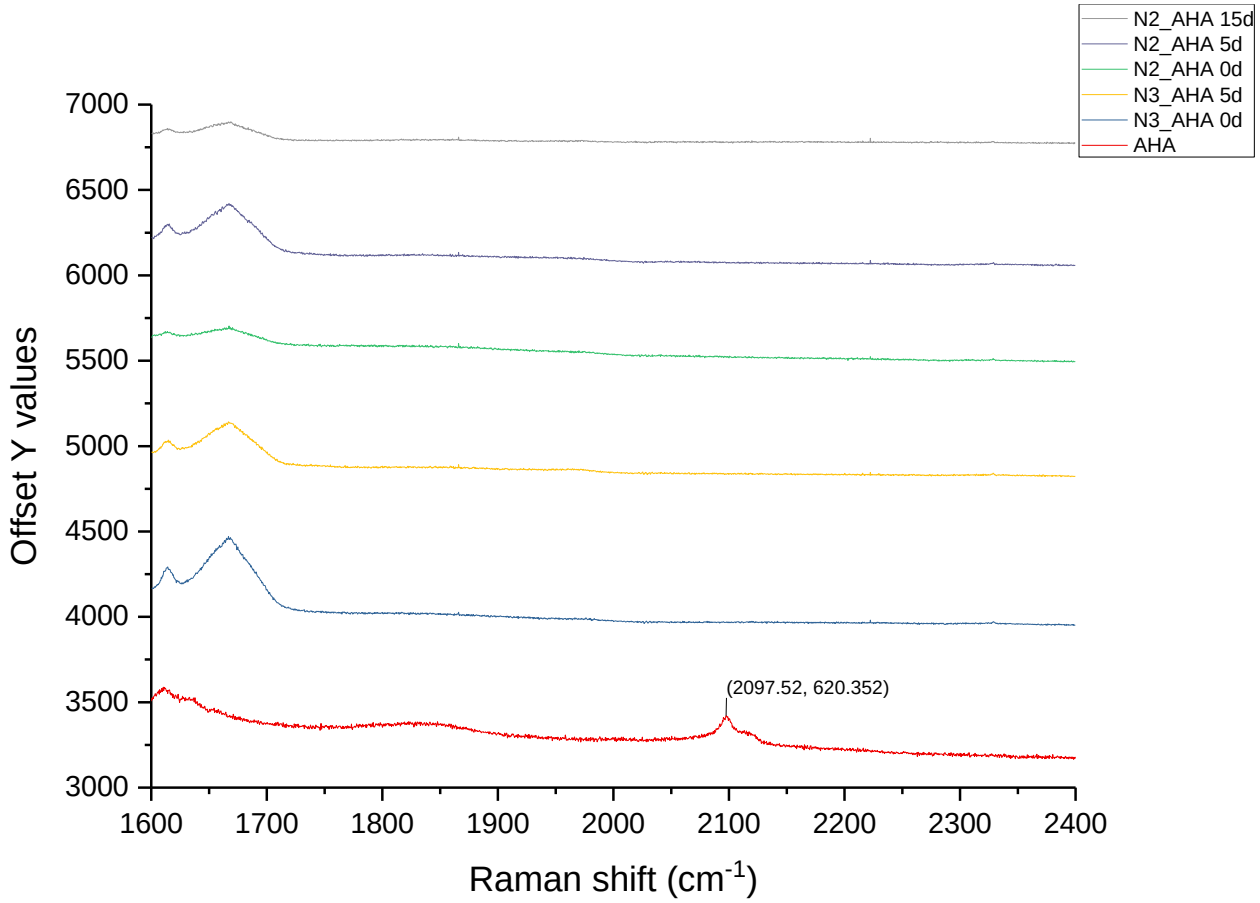

Figure 2.5: Raman spectra for N2_AHA and N3_AHA MAS silk samples, compared to pure AHA. Note the lack of a peak around 2097cm^{-1} in the silk samples. Acq t: 10s. Acq. number: 15. 0d: Control. 5d: Silks collected 5 days after the feeding regime. 15d: Silks collected 15 days after the feeding regime.

No discernible azide peaks can be seen from the silks obtained several days after feeding with AHA compared to the controls. As no signal could be detected by either IR or Raman, solid-phase approaches to probing the auxotrophic insertion of AHA were dismissed. In the following, results from in-solution methods are presented.

3.4 Mass Spectrometry and Proteomics for detection of AHA in silk proteins

3.4.1 Protein identification with PEAKS 8.5

The polymeric nature of spider silks limits the analytical possibilities in solution. One approach attempted in this work is the digestion of spider silks into their constituent peptides. These peptides can be analysed by mass spectrometry, using conventional bottom-up proteomic workflows.

However, one major challenge is that the genome of *N. edulis* has yet to be sequenced; as such, database searches – which is the most common approach in proteomic data analysis – were not possible. Consequently, the de-novo sequencing software PEAKS was used, which includes an initial de-novo sequencing step followed by database searches and homology/mutation searches (SPIDER searches) against known deposited sequences of related species of spiders, which included *N. clavipes* and *N. madagascarensis*.

Tables 2.5-2.8 are the results for the PEAKS database search for both MAS and MiS silk samples, which reflect the matches found when comparing the peptide sequences obtained from tandem mass spectrometry (MS/MS) against the PEAKS genetics database for selected *Nephila sp*.

Accession	-10lgP	Coverage	Coverage MAS_Major_amp	#Peptides	#Unique	PTM	Avg. Mass	Description
Proteins								
tr|Q2VLH2|Q2VLH2_9ARAC	204.55	33%	33%	100	12	d o c	172570	Major ampullate spidroin 2-like (Fragment) OS=Nephila inaurata madagascariens...
tr|Q9BIT7|Q9BIT7_9ARAC	201.22	29%	29%	91	4	d c	159382	Major ampullate spidroin 2-like protein (Fragment) OS=Nephila inaurata madaga...
tr|Q692G2|Q692G2_NEPCL	129.85	54%	54%	32	4	d c	31389	Major ampullate spidroin 1 (Fragment) OS=Nephila clavipes PE=4 SV=1
P19837|SPD1_NEPCL	124.21	56%	56%	43	13	d c	60585	Spidroin-1 (Fragment) OS=Nephila clavipes PE=1 SV=3
tr|O46171|O46171_NEPCL	123.94	44%	44%	31	6	d c	44107	Spidroin 1 (Fragment) OS=Nephila clavipes PE=2 SV=1
tr|O46172|O46172_NEPCL	117.76	49%	49%	31	2	d c	49410	Dragline silk protein spidroin 1 (Fragment) OS=Nephila clavipes PE=4 SV=1
tr|Q9BIT4|Q9BIT4_9ARAC	116.57	52%	52%	23	6	d	21311	Major ampullate spidroin 1 (Fragment) OS=Nephila senegalensis GN=MaSp1 PE...
tr|Q692G3|Q692G3_NEPCL	110.66	56%	56%	28	0	d c	32145	Major ampullate spidroin 1 (Fragment) OS=Nephila clavipes PE=4 SV=1
tr|Q692G4|Q692G4_NEPCL	110.39	46%	46%	25	1	d c	35903	Major ampullate spidroin 1 (Fragment) OS=Nephila clavipes PE=4 SV=1
tr|B2MUD4|B2MUD4_NEPCL	106.21	49%	49%	21	0	d	21510	Major ampullate spidroin 1 (Fragment) OS=Nephila clavipes PE=2 SV=1
tr|Q9BIT6|Q9BIT6_9ARAC	104.09	41%	41%	19	3	d	19885	Major ampullate spidroin 1 (Fragment) OS=Nephila inaurata madagascariensis G...
tr|B5SYS5|B5SYS5_NEPCL	92.26	40%	40%	15	5	d o	24900	Major ampullate spidroin 1A (Fragment) OS=Nephila clavipes GN=MaSp1A PE=1...
tr|B5SYS6|B5SYS6_NEPCL	89.26	50%	50%	16	8	d o c	24777	Major ampullate spidroin 1B (Fragment) OS=Nephila clavipes GN=MaSp1B PE=4 ...
tr|Q692G5|Q692G5_NEPCL	89.06	51%	51%	14	2	d	21948	Major ampullate spidroin 1 (Fragment) OS=Nephila clavipes PE=4 SV=1
tr|Q5UNL0|Q5UNL0_NEPPI	69.23	25%	25%	8	1		14473	Dragline silk spidroin 1 (Fragment) OS=Nephila pilipes PE=4 SV=1
tr|Q8WSZ3|Q8WSZ3_NEPCV	58.59	18%	18%	5	1		25396	Dragline silk protein spidroin 2 (Fragment) OS=Nephila clavata PE=2 SV=1
tr|Q9BIT5|Q9BIT5_9ARAC	57.90	8%	8%	5	0		48361	Major ampullate spidroin 2 (Fragment) OS=Nephila inaurata madagascariensis G...
P46804|SPD2_NEPCL	34.77	8%	8%	4	0		54184	Spidroin-2 (Fragment) OS=Nephila clavipes PE=2 SV=1

Table 2.5: Results of PEAKS database search for MAS

Accession	-10lgP	Coverage	Coverage MIS_minor_amp	#Peptides	#Unique	PTM	Avg. Mass	Description
Proteins								
tr|Q2VLH2|Q2VLH2_9ARAC	149.54	22%	22%	30	5	dc	172570	Major ampullate spidroin 2-like (Fragment) OS=Nephila inaurata madaga...
tr|Q9BIT7|Q9BIT7_9ARAC	143.94	18%	18%	26	1	dc	159382	Major ampullate spidroin 2-like protein (Fragment) OS=Nephila inaurata ...
tr|Q692G2|Q692G2_NEPCL	107.36	41%	41%	14	2		31389	Major ampullate spidroin 1 (Fragment) OS=Nephila clavipes PE=4 SV=1
P19837|SPD1_NEPCL	103.80	58%	58%	33	12	dc	60585	Spidroin-1 (Fragment) OS=Nephila clavipes PE=1 SV=3
tr|O46171|O46171_NEPCL	102.63	40%	40%	19	5	c	44107	Spidroin 1 (Fragment) OS=Nephila clavipes PE=2 SV=1
tr|O17434|O17434_NEPCL	94.85	33%	33%	34	32	dc	79082	Minor ampullate silk protein MiSp1 (Fragment) OS=Nephila clavipes PE=2...
tr|Q8WSW4|Q8WSW4_NEPCL	88.97	37%	37%	18	1	c	52104	Dragline silk protein (Fragment) OS=Nephila clavipes PE=4 SV=1
tr|Q692G3|Q692G3_NEPCL	87.09	54%	54%	17	0	c	32145	Major ampullate spidroin 1 (Fragment) OS=Nephila clavipes PE=4 SV=1
tr|Q692G4|Q692G4_NEPCL	84.44	45%	45%	16	2	dc	35903	Major ampullate spidroin 1 (Fragment) OS=Nephila clavipes PE=4 SV=1
tr|Q9BIT4|Q9BIT4_9ARAC	83.37	41%	41%	9	4	d	21311	Major ampullate spidroin 1 (Fragment) OS=Nephila senegalensis GN=Ma...
tr|B2MUD4|B2MUD4_NEPCL	82.03	44%	44%	11	1	c	21510	Major ampullate spidroin 1 (Fragment) OS=Nephila clavipes PE=2 SV=1
tr|B5SYS6|B5SYS6_NEPCL	73.53	29%	29%	5	1	do	24777	Major ampullate spidroin 1B (Fragment) OS=Nephila clavipes GN=MaSp1...
tr|B5SYS5|B5SYS5_NEPCL	73.17	26%	26%	5	1	o	24900	Major ampullate spidroin 1A (Fragment) OS=Nephila clavipes GN=MaSp1...
tr|Q9BIT6|Q9BIT6_9ARAC	72.23	45%	45%	9	2		19885	Major ampullate spidroin 1 (Fragment) OS=Nephila inaurata madagascari...
tr|Q692G5|Q692G5_NEPCL	68.95	46%	46%	11	2	c	21948	Major ampullate spidroin 1 (Fragment) OS=Nephila clavipes PE=4 SV=1
tr|Q2LC34|Q2LC34_9ARAC	37.16	12%	12%	3	1		32188	Minor ampullate fibroin 1 (Fragment) OS=Nephila antipodiana PE=1 SV=1
tr|A0A076L2S1|A0A076L2S1...	24.78	11%	11%	1	1		7157	BLTX573 OS=Nephila pilipes PE=2 SV=1
tr|A0A076KZX8|A0A076K...	24.78	10%	10%	1	1		8061	BLTX571 OS=Nephila pilipes PE=2 SV=1
tr|A0A076KUF1|A0A076...	24.78	4%	4%	1	1		18875	BLTX205 OS=Nephila pilipes PE=2 SV=1

Table 2.6: Results of PEAKS database search for MiS

Spidroin 1, Spidroin 1A, Spidroin 1B entries from *Nephila clavipes* and Spidroin-2 from *Nephila madagascarensis* are the top hits, as shown by the degree of coverage and numbers of peptide matches. Evidence suggests that the *Nephila clavipes* Spidroin-2 protein differs slightly from other *Nephila* species. The results are similar for both MAS and MiS samples.

3.4.2 Post-translational modification (PTM) analysis

Spider silks are heavily post-translationally modified, with single amino acid variations occurring frequently131. This is indeed observed in the PTM and SPIDER homology search using PEAKS 8.5, with sequence coverage increasing drastically. Results for both MAS and MiS show that identified sequences seem to be well conserved with few amino acid mutations found.

Accession	-10lgP	Coverage	Coverage MAS_Major_amp	#Peptides	#Unique	PTM	Avg. Mass	Description
Proteins								
tr|Q2VLH2|Q2VLH2_9ARAC	215.66	42%	42%	152	150	dcnoedddbPnnP	172570	Major ampullate spidroin 2-like (Fragment) OS=Nephila inaurata ma...
tr|Q692G2|Q692G2_NEPCL	133.15	54%	54%	37	6	dceeePoiX	31389	Major ampullate spidroin 1 (Fragment) OS=Nephila clavipes PE=4 S...
P19837|SPD1_NEPCL	129.52	57%	57%	54	15	dcneeeePfPmmldX	60585	Spidroin-1 (Fragment) OS=Nephila clavipes PE=1 SV=3
tr|O46171|O46171_NEPCL	126.38	48%	48%	35	6	dceeePfPoiX	44107	Spidroin 1 (Fragment) OS=Nephila clavipes PE=2 SV=1
tr|Q9BIT4|Q9BIT4_9ARAC	122.82	59%	59%	31	10	dePenddX	21311	Major ampullate spidroin 1 (Fragment) OS=Nephila senegalensis GN...
tr|Q9BIT6|Q9BIT6_9ARAC	108.13	65%	65%	24	5	daoX	19885	Major ampullate spidroin 1 (Fragment) OS=Nephila inaurata madaga...
tr|B5SYS5|B5SYS5_NEPCL	97.23	54%	54%	20	8	donUbX	24900	Major ampullate spidroin 1A (Fragment) OS=Nephila clavipes GN=M...
tr|B5SYS6|B5SYS6_NEPCL	91.94	51%	51%	19	10	docPoUX	24777	Major ampullate spidroin 1B (Fragment) OS=Nephila clavipes GN=M...
tr|Q692G5|Q692G5_NEPCL	91.70	53%	53%	16	2	deo	21948	Major ampullate spidroin 1 (Fragment) OS=Nephila clavipes PE=4 S...
tr|Q9BIT5|Q9BIT5_9ARAC	60.76	13%	13%	6	3	t	48361	Major ampullate spidroin 2 (Fragment) OS=Nephila inaurata madaga...
tr|O17434|O17434_NEPCL	23.55	4%	4%	2	2		79082	Minor ampullate silk protein MiSp1 (Fragment) OS=Nephila clavipes ...

Table 2.7: PEAKS SPIDER search for MAS sample showing the highest scoring hits

Accession	-10lgP	Coverage	Coverage MIS_minor_amp	#Peptides	#Unique	PTM	Avg. Mass	Description
Proteins								
tr|Q2VLH2|Q2VLH2_9ARAC	180.04	41%	41%	81	8		172570	Major ampullate spidroin 2-like (Fragment) OS=Nephila inaurata mada...
tr|Q9BIT7|Q9BIT7_9ARAC	178.10	37%	37%	79	6		159382	Major ampullate spidroin 2-like protein (Fragment) OS=Nephila inaurat...
tr|Q692G2|Q692G2_NEPCL	115.52	50%	50%	22	5		31389	Major ampullate spidroin 1 (Fragment) OS=Nephila clavipes PE=4 SV=1
P19837|SPD1_NEPCL	111.01	61%	61%	45	14		60585	Spidroin-1 (Fragment) OS=Nephila clavipes PE=1 SV=3
tr|O46171|O46171_NEPCL	109.95	52%	52%	27	7		44107	Spidroin 1 (Fragment) OS=Nephila clavipes PE=2 SV=1
tr|O17434|O17434_NEPCL	105.23	48%	48%	59	59		79082	Minor ampullate silk protein MiSp1 (Fragment) OS=Nephila clavipes PE...
tr|O46172|O46172_NEPCL	102.93	57%	57%	32	1		49410	Dragline silk protein spidroin 1 (Fragment) OS=Nephila clavipes PE=4 ...
tr|Q9BIT4|Q9BIT4_9ARAC	97.06	53%	53%	19	11		21311	Major ampullate spidroin 1 (Fragment) OS=Nephila senegalensis GN=...
tr|Q692G3|Q692G3_NEPCL	96.41	63%	63%	27	0		32145	Major ampullate spidroin 1 (Fragment) OS=Nephila clavipes PE=4 SV=1
tr|B2MUD4|B2MUD4_NEPCL	87.61	50%	50%	17	1		21510	Major ampullate spidroin 1 (Fragment) OS=Nephila clavipes PE=2 SV=1
tr|B5SYS6|B5SYS6_NEPCL	82.15	33%	33%	8	3		24777	Major ampullate spidroin 1B (Fragment) OS=Nephila clavipes GN=MaS...
tr|B5SYS5|B5SYS5_NEPCL	79.86	35%	35%	7	2		24900	Major ampullate spidroin 1A (Fragment) OS=Nephila clavipes GN=MaS...
tr|Q692G5|Q692G5_NEPCL	74.58	52%	52%	15	2		21948	Major ampullate spidroin 1 (Fragment) OS=Nephila clavipes PE=4 SV=1
tr|A0A076L2S1|A0A076L2...	24.78	11%	11%	1	1		7157	BLTX573 OS=Nephila pilipes PE=2 SV=1

Table 2.8: PEAKS SPIDER search for MiS sample showing the highest scoring hits

3.4.3 Analysis of AHA incorporation

When searching the obtained tandem mass spectrum of peptides from the *N. edulis* silk digestion, no peptides containing AHA instead of Met were identified (searches with variable modification). Therefore, manual inspection was required to validate candidate sequences suggested by the de-novo sequencing algorithm.

AHA modified peptides could only be found in the data set of de-novo identified peptides. The following spectra shows exemplary confirmed identifications of azidohomoalanine (labelled as small m) in the de-novo data set. A hit was considered a reliable identification of AHA when the following criteria were met by manual inspection of each spectra:

- Individual fragmentation on AHA, presence in the b- and y-ion series
- Local ALC >60 % (reliable) or >80% (very reliable) on AHA and on neighbouring residues
- Intensity of the corresponding fragment peaks
- Positioning in the peptide sequence (on the sides is considered less reliable)
- Combinations with the amino acids such as V, S, K, D are seen critically. C-terminal combination AHA + T + K or AHA + S + K are seen very often and considered unreliable

These criteria are clearly very strict, however necessary to reliably identify peptides containing AHA. All spectra were manually confirmed by Simon Nadal.

De-novo results for MAS samples

331 peptides could be found with an ALC >70% (found 3227 total, 926 peptides containing Met or AHA) and 119 with an ALC > 80% (found 1897 total, 420 peptides containing Met or AHA), or which 9 could be certainly confirmed by manual inspection (# 2842, 3983, 5091, 5643, 6865, 7986, 8086, 9810, 15697).

The de-novo results of ALC >80% improved (more identifications) in PEAKS 8.5 by increasing the Fragment mass accuracy to 0.05 Da. With 50ppm and 0.6Da accuracy, 166 peptides could be found with an ALC >70% (found 3799 total, 423 peptides containing Met or AHA) and 63 with an ALC > 80% (found 1069 total, 169 peptides containing Met or AHA). This confirms the need for de-novo sequencing of as high a resolution as possible to avoid any false-positives from occurring.

Figures 2.6 displays exemplary MS/MS spectra from MAS which contain AHA to a high degree of confidence.

0 10 20 30 40 50 60 70 80 90 (%)
Color code: >90% 80-90% 60-80% <60%

PNAGAGAVGM(-4.99)AASAGPGGYGPGQQGPGAAAAAAAAGR, #7986

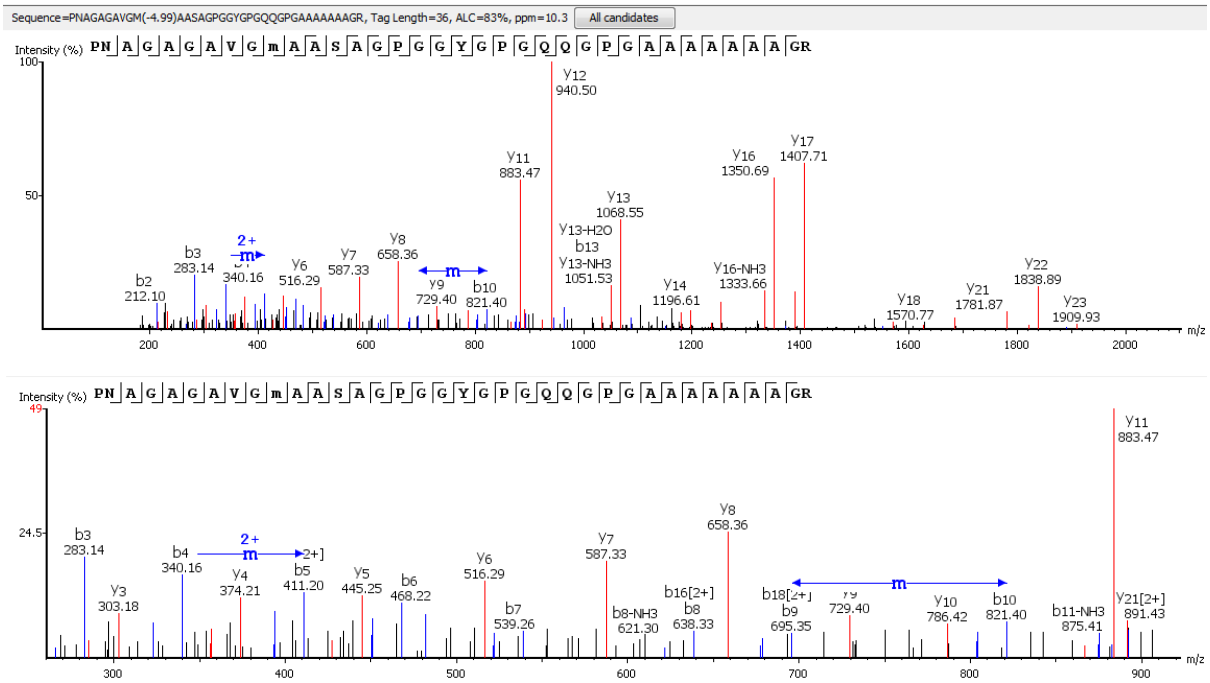

Figure 2.6: Examples of spectra that suggest the presence of AHA (designated as ‘m’) within the MAS peptides.

De-novo results for MiS samples

159 AHA-containing peptides could be found with an ALC >70% (found 2102 total, 756 peptides containing Met or AHA) and 48 with an ALC > 80% (found 1227 total, 321 peptides containing Met or AHA). Of the last set, 2 could be manually confirmed.

Figure 2.7 displays a spectra that shows confirmed identifications of azidohomoalanine (labelled as small m) in the de-novo data set (# 3279, 4614)

WMAATVM(-4.99)AR, #3279

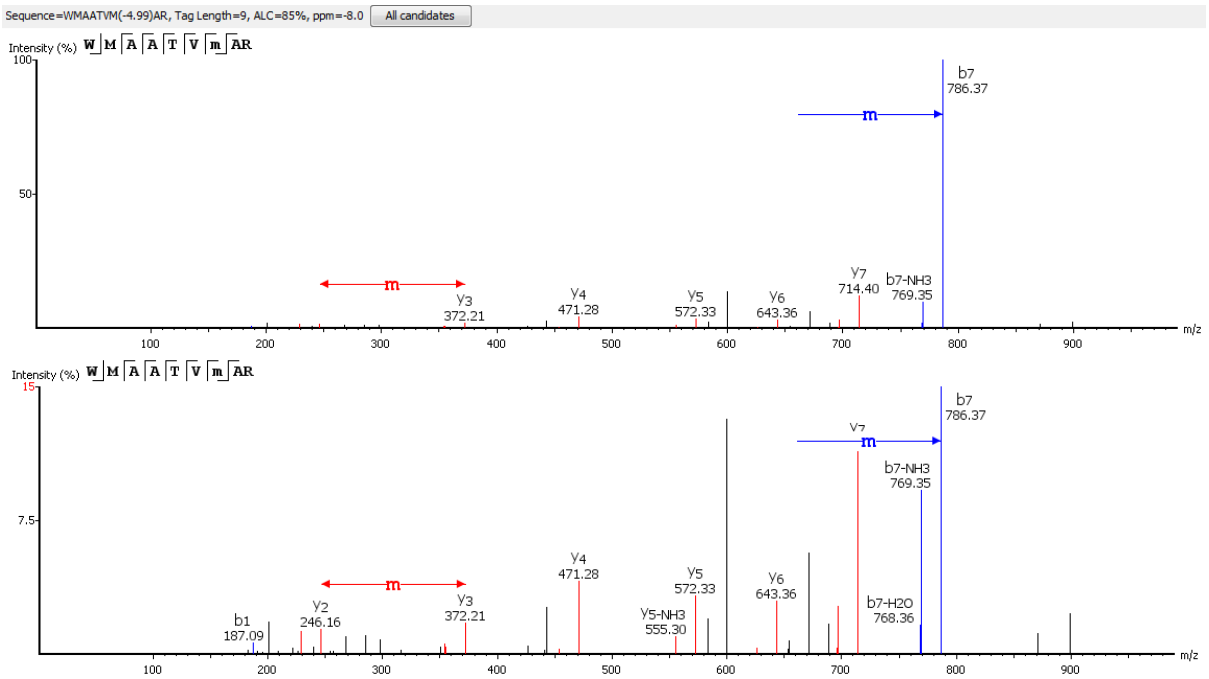

Figure 2.7: Examples of spectra that suggest the presence of AHA (designated as 'm') within the MiS peptides.

To date, bottom-up proteomics is one of the most sensitive methods for analysing proteins in their biological context. Nevertheless, the mass spectrometer still requires a population of identical peptides to be formed in order to observe their signal and acquire a tandem mass spectrum in the data-dependent acquisition mode. The unsupervised results suggested several peptide-spectrum matches that contain AHA, several of which could be manually validated despite the very stringent quality criteria that was applied. Taken together, this analysis suggests a trace level incorporation of AHA in spider silks.

3.5 Amino Acid Analysis (AAA) on spider silk samples

The decomposition of spider silks into their peptide components yielded promising results. As such, this logic was taken further and silks were hydrolysed to their constituent amino acids and analysed by a commercial service provider, Creative Proteomics.

However, Creative proteomics were not able to detect the presence of AHA within any of the samples. Additionally, they were not able to detect the presence of methionine within the samples either, which is a problem noted in previous work that attempt to detect Met through AAA as well[132–134]. Results containing the relevant spectra – as well as the procedure used – is in the Supporting Information (S2.2).

However, from literature as well as the results obtained from our proteomics and NMR experiments, we know that methionine is present within MAS silk proteins. This implies that that AAA – or at least the procedure and equipment used by Creative Proteomics – is not a sensitive enough technique for detecting Met or AHA in spider silk samples.

3.6 F-NMR spectroscopy

Analysis of the incorporation of AHA into spider silks is inherently restricted to conventional analytical methods described above. On the other hand, ^{19}F-labelled methionine is compatible with NMR spectroscopy, opening up new possibilities to track the incorporation of UAAs in spider silks.

Figure 2.8 presents the results obtained from the solid-state F-NMR experiments performed on MAS collected from spiders fed with triflourinated methionine.

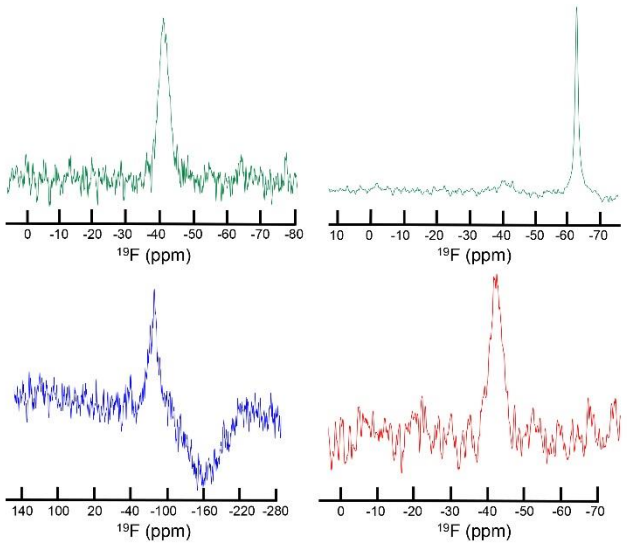

Top-left: MAS ^{19}F solid-state NMR with 30 kHz spinning for sample 1 obtained from $_{DL}$-($^{12}CF_3$)-trifluoromethionine.
Top-right: MAS ^{19}F solid-state NMR with 15 kHz spinning for sample 1 obtained from $_{DL}$-($^{12}CF_3$)-trifluoromethionine.
Bottom-left: MAS ^{19}F solid-state NMR with 15 kHz spinning for sample 2 obtained from $_{DL}$-($^{12}CF_3$)-trifluoromethionine.
Bottom-right: MAS ^{19}F solid-state NMR with 15 kHz spinning for sample 3 obtained from $_{DL}$-($^{13}CF_3$)-trifluoromethionine.

Figure 2.8: F-NMR spectra obtained from tested silk samples. Sample 1, 2 and 3 were obtained from N1, N2 and N3_CF_3 respectively, 15-20 days after the feeding regime. Control spectra were not displayed as there was no Fluorine signal obtained from the control samples. The fluorine signal is seen at -42ppm and -60ppm.

The peaks obtained are as one would expect from CF_3-Met in peptides (-42ppm in solution state). The solid-state NMR spectra obtained from the tested silk samples confirm the presence of CF_3-Met within the silk samples. No such signal was found in the control samples, thus eliminating the possibility of a false positive. This means we can safely assume that the $^{13}CF_3$-Met variant was successfully incorporated as well, since this would be the only

source of the signal in the sample. This result corroborates the previous findings obtained by proteomics on silks containing AHA, in that trace amounts of UAAs can be successfully incorporated into spidroins via feeding.

One of the tested samples displayed a peak at around -60ppm (Figure 2.8). We have several hypotheses as to why this is the case. Firstly, it is possible that the CF_3-Met within the peptide was oxidised; as mentioned before silk proteins tend to be post-translationally modified. Secondly, the chemical shift might be due to local flexibility of the CF_3-Met residue within the silk protein. Lastly, most of the CF_3-Met signal detected in that sample may be incorporated into different positions in the peptide chain, thus leading to a different chemical environment.

Furthermore, the position of the peaks suggest that it is highly unlikely that the CF_3-Met was converted into other amino-acids within the 20 day period. We hypothesise that this is because although natural methionine can act as a methyl group donor for other amino acids, the trifluorinated state of the methyl group in the CF_3-Met UAA may inhibit that process from occurring.

3.7 Click-chemistry on AHA silks

Another approach to expand the analytical possibilities for studying AHA incorporated into silks was to try a biorthogonal reaction of the azide moiety contained within AHA. Success in this approach would also open up many possibilities for functionalising silks in ways not possible before.

Unfortunately, both the control and the AHA fed spider silks fluoresced, with indiscernible levels of fluorescence between the two. It seemed that that Sulfo-Cy3-Alkyne fluorophore sticks too well to spider silks, so much so that the background fluorescence was too high for any signal from a click-reaction – if one had occurred – to be detected. This was despite vigorous washing of the two samples following the method outlined in the methods section.

4. Discussion and future work

This work proves that UAAs – both with chemical and structural changes – can be incorporated into spider silks via residue-specific incorporation. This is the first time that such a feat has been achieved and we believe this opens many avenues for the application of novel methods for studying silk protein structure and dynamics. The incorporation of $^{13}CF_3$ into silk proteins will allow 2D-NMR experiments to be performed. The Fluorine-Carbon correlation should allow researchers to decipher the structure and chemical environment around the targeted UAA as well as open the potential for monitoring dynamic structural changes within the protein by making use of the Nuclear Overhauser effect and by performing LIDOR experiments[92,93,135].

Temperature ramped NMR experiments can also be performed on silk dope which should theoretically allow researchers to monitor the polymerisation and fibrillation process of silk proteins as it occurs in real time, by monitoring signal changes in the NMR spectra over time. We tried performing such experiments in a pilot study by using standard silkworm dope and looking at the resulting T-ramped ^{1}H spectra (Supporting Information, S2.3). However, the signal-to-noise ratio obtained from the signals were far too low for any useful information to be deciphered.

As alluded to in the introduction, the successful incorporation of azido – or alkyne – UAAs will open up the possibility of functionalising silks with various cargo targets. This includes but is not limited to fluorophores, markers suitable for Mass Spectrometry, NMR probes, antibodies, pharmaceutical chemicals, and more. Consequently, such functionalised silks may be better suited for a variety of industrial or medical uses, as well as open opportunities for studying the structure and protein dynamics of altered silk proteins[66,70,89,119,136–138].

There are however gaps and challenges that I've identified in this chapter's work that needs to be addressed before such work can be done. First, the incorporation rate of the UAAs needs to be increased to yield a higher signal-to-noise ratio. Although my work has proven the presence of such UAA incorporation, the signal-to-noise (S/N) ratios remain too low for information regarding protein structure and dynamics to be reliably extracted. A high S/N would allow researchers to reliably determine the identity of neighbouring nuclei through the electro-magnetic interactions occurring between the target nuclei and its neighbours[50,55,94,135,139]. Increasing the incorporation rate by further modifying the feeding procedure, formulating a better artificial diet, or using genetically modified silkworms with amber-codon mutations[74,80,84,90] might enable such an increase.

Secondly, it would be ideal for the genome of *N.edulis* to be sequenced and readily available for use in proteomic studies. Due to the lack of a comprehensive sequence for *N.edulis*, our proteomic analyses had to be based on close relatives or performed de-novo. Being able to use the actual *N.edulis* sequence as a reference would not only save researchers a lot of time, but also increase our accuracy and confidence in making such analyses.

Lastly, follow up click-chemistry experiments need to be performed using different cargo-alkynes. Following the results of my click-chemistry reaction, I would recommend using a biotin-alkyne for the click-reaction, followed by both mass spectrometry and subsequent proteomic analysis, as well as Western blotting as tests to see if the reaction worked. This is important work to perform as it will allow researchers to functionalise silks in a myriad of ways should the reaction be successful and repeatable[66,72,73,89,116–119,123,138,140–143].

Acknowledgements

I thank Simon Nadal for helping me perform the Mass Spectrometry experiments on the AHA silk samples, for discussing and analysing the results from the proteomic analysis with me, and for providing lots of useful feedback during my write-up of this chapter. I thank Satoshi Kishigami for synthesising the trifluoro-methionine UAAs, for performing the solid-state F-NMR experiments, and for discussing and analysing the resultant NMR spectra.

Supporting Information

S2.1. Synthesis of DL-trifluoromethionine (Shibata's method)

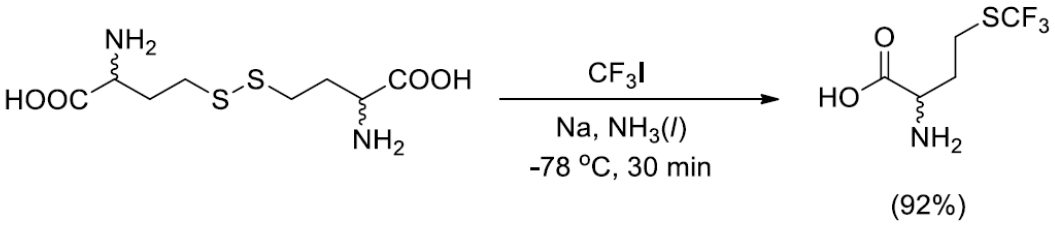

A 100 mL two-necked RB flask with a cold finger condenser attached was dried with a heat gun. DL-homocystine (1.0 g, 3.7 mmol) was added and dried under vacuum. The flask was cooled to -78°C by dry ice-acetone bath. Ammonia (~20 mL) was condensed to the flask through the cold finger to dissolve the powder under stirring. Sodium (0.36 g, 16 mmol) was cut into pieces and added to the solution until the solution turned deep blue. Trifluoromethyl iodide (0.76 mL, 9.3 mmol) was condensed through the cold finger and the reaction mixture was stirred at -78°C for 30 min. The flask was removed from the dry ice-acetone bath and the ammonia was left to evaporate. The resulting residue was dissolved in H2O (30 mL) and acidified by DOWEX® 50WX8 (H+) 100-200 until pH ≈ 2. The resulting suspension was loaded onto an ion exchange column (DOWEX® 50WX8 (H+) 100-200). The column was prewashed with H2O until the solution was neutral. The product was eluted by 0.5% NH4OH (aq). Fractions containing the product were combined and evaporated under vacuum, followed by freeze-drying to give the product as a white powder (1.4 g, 92%); Rf (3:1:1 EtOAc/AcOH/H2O v/v/v) = 0.52; 1 H NMR (400 MHz, D2O) δ = 2.23 (m, 2H, Hβ), 3.06 (m, 2H, Hγ), 3.78 (t, J 6.44, 1H, Hα); 13C NMR (100 MHz, D2O) δ = 25.42 (Cγ), 31.36 (Cβ), 53.50 (Cα), 129.89 (q, J 328.97, CF3), 174.25 (COOH); 19F NMR (375 MHz, D2O) δ = -41.18 (CF3); LRMS m/z (ESI+): measured: 204.1 (M + H+), calculated: 204.0306; IR: 2945, 2558, 2144, 1617, 1587, 1504, 1452, 1411, 1348, 1319, 1277, 1255, 1160, 1096 cm^{-1}.

S2.2. Amino Acid Analysis report and procedure from Creative Proteomics

Creative Proteomics
45-1 Ramsey Road, Shirley, NY 11967, USA
Tel: 1-631-275-3058 Fax: 1-631-614-7828
www.creative-proteomics.com
info@creative-proteomics.com

Analysis Report

Project Name	Targeted Metabolomics Analysis (Azidohomoalanine)
Sample Description	Silk
Sample Quantity	4
Order Number	CPMT02071902
Client	
Project Date	*2019-08*
Remark	

Part 1 Sample Preparation

1.1 Samples and Groups

4 silk samples for quantitative measurement of hydrolyzed amino acids in the collected samples, amino acids are quantified using a shimadzu LC20AD - API 3200MD TRAP HPLC- MS/MS.
Name: S1; S2; S3; S4.

1.2 Parameters

(1) MS parameters:
Ion source: +ESI, positive ion
Ion source temperature: 550°C
CUR: 20 psi
IS: +5500V
GS1: 50 psi
GS2: 60 psi

(2) LC parameters:
Column: MSLab 45+AA C18 15 cm×4.6 mm×5 μm column
Flow rate: 1.0 mL/min
Injection volume: 10 μL
Column temperature: 50°C
Mobile phase A: Pure water (1‰ formic acid); Mobile phase B: Acetonitrile (1‰ formic acid)

Time (min)	A (%)	B (%)
0.00	95	5
0.01	95	5
0.05	80	20
4.00	80	20
4.01	10	90
6.00	10	90
6.01	95	5
9.00	95	5

1.3 Analytical Procedures

(1) Add 6 mol/L HCl to the sample, fill N_2 to protect the environment.

(2) Seal up, digest for 21 h at 110°C.

(3) Transfer 100 μL digestion and enrich it to 20 μL, add 980 μL of water.

(4) Add 150 μL deproteinization reagent (methanol) and standard (100 ng/mL) to 50 μL sample.

(5) Cool, mix and vortex at 13200 rpm for 4 min.

(6) Transfer 50 μL for analysis.

Part 2 Analytical Results

2.1 Chromatograms

Standard (100 ng/mL)

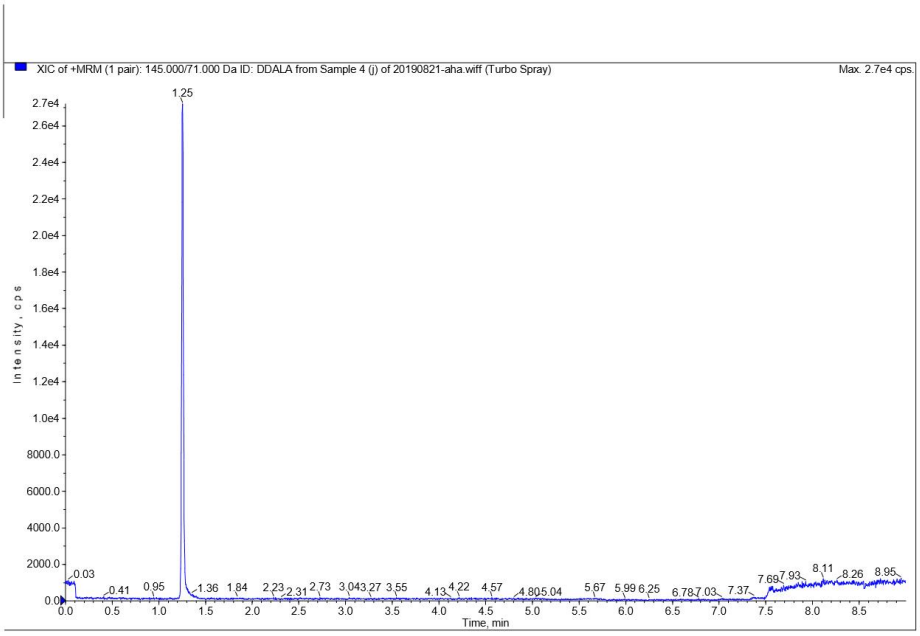

S1

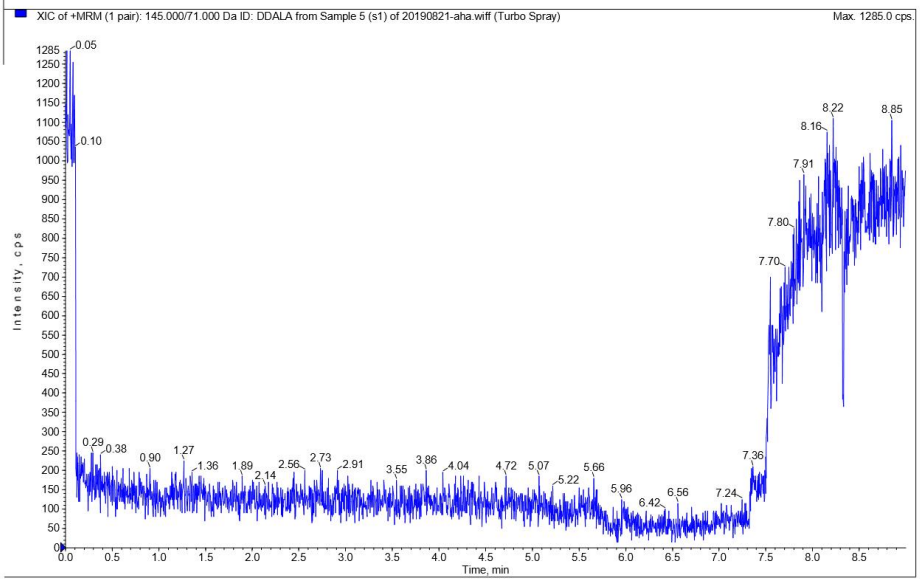
XIC of +MRM (1 pair): 145.000/71.000 Da ID: DDALA from Sample 5 (s1) of 20190821-aha.wiff (Turbo Spray)
Max. 1285.0 cps.
Intensity, cps
Time, min
0.05
0.10
0.29
0.38
0.90
1.27
1.36
1.89
2.14
2.56
2.73
2.91
3.55
3.86
4.04
4.72
5.07
5.22
5.66
5.96
6.42
6.56
7.24
7.36
7.70
7.80
7.91
8.16
8.22
8.85

S2

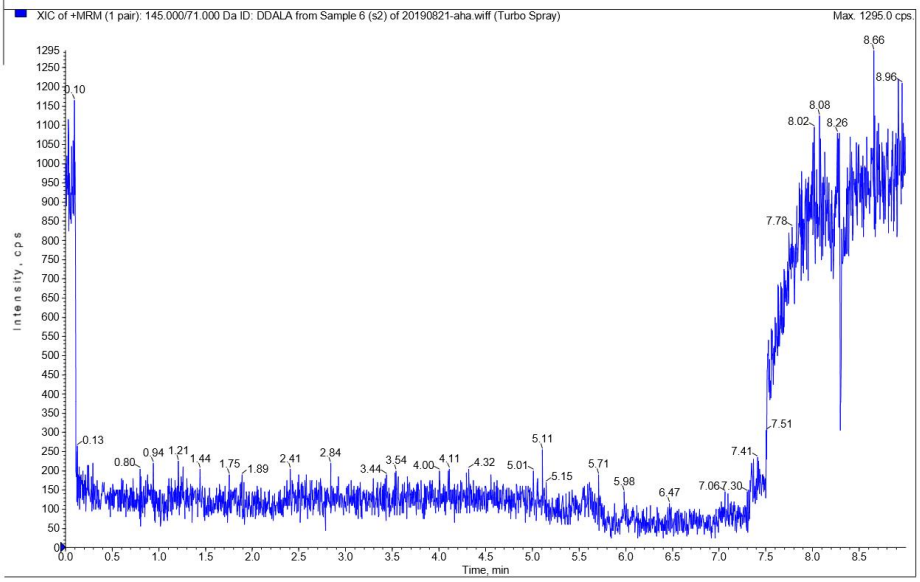
XIC of +MRM (1 pair): 145.000/71.000 Da ID: DDALA from Sample 6 (s2) of 20190821-aha.wiff (Turbo Spray)
Max. 1295.0 cps.
Intensity, cps
Time, min
0.10
0.13
0.80
0.94
1.21
1.44
1.75
1.89
2.41
2.84
3.44
3.54
4.00
4.11
4.32
5.01
5.11
5.15
5.71
5.98
6.47
7.06
7.30
7.41
7.51
7.78
8.02
8.08
8.26
8.66
8.96

S3

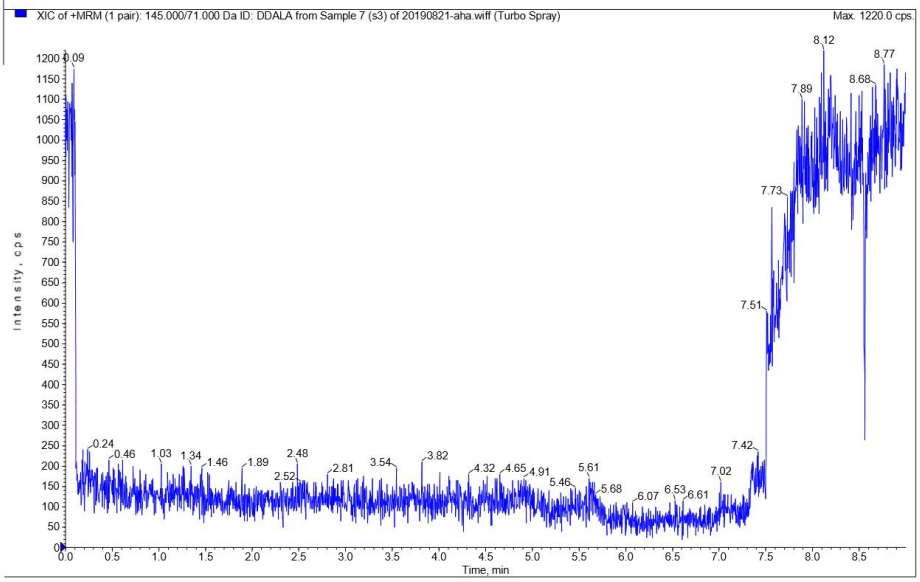
XIC of +MRM (1 pair): 145.000/71.000 Da ID: DDALA from Sample 7 (s3) of 20190821-aha.wiff (Turbo Spray)
Max. 1220.0 cps.
Intensity, cps
Time, min
0.09
0.24
0.46
1.03
1.34
1.46
1.89
2.48
2.52
2.81
3.54
3.82
4.32
4.65
4.91
5.46
5.61
5.68
6.07
6.53
6.61
7.02
7.42
7.51
7.73
7.89
8.12
8.68
8.77

S4

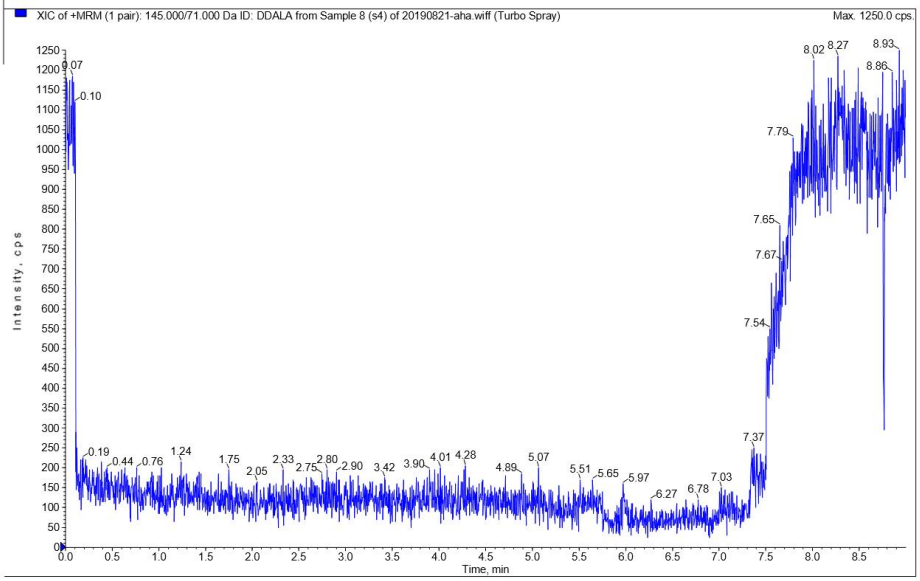

2.2 Calculation Results

No azidohomoalanine was detected in the samples.

A2. AAA of silk samples for presence of Methionine

Creative Proteomics
45-1 Ramsey Road, Shirley, NY 11967, USA
Tel: 1-631-275-3058 Fax: 1-631-614-7828
www.creative-proteomics.com
info@creative-proteomics.com

Analysis Report

Project Name	Targeted Metabolomics Analysis (Methionine)
Sample Description	Solution
Sample Quantity	4
Order Number	CPMT02071902-02
Client	
Project Date	*2019-10*
Remark	

Part 1 Sample Preparation

1.1 Samples and Groups

4 solution samples for quantitative measurement of hydrolyzed amino acids in the collected samples, amino acids are quantified using a shimadzu LC20AD - API 3200MD TRAP HPLC- MS/MS.
Name: S1; S2; S3; S4.

1.2 Parameters

(1) MS parameters:
Ion source: +ESI, positive ion
Ion source temperature: 550°C
CUR: 20 psi
IS: +5500V
GS1: 50 psi
GS2: 60 psi

(2) LC parameters:
Column: MSLab 45+AA C18 15 cm×4.6 mm×5 μm column
Flow rate: 1.0 mL/min
Injection volume: 10 μL
Column temperature: 50°C
Mobile phase A: Pure water (1‰ formic acid); Mobile phase B: Acetonitrile (1‰ formic acid)

Time (min)	A (%)	B (%)
0.00	95	5
0.01	95	5
0.05	80	20
4.00	80	20
4.01	10	90
6.00	10	90
6.01	95	5
9.00	95	5

1.3 Analytical Procedures

50 μL of the solution was injected for analysis.

Part 2 Analytical Results

2.1 Chromatograms

Standard (100 μmol/L)

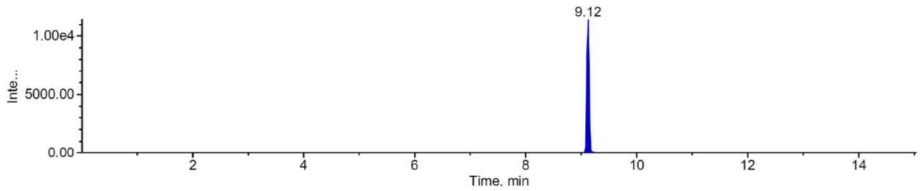

S1

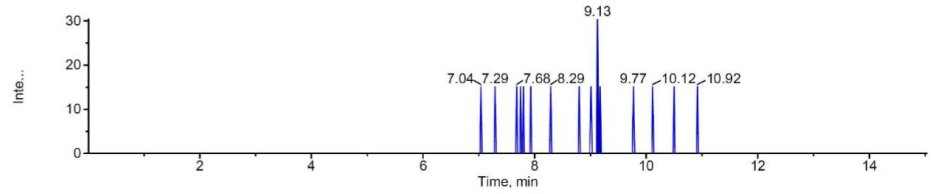

S2

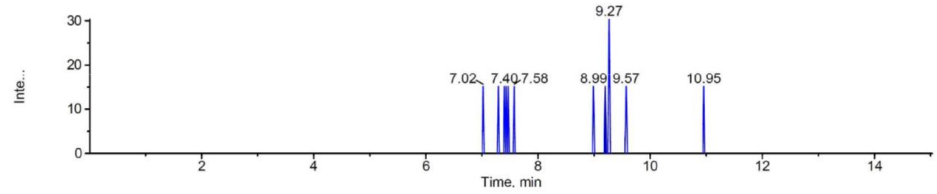

S3

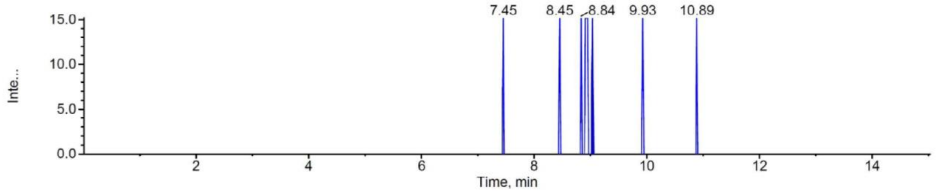

S4

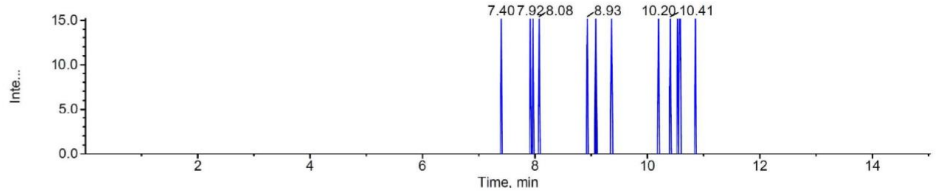

2.2 Calculation Results

No methionine was detected in the samples.

S2.3. Pilot experiment: Solution state NMR on silkworm dope

Silkworm dope was extracted from Vth instar silkworms using methods detailed elsewhere (Frydrych, Greenhalgh, Vollrath, 2019). **N.B. These worms have been stored in a fridge at 4 Celcius for a week beforehand due to timing issues. As a result, the silk will not be as pristine as silks harvested from 'fresh' silkworms.**

The resulting silk dope was carefully injected into a NMR tube. A temperature ramp was applied and 1D H-spectra for the sample were obtained at 25°C, 40°C, 50°C and 60°C. At each designated temperature, the sample was left to equilibrate for 30mins. After obtaining the spectra at 60°C, the sample was allowed to cool back down to 25°C, before another H-spectra was obtained. The result is shown below, with each coloured line representing an independent run:

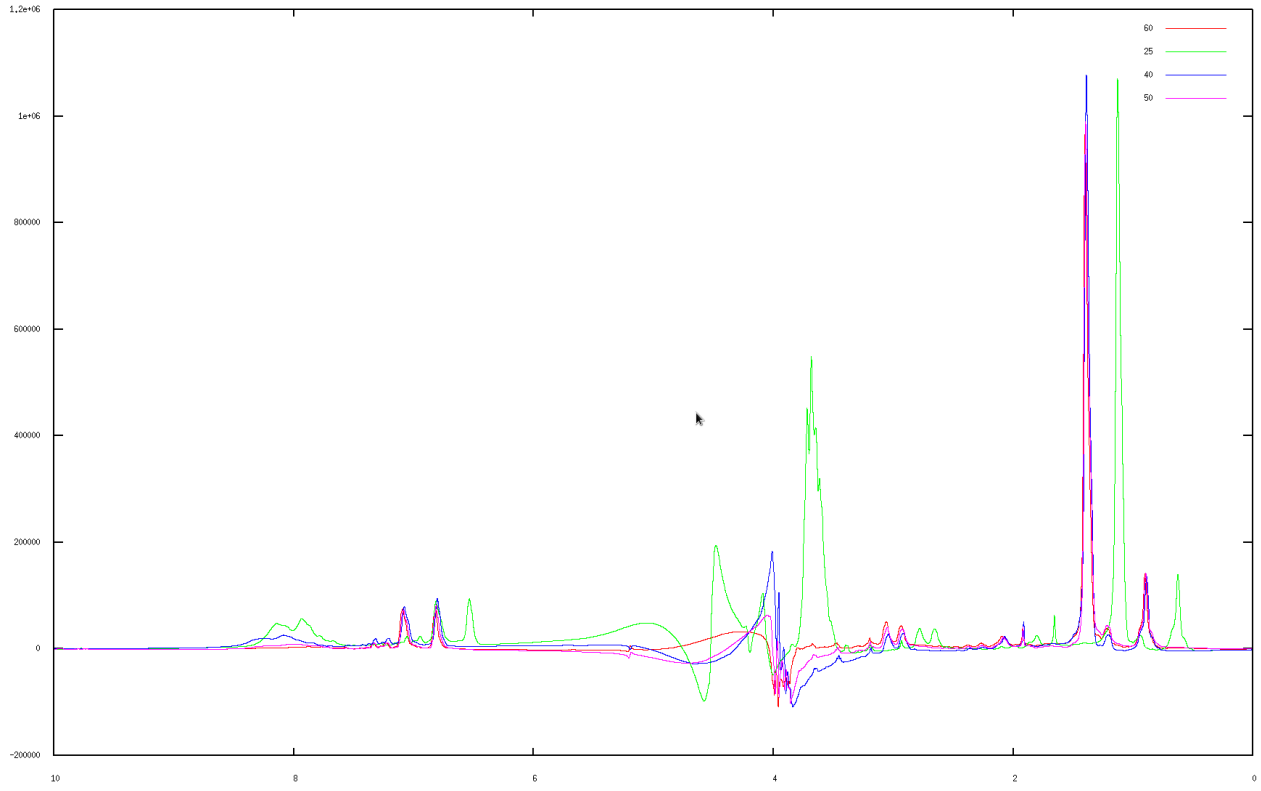

From the results, we can see that the H-spectra is largely dominated by the signal from Alanine residues within silks, with several aromatic Hydrogens being displayed as well. It seems that raising the temperature does not significantly change the spectra; this implies that either the sample has already gelled/undergone a transition prior to testing, or that conditions within the sample (e.g. concentration might be too high) might not be suitable to allow for transitions to occur.

We also performed diffusion gradient experiments on the sample at 25°C. Signals were still obtained despite a very strong gradient being applied, implying that the molecules within the sample are massive and do not move very much. This could be further support for the idea that the silk has already undergone partial transition before the sample was tested.

Chapter 3: Incorporation of fluorophore dyes into spider and silkworm silks

1. Introduction

Silks have long been lauded for their impressive combination of strength, toughness and flexibility [4,43,144], a triad of properties rarely attainable in both natural and synthetic polymers. Several decades worth of research have revealed a myriad of factors that contribute to the mechanical properties of silks: hierarchy from the nanoscale [41,45,145], highly-ordered crystalline structures interspersed within a matrix of less-ordered 'amorphous' regions [44,146], a variety of molecular motifs conferring different properties to the fibre [29] to name a few. Due to its highly complicated nature, various techniques are required to study the different aspects of silk structure. Among them include X-ray Diffraction [147,148], Fourier Transformed Infrared Spectroscopy [149–151], Raman Spectroscopy [28,152,153], Nuclear Magnetic Resonance [30,47,48,53] and Neutron Scattering [154]. Nevertheless, gaps remain in our knowledge regarding silk structure – specifically in our knowledge of the non-crystalline regions and the spatial-relationship between the crystalline and non-crystalline regions – and researchers are constantly in search of novel techniques to unravel silk's mysteries.

Fluorescence microscopy has been employed as a technique for studying cell biology for little over a century [155]. Among its uses are to identify structures within cells, studying protein dynamics, and to follow synthetic pathways of proteins of interest[156–160]. In the past two decades or so, newer techniques including STORM, PALM, STED [161] – in combination with suitable fluorescent dyes [162] – have allowed researchers to surpass the resolution previously imposed by the diffraction limit of visible light, enabling them to obtain fluorescent images with micron-level - or even sub-micron [156] – resolution. Only recently has there been some interest in inserting fluorescent dyes into silkworm silks with the goal of

discovering new methods for dying silks. Example of works include feeding Rhodamine based dyes to silkworms[99,100], genetically modifying silkworms to express silk proteins containing fluorescent proteins [163] and feeding fluorescent carbon nanodots to silkworms[164]. There are several potential advantages that fluorescence microscopy has over previous techniques that have been used in the past to study silks; the most prominent being that it is potentially less laborious to prepare samples for analysis, it is a spatially-resolved (as opposed to bulk-averaging), and there is no need for long range periodicity of motifs in order to obtain images, potentially allowing us to study structures in the elusive 'amorphous' regions.

Despite the recent interest, the previous works mentioned do not emphasize using fluorescence as a method for further probing structure; rather they focus more on the industrial applications of fluorescent silks. Given that this field is so new, there is also a need to replicate the work to ensure that the insertion of fluorescent dyes into silks is easily replicable across different labs. Additionally, there has been no work done on spider silks, which is arguably of more interest as a model-biomaterial compared to silkworm silks due to its superior mechanical properties. The lack of focus on spider silks is understandable; at the time of writing there are no viable methods for genetically modifying spiders and dying spider silks externally is difficult since spider silks are sensitive to external conditions and treatments. In particular, spider silks will supercontract when exposed to water, subsequently altering the structure of the native spider silk fibres, though this process is reversible[35,165–167]. Ideally, we would aim to dye spider silks in a manner that maintains their native state for study.

I will experimentally test the viability of feeding Rhodamine B (RhB) to spiders and silkworms as a method for dying their silks. Rhodamine B is chosen as my dye of choice as

its spectral properties are well known, it has been shown to go into silkworm silks via feeding with purportedly little to no effect on the behavior and growth of the silkworms, is easily obtainable and soluble in water. I will then test the effects of RhB on the mechanical properties of spider silks. I will also analyse the fluorescence spectra of RhB within spider and silkworm silks to see if there are any results of interest – such as whether the fluorophores display interactions with the silk motifs or whether there are patterned in a specific manner – and whether we can utilize the fluorescence of RhB within silks to unpick details regarding silks' structure, both crystalline and non-crystalline. Finally, I will try feeding spiders with dyes suitable for super-resolution fluorescence microscopy, as their inclusion may allow researchers to utilize techniques such as PALM or STORM for studying the structure of spider silks with potentially nanoscale spatial-resolution[156–158,162].

2. Materials and Methods

2.1 Chemicals

Rhodamine B (95%), Alexa488-NHS ester and Sypro® Orange was obtained from Sigma-Aldrich and used without further purification. ATTO488-COOH was obtained from ATTO-TEC GmbH and used without further purification. Structures of RhB and ATTO488-COOH can be found in Figure 3.1.

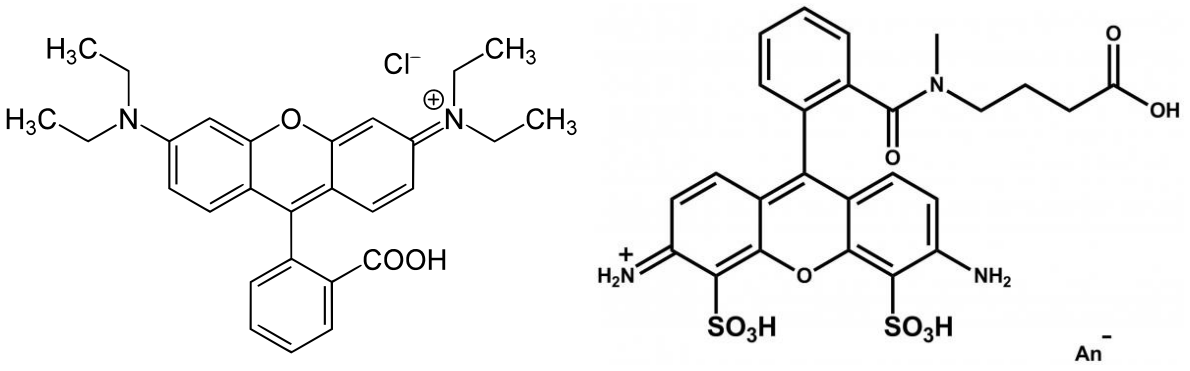

Figure 3.1: Left: Structure of Rhodamine B. Right: Structure of ATTO488-COOH.

2.2 Preparation of silkworm feed

Silkworm feed was obtained as a hydrated paste from the silkworm supplier (CREA-API Unità di Ricerca di Apicoltura e Bachicoltura). Modified feed was prepared by thoroughly mixing Rhodamine B into the feed.

2.3 Culturing of silkworms

Bombyx mori silkworms in their V^{th} instar were obtained from a supplier (CREA-API Unità di Ricerca di Apicoltura e Bachicoltura) and initially cultured on normal silkworm feed. On specific days of the V^{th} instar, a random group of silkworms were transitioned to the modified feed. The rest were cultured on normal feed until they begun spinning cocoons to act as a control.

The growth, weight and behaviour of the silkworms were recorded daily to see if they differed from the control treatment. The designations of silkworm batches, the concentration of the feed used, and the day in which a random group of silkworms were transitioned to the RhB feed is shown in Table 3.1.

Silkworm batch	Sample size in the control group	Sample size in the treatment group	Day of initial RhB feeding from day 0 of their V^{th} instar	RhB concentration
Apr2017	100	105	4	0.04wt%
May2017	88	70	2	0.01wt%
Jun2017	90	70	1	0.01wt%

Table 3.1: Information related to silkworms from different experimental batches. 0.04wt% was used as that was close to the concentration used in past literature[100,168]. 0.01wt% was used as a safer, more conservative feeding regime.

2.4 Sample collection and processing

Cocoons spun by the silkworms were collected and kept in a freezer at -4°C until analysis. Cocoons were divided into three layers: an outer layer, a middle layer and an inner layer. This was done by carefully separating the cocoon layers with tweezers.

To obtain liquid silk dope, silkworms were dissected to collect their silk glands. Silkworms that have just begun spinning cocoons were selected and dissected by decapitation in a Petri dish filled with type I water. The silk glands were carefully extracted and cleaned in type I water. Subsequently, the posterior and anterior sections of the silk glands were cut off using a scalpel, leaving the middle (storage) section of the silk gland which was then drained into a container containing an extraction buffer which consisted of 10mM of Ammonium Acetate (pH adjusted to 7.3 using 1% NH_4OH). The container with the silk glands was then covered with cling film and kept in the fridge overnight at 4˚C. After leaving it overnight, excess extraction buffer and solubilised sericin was removed using a 3mL Pasteur pipette. The removal of excess buffer was done slowly and with care to prevent shearing of the sample. Subsequently, the Native Silk Fibroin (NSF) was filtered using a fine nylon mesh to remove any excess epithelium and any converted silk. The NSF is then stored in the fridge at 4˚C for up to 4 days. Some normal NSF was doped with 0.01wt% RhB; the purpose of this was to see whether the process of doping the silk outside of the worm makes a difference to the mechanical properties of the silks compared to silks doped with RhB via feeding. The NSF is then spun into artificial fibres using a custom rig. Figure 3.2 shows silkworm cocoons dyed with RhB, as well as fibres spun from NSF.

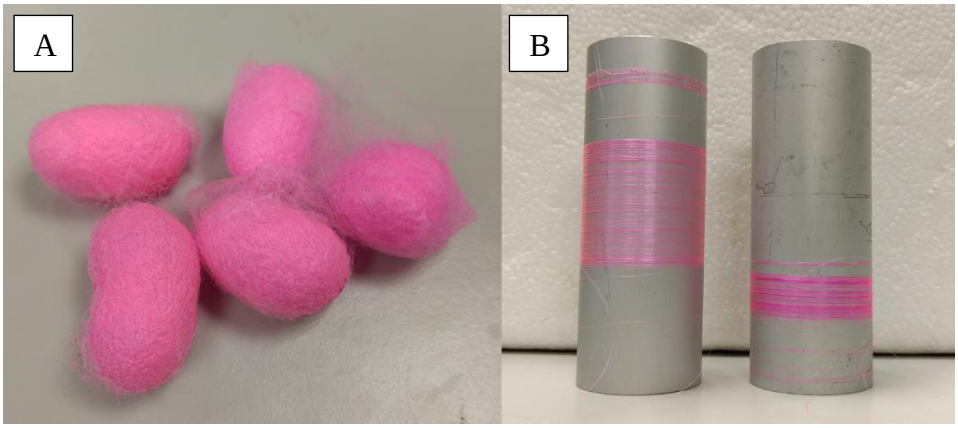

Figure 3.2**: (**A) Cocoons collected from worms fed with 0.5mg RhB per 1g of feed. (B) Left: Artificial fibres spun from silk collected from worms that were fed RhB. Right: Artificial fibres spun from NSF that was doped with RhB during the NSF processing step.

2.5 Differential Scanning Fluorimetry on silkworm silk dope

2mg of 2% Sypro Orange was diluted with 98µL of Type I dH_2O. 5µL of the diluted Sypro Orange was aliquoted into 0.2mL Eppendorf tubes. Subsequently, 20µL of RhB NSF extracted from silkworms fed with 0.01wt% RhB feed was aliquoted into the Eppendorf tubes. The tubes were then inverted multiple times to allow the sample to mix with the Sypro Orange.

All samples were measured in 0.2 ml Eppendorf tubes on the Rotor-Gene Q real-time PCR by Quiagen (www.quiagen.com) using the following temperature program (i) hold at 25°C for 7 minutes (ii) ramp from 25°C to 95°C in 0.4°C steps (hold for 10 Seconds at each step). Each measuring step lasted 30 seconds. The Eppendorfs were always closed and positioned as soon as samples had been prepared in order to minimize evaporation. The nature of the measurement (rapid spinning generating centripetal forces) minimizes the possibility of bubble formation during a temperature ramp and the sealed Eppendorfs prevent evaporation from the sample as the temperature is raised.

2.6 Handling of spiders and silk collection

Nephila edulis were used as the organism of choice due to their availability and ease of handling their silks. Individual spiders were placed on polystyrene platforms and held in place with a mesh, which contained a hole where the spinnerets of the spiders were exposed. The spiders were then examined under a dissection microscope to identify the location of the different spinnerets. Individual silk fibres were then pulled from the Major Ampullate spinneret onto a calibrated motorized spool. Major Ampullate Silk (MAS) was reeled as single fibres at a rate of 20mm s^{-1}, 30mm s^{-1}, and 40mm s^{-1} for tensile testing; these reeling speeds conform to natural reeling speeds of spiders in natural conditions [169,170]. The temperature and humidity of the reeling conditions were recorded for each reeling session. Silk at the very start of the reeling procedure was not used. Collected samples were stored on spool segments under lab conditions (20°C, 40% RH).

Spiders were reeled prior to any treatment with fluorescent dye solutions; these samples served as controls for the experiment. Spiders were then fed up to 40µL of dye solution daily using a P20 Gilson Pipette. The types of dye solution fed to each spider is listed in Table 3.2. The spiders were reeled 5 days after daily feeding of the solution. In addition, webs were collected for study if the spiders built any during the 5 day period.

Spider	Treatment	Reeling speed (mm s^{-1})
N0_RhB	0.025wt% RhB + 0.25% Sucrose	20
N1_RhB	0.01wt% RhB + 0.5% Sucrose	20
N2_RhB	0.01wt% RhB + 0.5% Sucrose	20
N3_RhB	0.025% RhB + 0.5% Sucrose	20, 30, 40
N4_RhB	0.025% RhB + 0.5% Sucrose	20, 30, 40
N5_RhB	0.05% RhB + 0.5% Sucrose	20
N6_RhB	0.01% RhB + 0.5% Sucrose	20
N7_RhB	0.05% RhB + 0.5% Sucrose	20
N8_RhB	0.025% RhB + 0.5% Sucrose	20
N9_RhB	0.05% RhB + 0.5% Sucrose	20
N1_ATTO488	0.52 mM ATTO488-COOH + 0.5% Sucrose	20
N2_ATTO488	0.52 mM ATTO488-COOH + 0.5% Sucrose	20
N3_ATTO488	0.52 mM ATTO488-COOH + 0.5% Sucrose	20
N1_Alexa488	0.52 mM Alexa488-NHS ester + 0.5% Sucrose	20
N2_Alexa488	0.52 mM Alexa488-NHS ester + 0.5% Sucrose	20

Table 3.2: List of spiders and the respective treatments. 0.52 mM is the molarity of a 0.025 wt% RhB solution. 0.05wt% was used as that was close to the concentration used in past literature[100,168] . 0.01wt% and 0.025wt% were used as safer, more conservative doses to see the effect of RhB concentration on spider behaviour and silk properties.

2.7 Cross-sectional Area Measurement

CSA information is necessary to calculate the mechanical property parameters of interest from silks.

The artificial silkworm fibres produced in this project were embedded in a plastic resin, then cut on both ends. The resin was then mounted onto SEM stubs and then sputter coated with gold/palladium metal for 150 seconds at 18 mA. They were then viewed using a Jeol Neoscope JCM-5000 SEM to visualize the fibres. Images of the fibres were taken using the SEM, which were then subsequently analysed using ImageJ to obtain the cross-sectional areas of the fibres.

Cardboard frames containing single MAS fibres were mounted onto SEM stubs with conductive tape. Samples were then sputter coated with gold/palladium metal for 150 seconds at 18 mA, giving the samples a coating of 12.5nm (Quorum Technologies SC7620). Samples

were then viewed using a Jeol Neoscope JCM-5000 SEM. Images of the fibres were taken using the SEM, which were then subsequently analysed using ImageJ to obtain the diameters of the fibres. For each treatment group, 6 fibres were measured, with 3 measurements made per fibre. The results were then averaged to obtain an average diameter. Individual MAS fibres were observed to be cyllindrical and the cross-sectional area was calculated using the formula:

$$A = \pi \left(\frac{d}{2}\right)^2$$

2.8 Tensile Testing & Statistical testing

All tensile tests were performed on a Zwick ZwickiLine Z0.5 which is equipped with a 5N load cell.

Single silk fibres were mounted onto individual 15 mm cardboard frame with an aperture of 10.4mm x 5mm.. The sides of the frames were then cut and removed, allowing the force to go through the fibre during testing. Slack was then introduced to the fibres to remove any pre-tension that might have originated from the reeling or mounting procedures. The fibres were tested at a strain rate of 20% strain/min. The temperature and humidity of testing conditions were always recorded.

To reduce the effects of intrinsic factors on the tests, all control and treatment samples from the same spider were always tested on the same day, and samples were never tested when the temperature and humidity of the testing conditions exceeded critical values known to trigger a glass transition in silks [35].

Stress-strain profiles from individual fibres were obtained and summarized in Microsoft Excel. Parameters of interest – Young's Modulus, strain at break, and toughness (energy

absorbed before total failure) – were obtained from the data. The data was then exported as CSV files for statistical analysis using R.

A linear mixed-effect model with random intercepts was applied to the datasets. 'Treatment' (i.e. the presence of RhB within silks) was taken to be the fixed effect of interest, whereas individual spiders were considered a random effect in the model. This allows the model to account for intraspecific variation within the dataset. The Welch-Satterthwaite equation was applied as a test to determine if there are any statistically significant differences in the results. Assumptions of normality, independence of samples, and equal variances of residues were tested and met.

2.9 Fluorescence imaging

Silkworm cocoon segments were mounted onto glass slides and imaged using a Leica DMi 8 Fluorescence Optical microscope. Fibres were excited using a 488nm and 540nm laser and the resulting image was recorded.

Fluorescence imaging was also used to determine the presence of fluorescent dyes in spider silk samples, as the fibres were too thin to determine any presence of the dyes with the naked eye. Silk fibres that were mounted onto glass slides were either imaged using an Olympus FV3000 confocal fluorescence microscope, or a Leica SP8. In the case of the images recorded using the Leica SP8, the emission spectra were recorded with time gating to remove Raman scattering produced by the crystalline regions within the protein core. The images were then analysed using ImageJ with an OlympusViewer plugin to obtain the fluorescence spectra of the fibres.

2.10 Two-Photon Excitation Polarisation under different strains

Changes in fluorescence signal as a function of the polarization angle of the excitation light were measured using a custom-built two-photon fluorescence microscope as described here 163.

Samples were excited in the two-photon mode at 780 nm using a Ti:Sa laser (HP Mai Tai DeepSee, Spectra Physics, Mountain View, CA). The laser power is controlled using a motorized half-wave plate together with a polarizer. The objective used was a CFI S Plan Fluor ELWD 40× objective (NA = 0.6) (Nikon).

Before passing through the objective, the excitation light passes through a rotatable half-wave plate to control the polarization angle (ϕ) of the light. After each image is collected, the half-wave plate rotates 10° corresponding to a 20° rotation of the polarization of the light. The angle at which the light is polarized parallel and perpendicular to the stage is found.

The sample is then imaged 19 times – corresponding to a complete rotation of 360° – of the excitation light. These images show the intensity of the autofluorescence as a function of the polarization angle of the excitation light.

The resulting fluorescence signal is passed through a tube lens and a 525 ± 25 nm bandpass filter (Semrock) before entering a Hamamatsu H7422P-40 photomultiplier. After acquiring intensity images of the autofluorescence, the images were computed with SimFCS software.

The sample was imaged at different strain values. To achieve this, samples were mounted on a custom-built force pulley that could be mounted on the microscope. A miniature linear actuator – with 60 mm of travel (TLA60A-S, Zaber Technologies Inc. Vancouver, Canada) – pushes a TSB60M translation stage, 60 mm travel (Zaber Technologies Inc.Vancouver, Canada), which in turn pulls on the end of the fiber. The other end is fixed to a UF1 isometric force sensor, 0−50 g (Applied Measurements Ltd., Mercury House Calleva Park,

Aldermaston, Berkshire, U.K.), which measures the force exerted by the fiber upon elongation. The force pulley is controlled via LabVIEW using an NI USB card NI USB-6211. The force pulley was then set to pull the fiber at a constant speed of 0.05 mm/s.

For each strain value, the intensity of fluorescence as a function of polarization angle is measured at three different locations on a single fiber. This is then repeated for different fibers. For each fiber, the mean autofluorescence intensity per area is found for each strain value. The total mean autofluorescence intensity is then found for all fibers at each strain value. These are then plotted as a function of the polarization angle of excitation light. The entire setup is described in Figure 3.3.

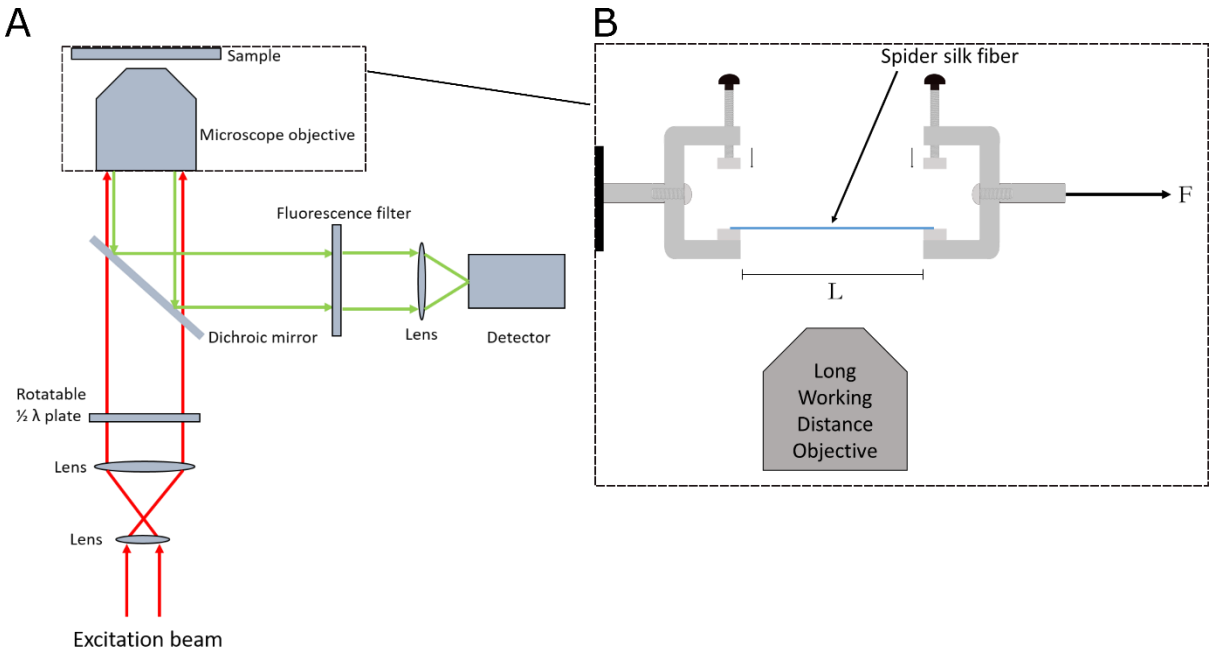

Figure 3.3: Microscopy set-up for two-photon polarization measurements in strain-induced fibres. Adapted with permission from [172].

3. Results

3.1 Presence of RhB in silkworms, spiders and their silks

Detection of RhB within silkworms is straightforward: the silkworms take on a pink colouration a few hours after ingesting the RhB feed (Figure 3.4). Dissection of the silkworms reveal that the RhB enters the majority of organs within the silkworm albeit to different extents (Figure 3.5). The silks spun by these silkworms are also pink in colour (Figure 3.6) and fluoresce when excited by lasers or lights with an excitation wavelength between 450nm – 540nm (Figure 3.6).

Figure 3.4: Left: Silkworms prior to ingesting the RhB doped feed. Right: Silkworms after a day of ingesting the RhB feed.

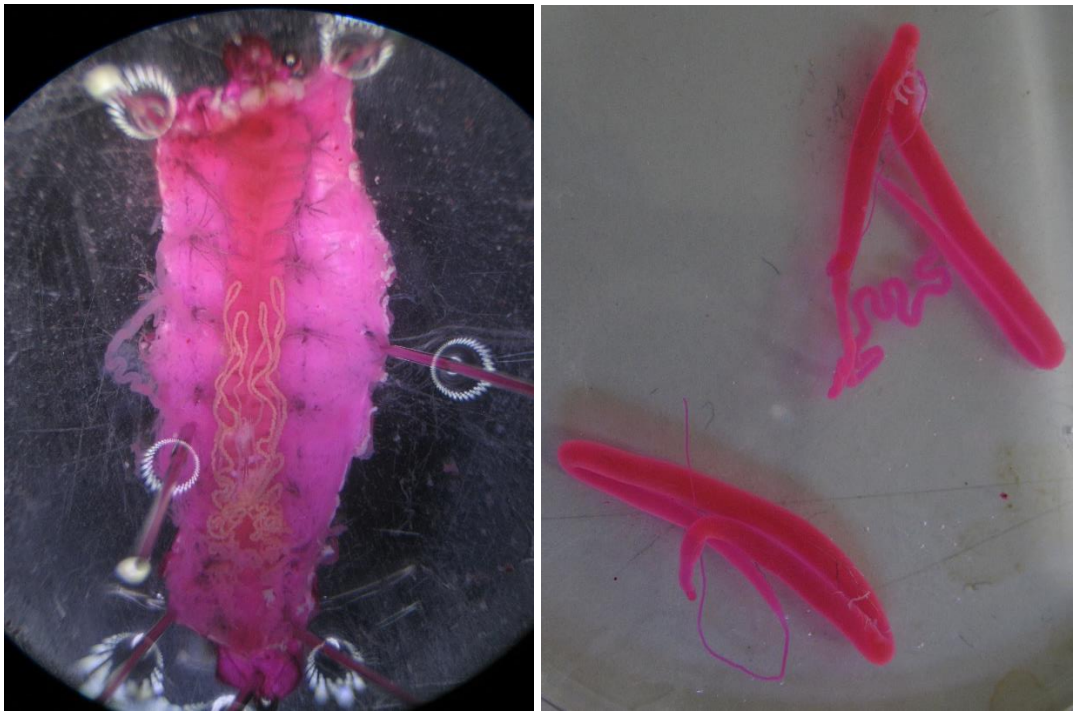

Figure 3.5: Left: Dissected silkworm – silk glands removed - after 1 day of ingesting RhB feed. Right: Dissected silkworm glands after a day of ingesting RhB feed.

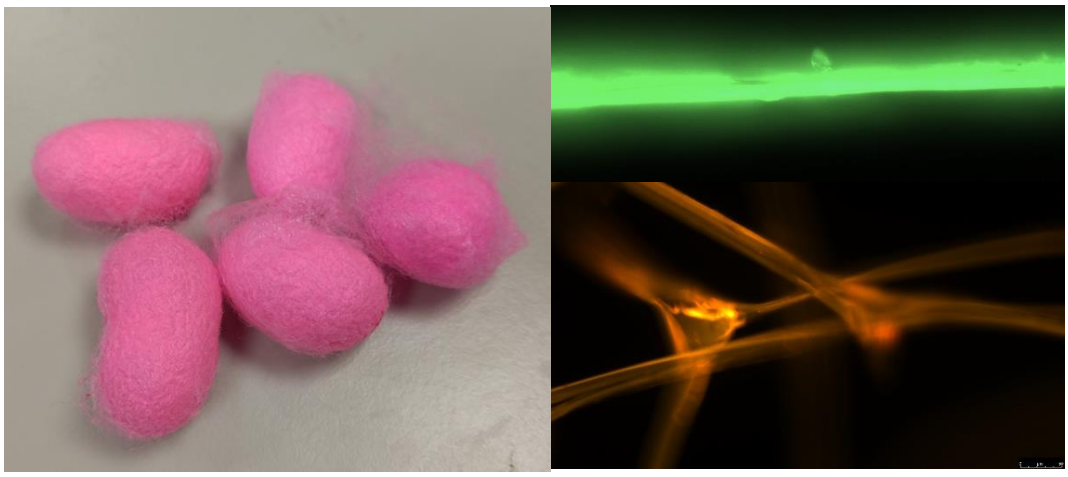

Figure 3.6: Left: Silkworm cocoons spun by silkworms fed with RhB feed. Right: RhB silkworm silks excited by a 488nm light (top) and a 540nm light (bottom). Scale bars (25μm) on the bottom right.

In the case of spiders, eyeballing either the spider or the silks obtained was not sufficent to confirm the presence of RhB. However, the silks from spiders fed with an RhB solution do fluoresce when excited with lasers with the excitation wavelength of 488nm (Figure 3.7). The presence of RhB was detected in MAS, MiS and the Capture Spiral (CS) silks. Figure 3.8 display results from the control samples.

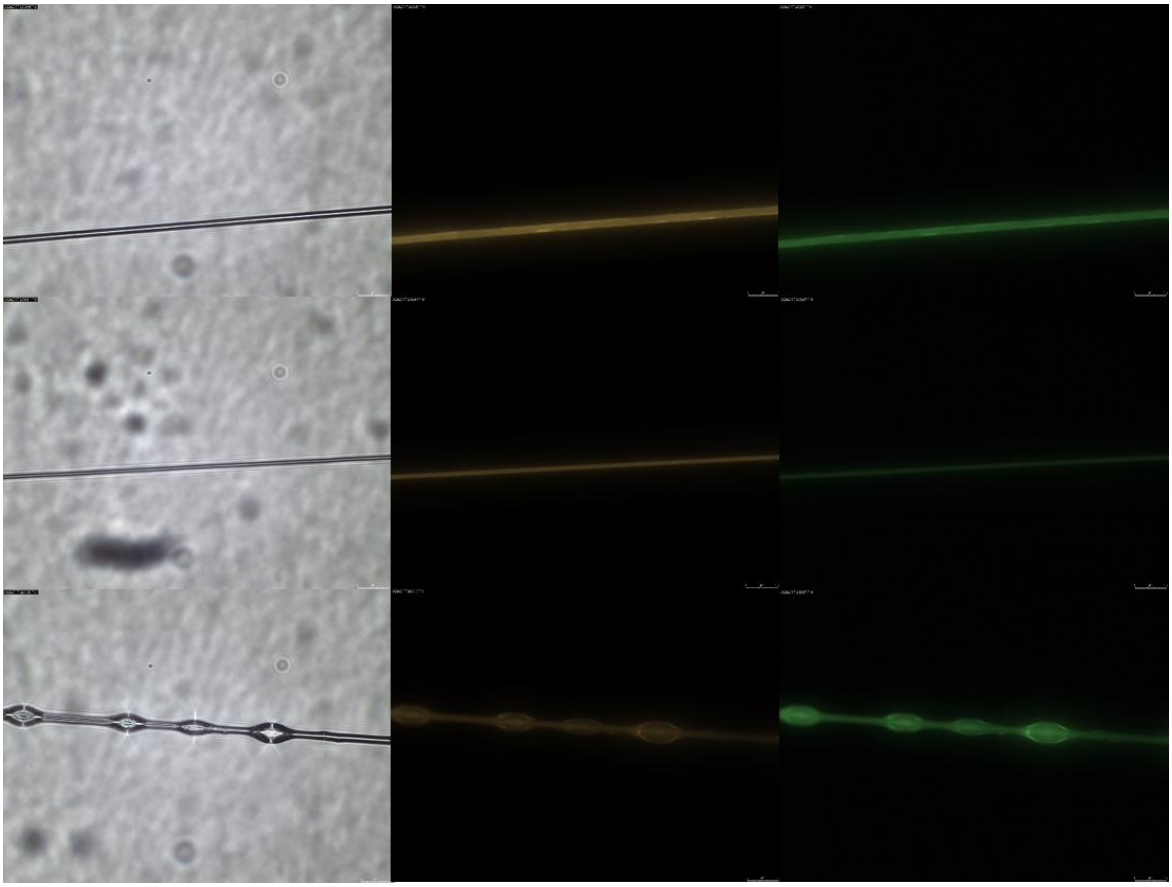

Figure 3.7: Spider Major Ampullate silk (top row), Minor ampullate silk (middle row), and Capture Spiral silk (bottom row). Left column: Silks under white light. Middle column: Silks excited by a 540nm light. Right column: Silks excited by a 488nm light. Scale bars (25μm) on the top right.

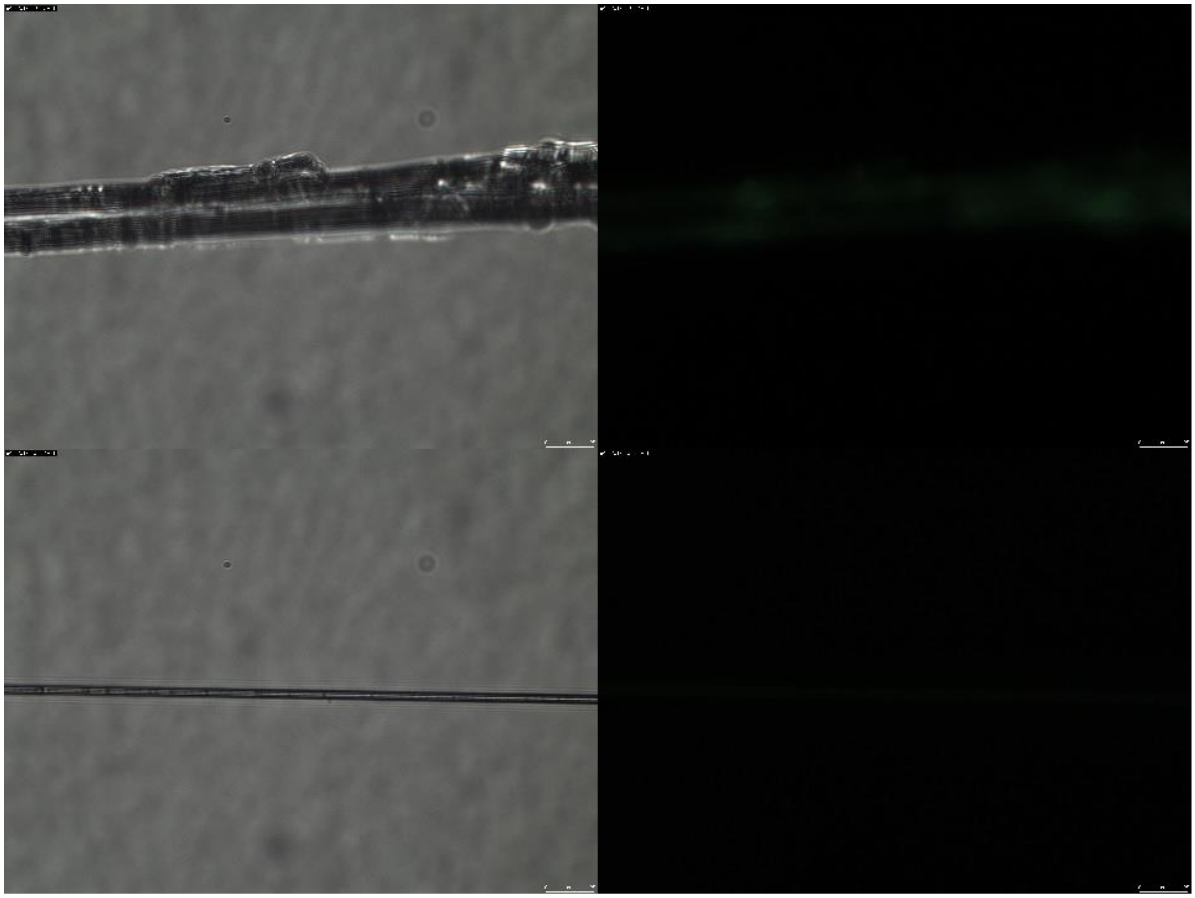

Figure 3.8: Control silkworm (top row) and spider (bottom row) samples. Left columns: Silks under white light. Right column: Fluorescence imaging using 488nm light. There is mild fluorescence attributed to autofluorescence.

3.2 Effect of RhB on the growth of silkworms and spiders

The growth rate of the silkworms – represented by proxy using their weight per day – is shown in Figure 3.9.

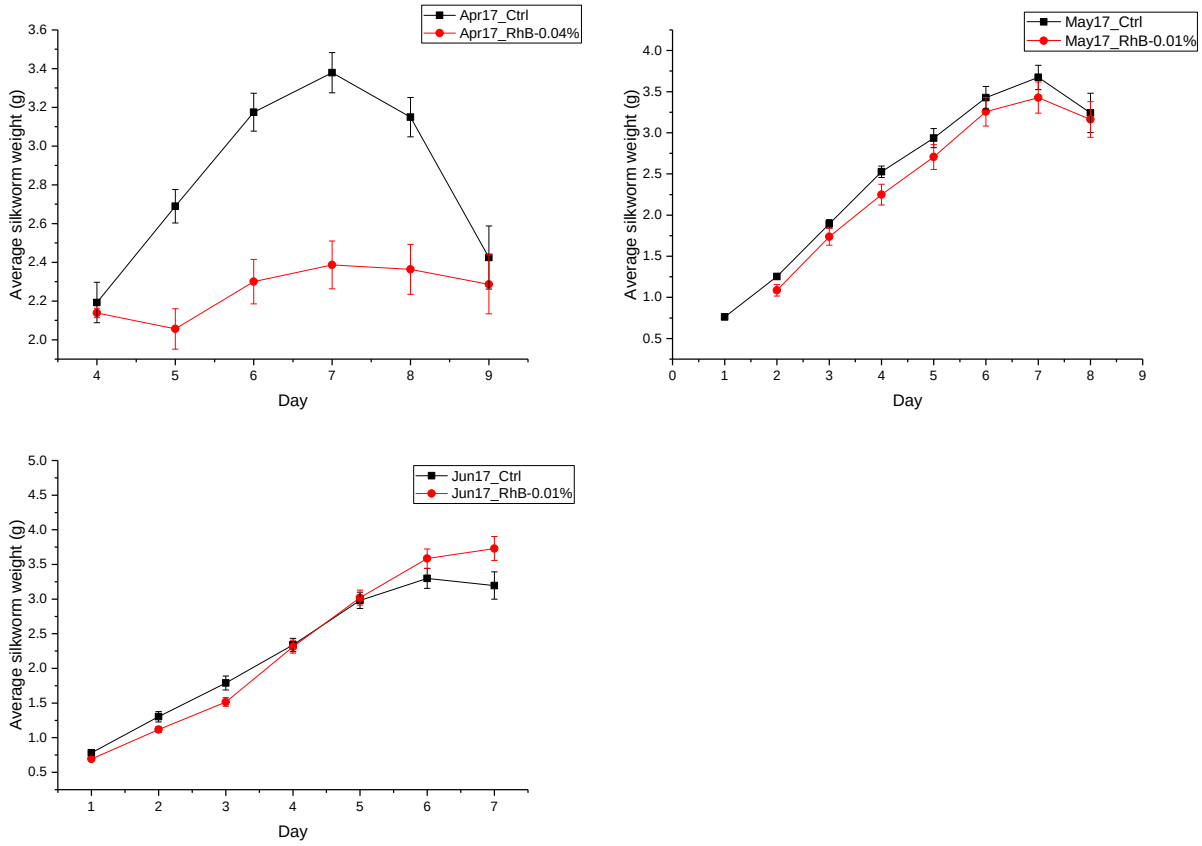

Figure 3.9: Silkworm growth data.

Silkworms fed with the feed containing 0.01wt% RhB showed little to no difference in growth rate compared to controls and began spinning cocoons around the same period as the control silkworms. The silkworms from the two different groups also did not differ behaviourally for silkworms fed with the 0.01wt% RhB feed.

In contrast, silkworms fed with the 0.04wt% RhB feed showed a marked decrease in growth rate, were less active than their control counterparts, and began the cocoon spinning process up to 4 days later than the controls. Additionally, the spinning behaviour of the silkworms fed with RhB at this concentration was impaired as well; some spun sheets of silks as opposed to cocoons while others failed to spin entirely. This suggests that this concentration of RhB in

the silkworms' system is detrimental to silkworm growth and behaviour; which contradicts data seen in Tansil's work where it was claimed that silkworms did not display any detrimental changes in behaviour[100].

Note the drastic decrease in silkworm weight in the control group for the Apr2017 batch. This is normal silkworm behaviour; the silkworms reduce their food intake and purge their GI in preparation for the cocoon spinning process. The start of this process is also captured in both treatment groups in the May2017 batch starting from 'Day 7'.

As for the spiders, there was seemingly no change in the behaviour of the spiders fed with the RhB solutions compared to the controls when visually monitored.

3.3 Digital Scanning Fluorimetry data on silkworm silk dope

Figure 3.10 displays the averaged DSF first derivative spectra for silkworm dopes obtained from silkworms fed with 0.01% RhB feed across two colour channels.

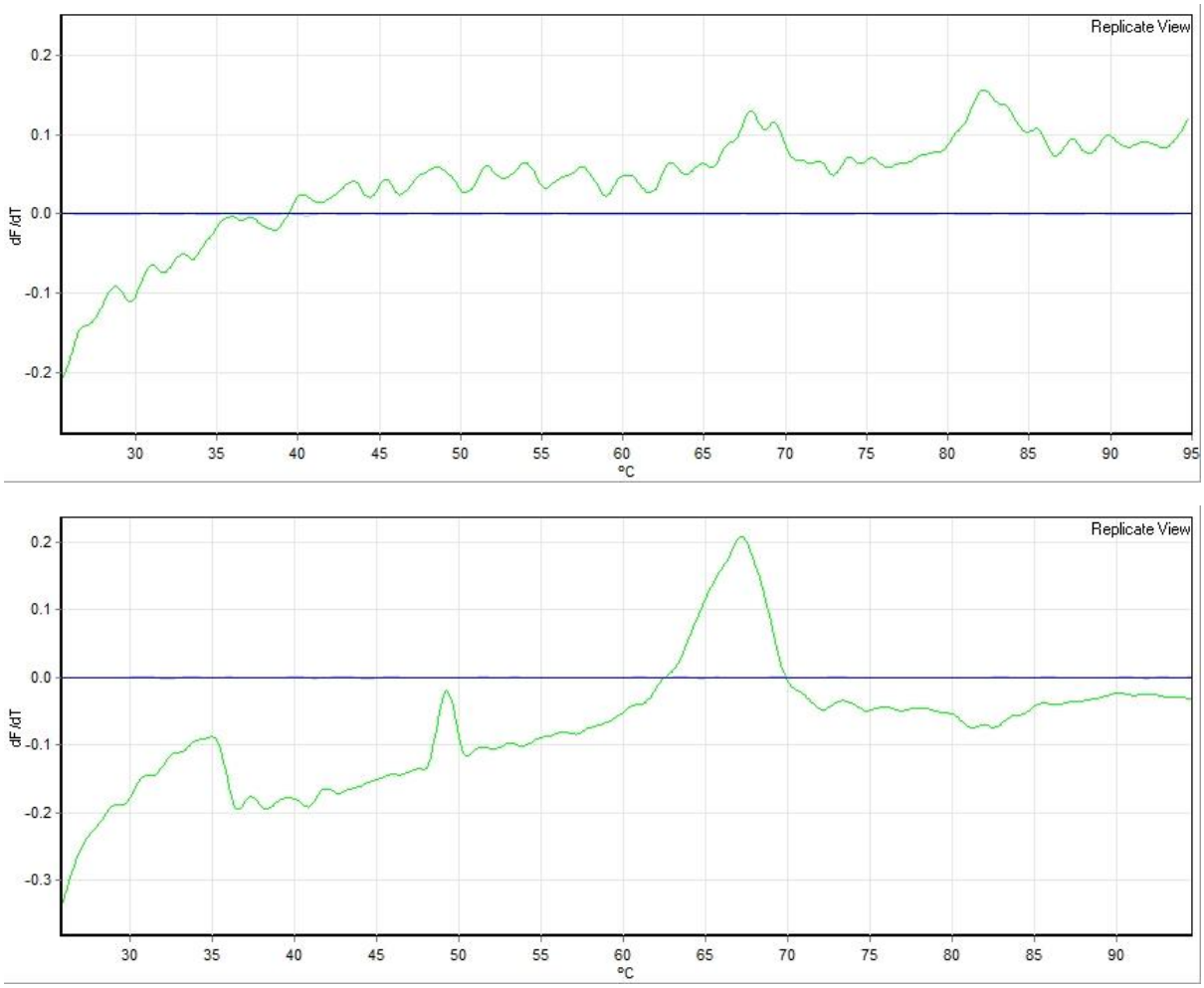

Figure 3.10: DSF first derivative curves obtained from fluorescence signals for NSB RhB 0.01%. Top: Averaged DSF spectra obtained from the green channel (λ_{ex}: 470nm, λ_{em}: 510nm). Bottom: : Averaged DSF spectra obtained from the orange channel (λ_{ex}: 585nm, λ_{em}: 610nm)

Typically, the green channel is used for analysing the DSF spectra of *Bombyx mori* silks due to the higher dynamic range afforded by this channel[173]. However, from our results it seems likely that the RhB signals are interfering with the emission spectra obtained by generating a very high background, making it hard to decipher any useful information from the spectra without further replicates. Consequently, we used data from the orange channel to analyse the DSF spectra, which does seem to yield useful data and still have decent dynamic range.

Of interest in the spectra is the instability temperature – often denoted in DSF silk literature as T_i – and refers to the point at which temperature induced instability of hydrogen interactions which causes molecular reconfiguration and allows Sypro-Orange to interact with motifs within the silk proteins. The T_i obtained from the spectra seems to be 67°C as shown by the peak seen at that temperature, which is typical of standard *B. mori* silks, which implies that low concentrations of a perturbing dye such as RhB doesn't seem to significantly affect the stability of the silk feedstock.

There is another peak seen at around 47°C. Literature suggests that this peak is a result of the denaturation of sericin[174]. Another possibility is that this peak is a result of the reconfiguration or disruption of micellar structures in the silk dope (*personal comm.* Alex Greenhalgh, 2021).

3.4 Fluorescence spectra

Figure 3.11 displays information about the fluorescence spectra of the experimental RhB solutions, the MAS from spiders fed with the different RhB solutions and a comparison in emission peaks for the RhB solutions, as well as MAS dyed with RhB via feeding vs dyed post-reeling.

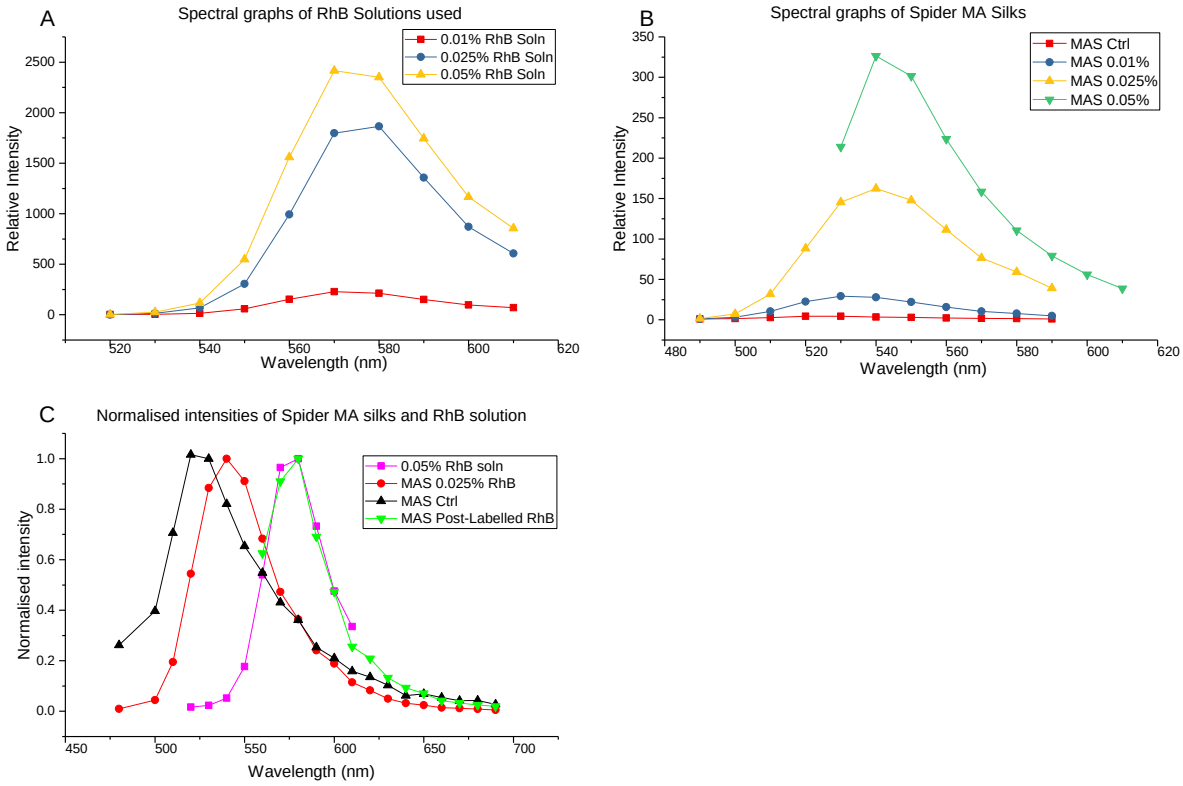

Figure 3.11: (A) Fluorescence spectra of the RhB solutions used in the experiment. (B) Fluorescence spectra of the MAS fibres obtained from the experiment, as well as a control. (C) Normalised fluorescence spectra of a representative RhB solution, control MAS, representative MAS from a spider fed with RhB, and MAS fibres dyed post-spinning. All spectra were obtained by exciting samples with a 488nm laser.

The fluorescence spectra of all the RhB solutions used in this experiment is typical of RhB in water or in ethanol, with an emission peak at approximately 580nm. The intensity of the fluorescence response is also concentration dependent, which is not surprising.

The intensity of the fluorescence spectra of MAS silks collected from spiders fed with the RhB solutions also display a concentration dependence, indicating that the spiders

accumulate a larger amount of RhB in their system when a higher dosage is used and that the spiders are not able to expel the RhB from their systems faster than they intake it.

What is interesting to note is that the RhB in the silks respond differently from RhB in solution: the RhB in silks have an emission peak at approximately 540nm as opposed to the expected 580nm, a 40nm blue-shift.

This shift can be more easily seen in the normalised fluorescence spectra in Figure 3.11 (C). Interestingly, MAS fibres dyed with RhB post-spinning display the typical fluorescence spectra of RhB in solution i.e. the blue-shift only occurs when the dye is fed to the spider, and when the spider incorporates the dye into the silks as part of its natural spinning process.

Literature suggests that this response could be a result of RhB forming dimers which occurs when a critical concentration of RhB in solution is reached [168,175,176], so it is possible that conditions within the silk gland favour the dimer formation of RhB. However, I also cannot rule out the possibility of the RhB molecules interacting with specific motifs in the silks, or if the RhB molecules have been chemically modified after passing through the spider's system.

3.5 Polarisation data

Figure 3.12 displays data from the two-photon polarisation experiments, which allows us to see whether the RhB molecules are oriented in any specific orientation, or whether the distribution is random.

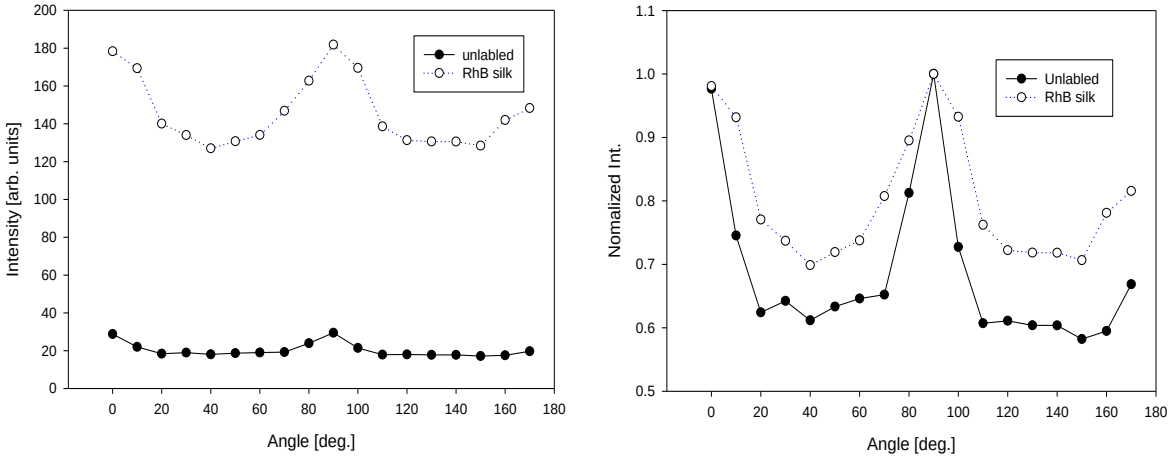

Figure 3.12: (Left) Averaged (N=5) fluorescence intensity as a function of the polarisation angle of excitation light for RhB MAS fibres and control MAS fibres. (Right) Normalised intensity as a function of the polarisation angle of excitation light for RhB MAS fibres and control MAS fibres

Comparing the emission intensities of silks from RhB fed spiders against control MAS, we see a large difference not only in absolute intensity, but also in their respective amplitudes over the full range of angles. The RhB doped silks have a relative change of c.a. 50% whereas the controls only have a change of about 25%, relative to the maximum intensity. The peak obtained from RhB is also wider, suggesting that the RhB molecules within the silks are not as well oriented as the auto-fluorescent motifs in silks. It is interesting to note that the spectral graph obtained from the RhB doped silks suggest that the distribution of RhB molecules within the silks are not random and are not distributed in a Gaussian manner either[172] (Figure 3.13). It seems that the RhB molecules are oriented along the longitudinal axis of the silk fibre, likely by interacting with protein motifs within the silks during the fibrillation process, or flow-oriented as a result of the highly shear-induced spinning process (less likely compared to the former interpretation.

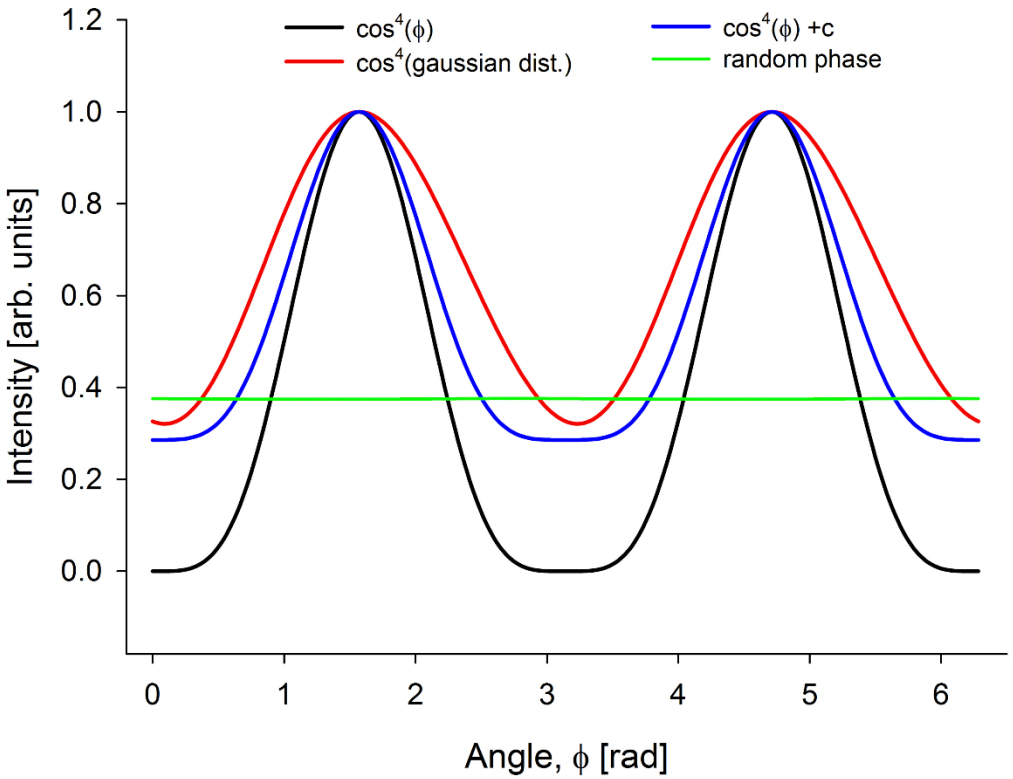

Figure 3.13: Modelled[172] emission intensity spectra as a function of the angle of polarisation of two-photon excitation light for different fluorophore (dipole) distribution types. Black line: samples with all fluorophores aligned in the same direction. Red line: samples with fluorophores oriented in a Gaussian distribution with a mean value of $\pi/2$ and a variance of 0.7rad. Blue line: Samples with a mix of highly oriented dipoles along the fibre axis, and some randomly oriented dipoles. Green line: samples with randomly distributed dipoles. Adapted with permission from [172].

Figure 3.14 displays data for two-photon polarisation experiments performed in tandem with induced strain. This allowed us to compare the polarisation response of RhB versus the auto-fluorescent motifs when the fibres are stretched.

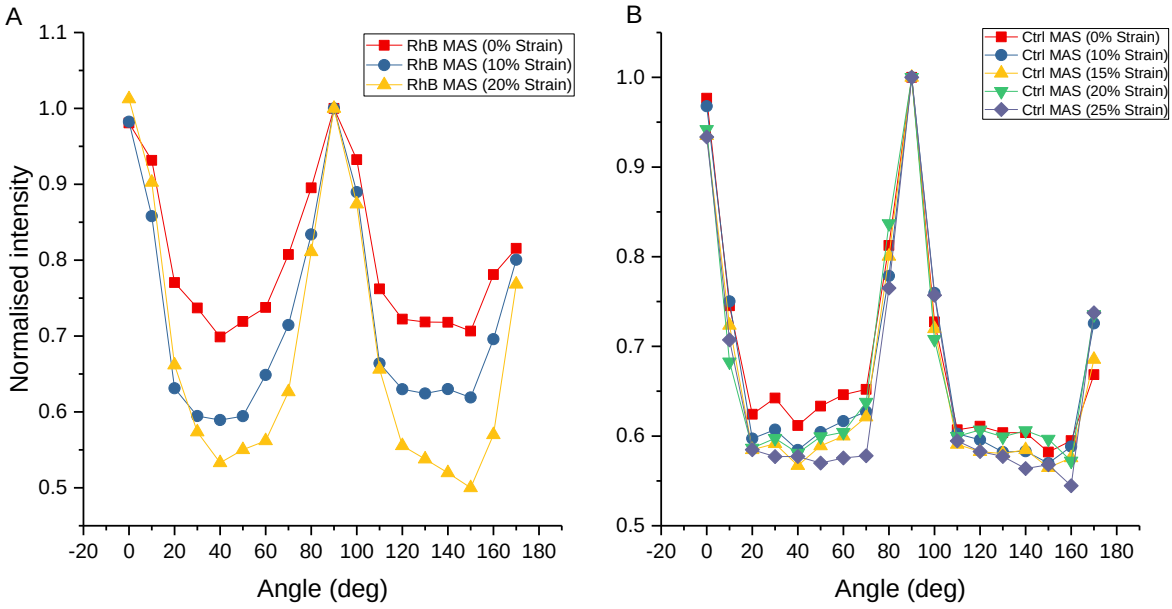

Figure 3.14: (A) Normalised fluorescence intensity as a function of the polarisation angle of excitation light for RhB MAS fibres at various strain values. (B) Normalised fluorescence intensity as a function of the polarisation angle of excitation light for control MAS fibres at various strain values. Intensity values are normalised based on the maximum intensity for each individual spectra.

From Figure 3.14 (A), we observe a relative amplitude increase as the fibres are strained. This leads us to believe that as the fibres are strained, more RhB dipoles are being oriented along the longitudinal axis of the silk fibre. This increase in relative amplitude also occurs to a lesser extent for auto-fluorescent motifs in standard silks as seen in Figure 3.14 (B). Thus, the introduction of strain within the fibres orients the RhB dipoles to a greater extent compared to the auto-fluorescent motifs present within spider silk fibres.

This combination of results – the blue-shift of RhB seen in Fig 3.11, the polarisation data shown in Fig 3.12, and the relationship of the polarisation response with strain as shown in Fig 3.14 – suggest that RhB is not randomly distributed across the silk fibre but are possibly interacting specifically and aligning with certain regions or motifs of silk fibres.

3.6 Tensile tests

Figure 3.15, 3.17 and 3.19 display representative stress-strain graphs for the tested samples, grouped by the different treatment groups. Figures 3.16, 3.18 and 3.20 display parameters of interest obtained from the stress-strain data (Young's Modulus (YM), Maximum Strain at break (MaxStrain) that has been summarised into box-and-whisker plots. Tables 3.3-3.5 display results from the applied mixed-effect model.

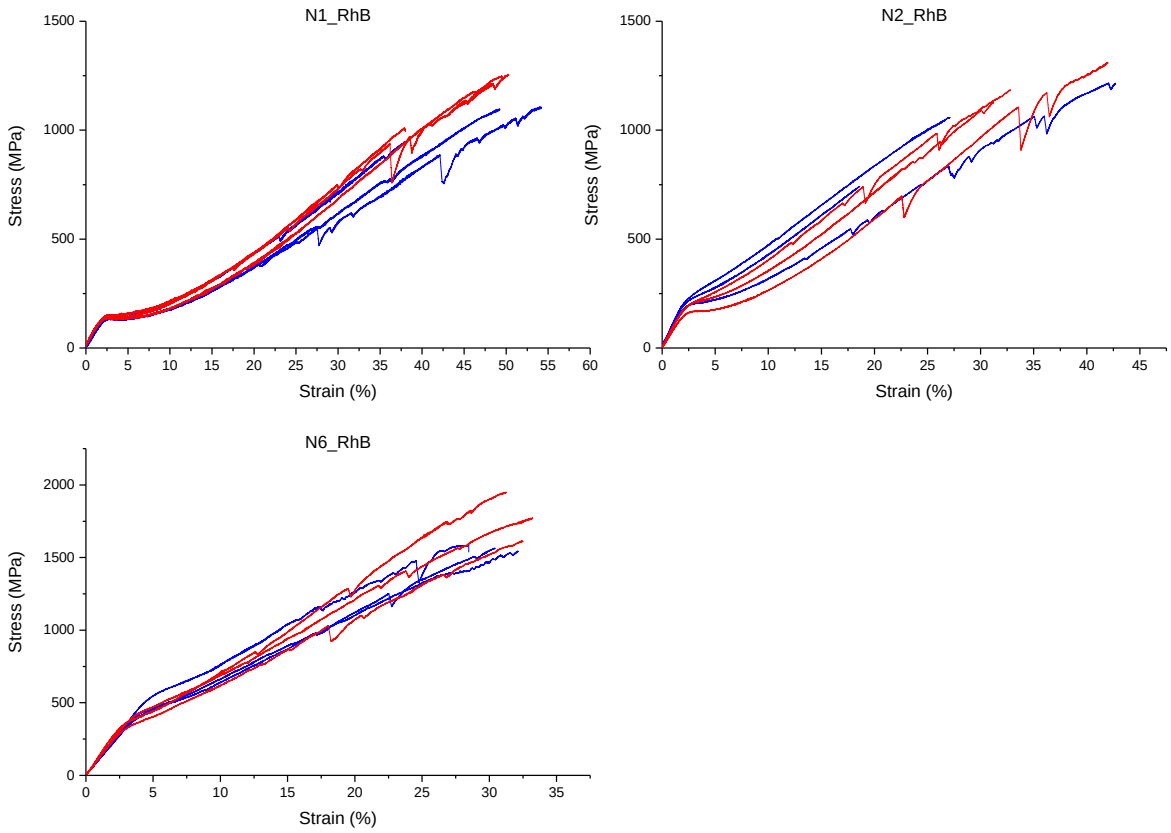

Figure 3.15: Representative stress-strain graphs from silks collected from spiders fed with 0.01% RhB solution. Blue lines represent control samples. Red lines represent samples collected from spiders 5 days after the feeding regime.

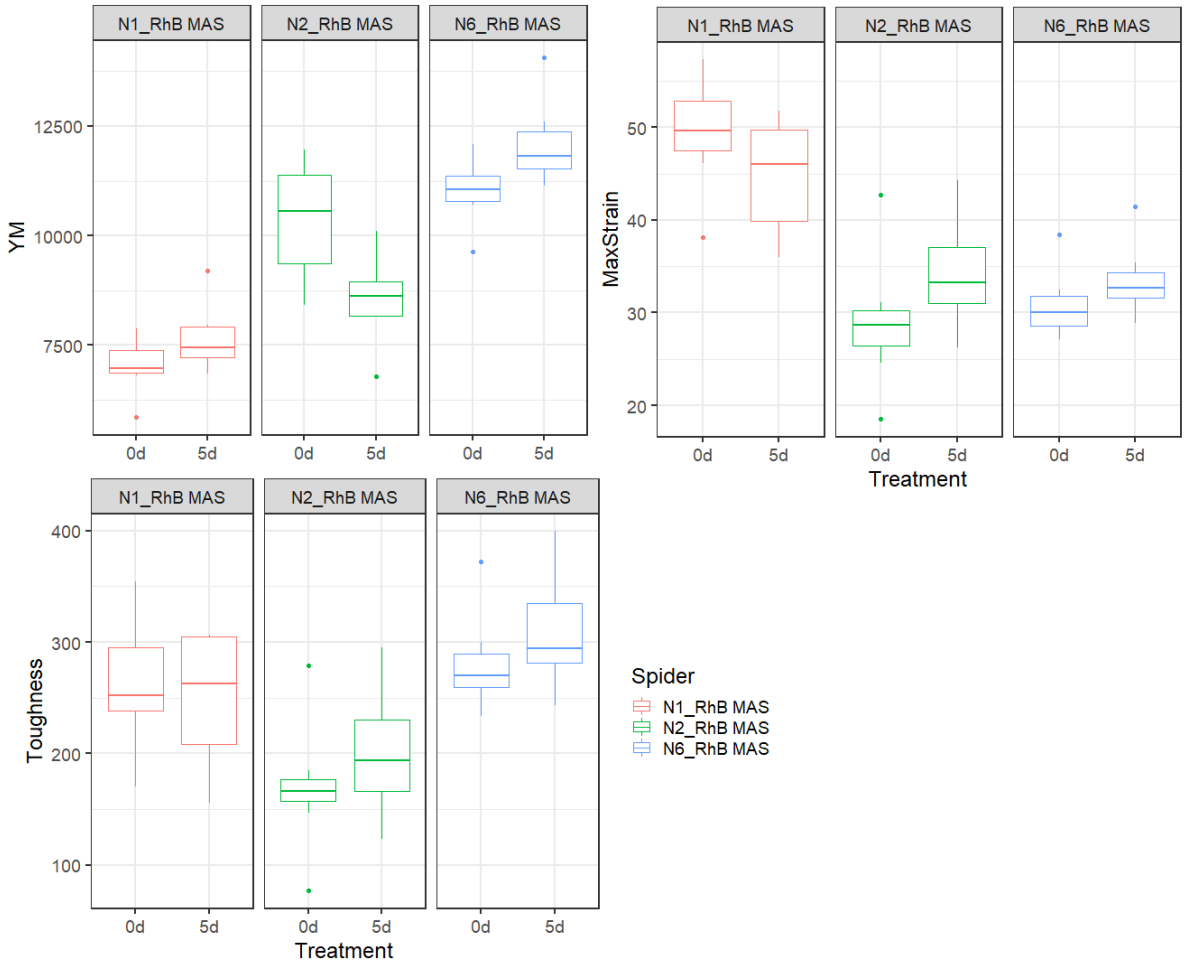

Figure 3.16: Results from spiders fed with 0.01% RhB solution. 0d: control samples. 5d: silks collected from spiders fed with RhB after 5 days. The centre line of the box plot represents the median, the bottom and top portions of the box represent data within the first and third quartile respectively, the dots outside the box plot represent outliers.

Treatment	Parameter	Effect size	df	t-value (T)	p-value (P)	Marginal coefficient	Conditional coefficient
0.01% RhB Solution	Young's Modulus (MPa)	14.46 ± 292.81	49	0.049	0.9608	1.334121e-05	0.7209641
0.01% RhB Solution	Maximum Strain (%)	1.34 ± 1.53	49	0.877	0.3850	0.005674673	0.6234052
0.01% RhB Solution	Toughness (MJ/m^3)	16.18 ± 14.24	49	1.136	0.2615	0.01477812	0.415911

Table 3.3: Results from the Mixed-effects model analysis for samples from spiders fed with 0.01% RhB Solution.

The results suggest no significant changes in the three mechanical property parameters examined, and there are no trends (net positive or net negative) in improvement or degradation of the three parameters that were examined. Additionally, the marginal and

conditional coefficient values indicate that only a miniscule proportion – quantified in Table 3.3 – of the variation seen in the dataset is explained by the fixed effect, with most of the variation being explained by the random effect (intraspecific variation). Thus, it is highly unlikely that an inclusion of RhB at this concentration elicits any effect on the mechanical properties of spider silks.

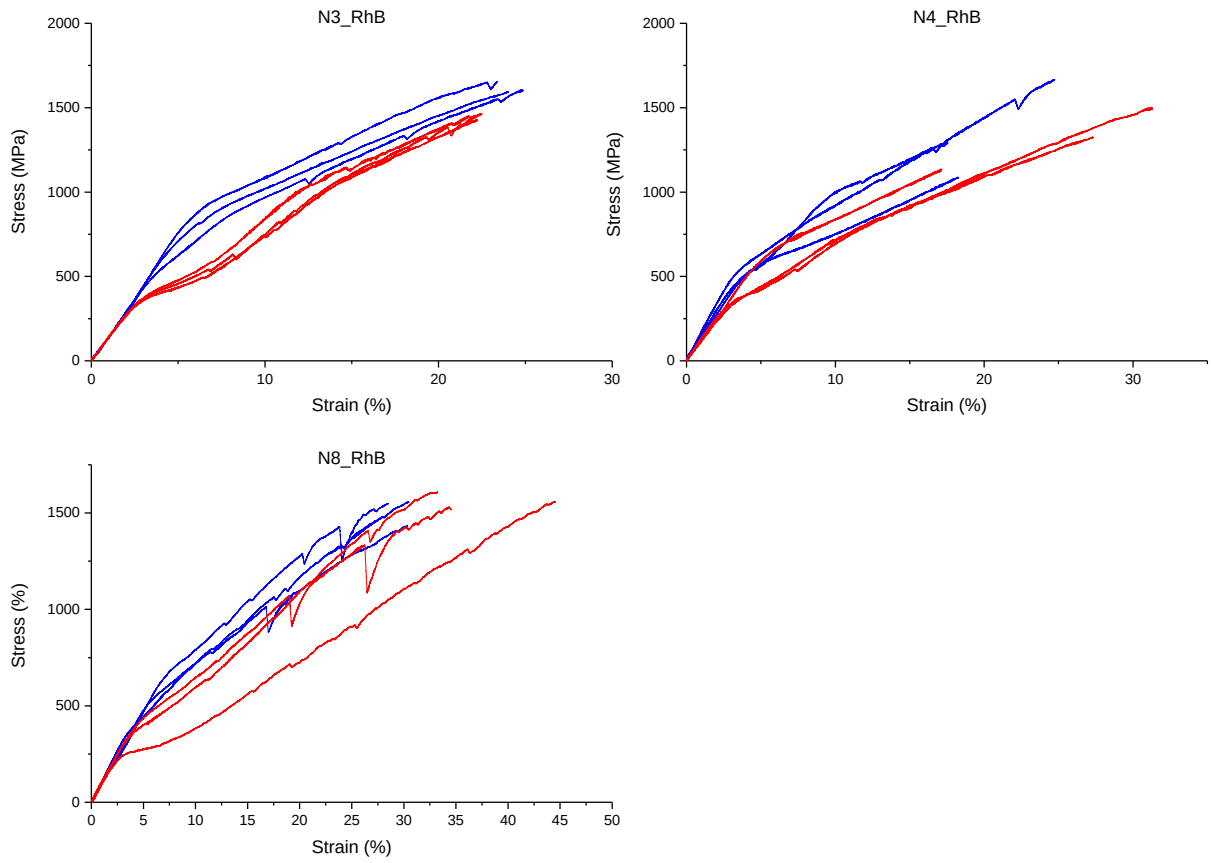

Figure 3.17: Representative stress-strain graphs from silks collected from spiders fed with 0.025% RhB solution. Blue lines represent control samples. Red lines represent samples collected from spiders 5 days after the feeding regime.

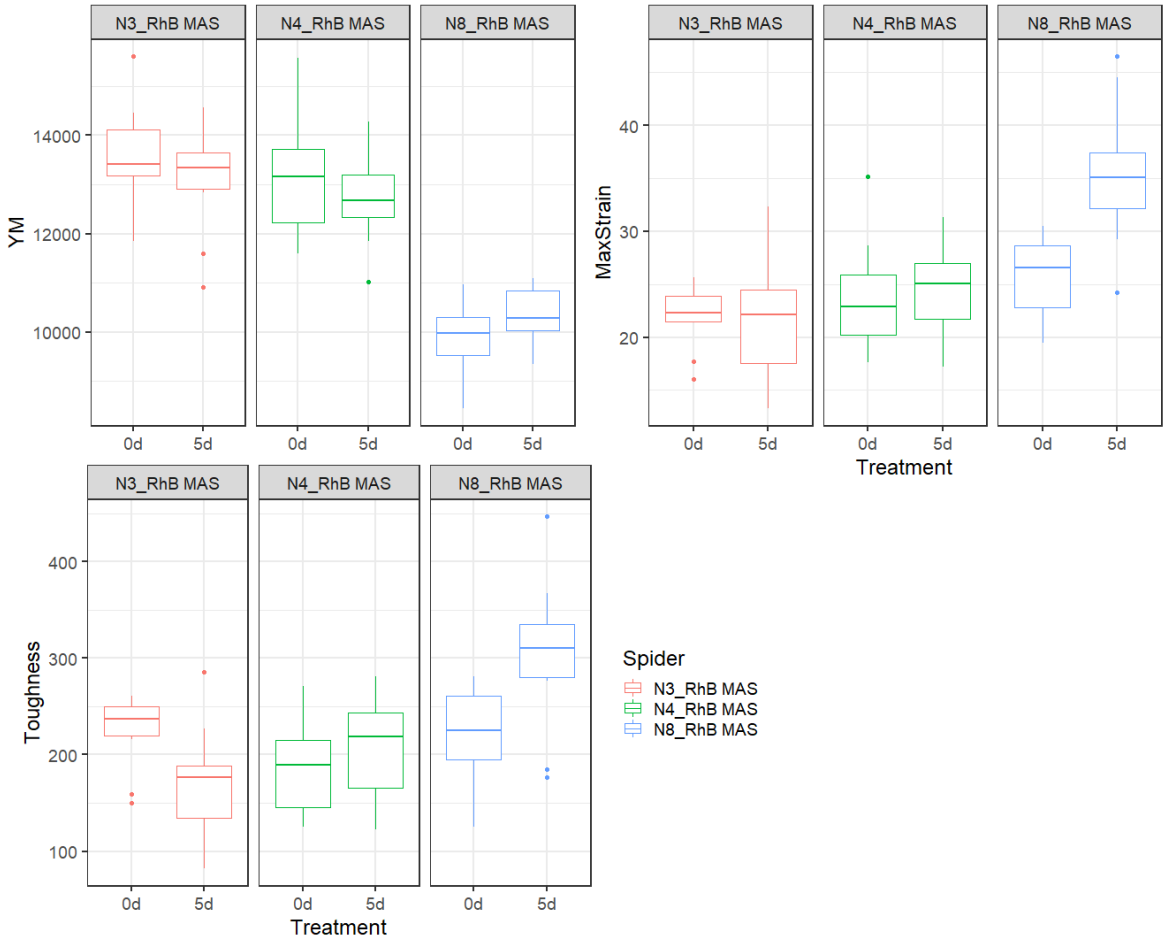

Figure 3.18: Results from spiders fed with 0.025% RhB solution. 0d: control samples. 5d: silks collected from spiders fed with RhB after 5 days. The centre line of the box plot represents the median, the bottom and top portions of the box represent data within the first and third quartile respectively, the dots outside the box plot represent outliers.

Treatment	Parameter	Effect size	df	t-value (T)	p-value (P)	Marginal coefficient	Conditional coefficient
0.025% RhB Solution	Young's Modulus (MPa)	-174.66 ± 257.94	58	-0.677	0.501	0.00248137	0.6754521
0.025% RhB Solution	Maximum Strain (%)	3.268 ± 1.365	58	2.394	< 0.05	0.06245584	0.346574
0.025% RhB Solution	Toughness (MJ/m^3)	17.36 ± 16.20	58	1.073	0.2878	0.01493259	0.2221745

Table 3.4: Results from the Mixed-effects model analysis for samples from spiders fed with 0.025% RhB Solution.

The results from silks collected from spiders fed with a 0.025% RhB solution suggest no significant changes ($P < 0.05$) in the Young's Modulus and Toughness of the silks, and a

significant change in the maximum strain of silks, whereby the maximum strain seems to increase. However, there are several factors to consider before accepting this result as conclusive. Firstly, closer inspection of the data reveals that this significance largely originates only from results collected from N8_RhB, with silks from the other two spiders showing no change. In addition, the increase of 8% seen in samples from N8_RhB is within the bounds of natural variation of silk properties simply due to temporal effects [169]. Furthermore, results obtained from spiders fed with a higher dosage of RhB (Fig. 3.19 and Table 3.5) did not display any improvement in strain, nor were there any consistent trends in the change in maximum strain of silks. The marginal and conditional coefficient values – shown and quantified in Table 3.4 – also indicate that only a small proportion of the variability within the dataset is explained by the fixed effect, with the remaining variability being explained by the random effect or due to factors not captured within the model (i.e. temporal variation and error). Therefore, it is likely that the significance of this result arose from natural temporal variation in the mechanical properties of silks, which is large and could not be captured in the model.

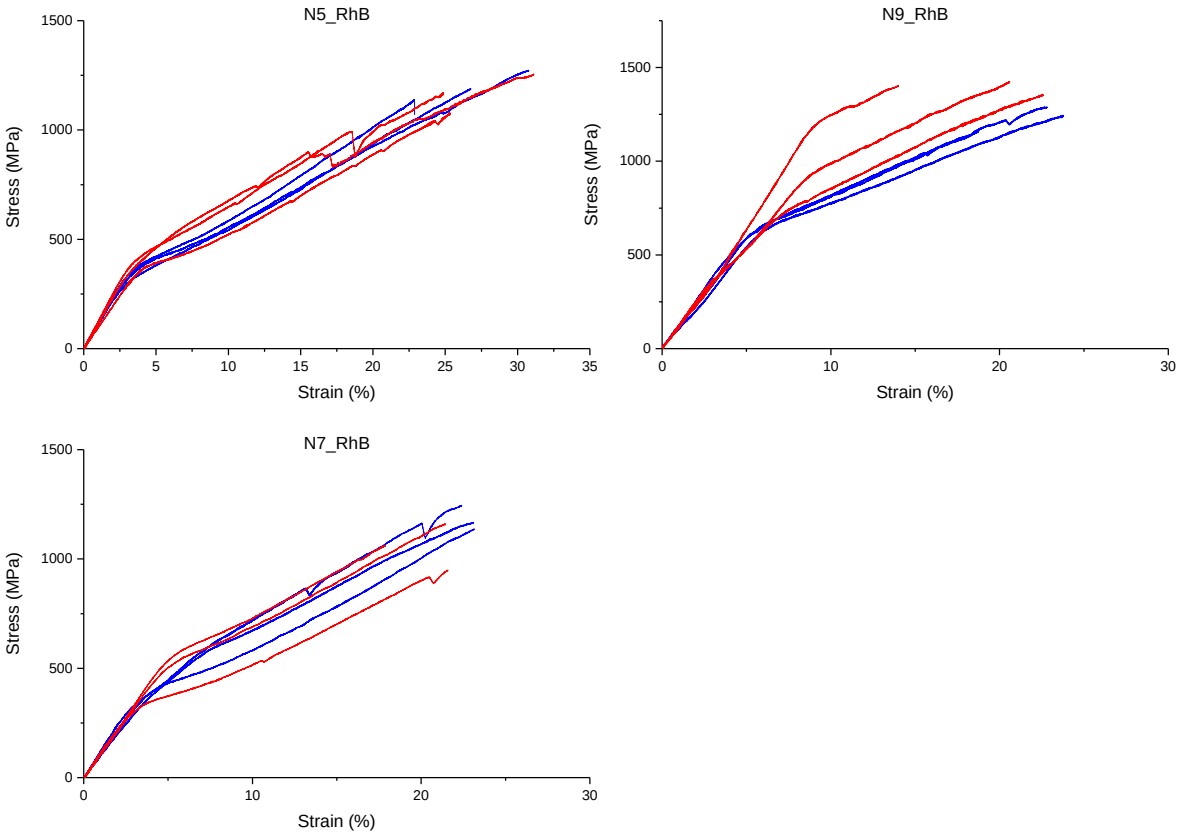

Figure 3.19: Representative stress-strain graphs from silks collected from spiders fed with 0.05% RhB solution. Blue lines represent control samples. Red lines represent samples collected from spiders 5 days after the feeding regime.

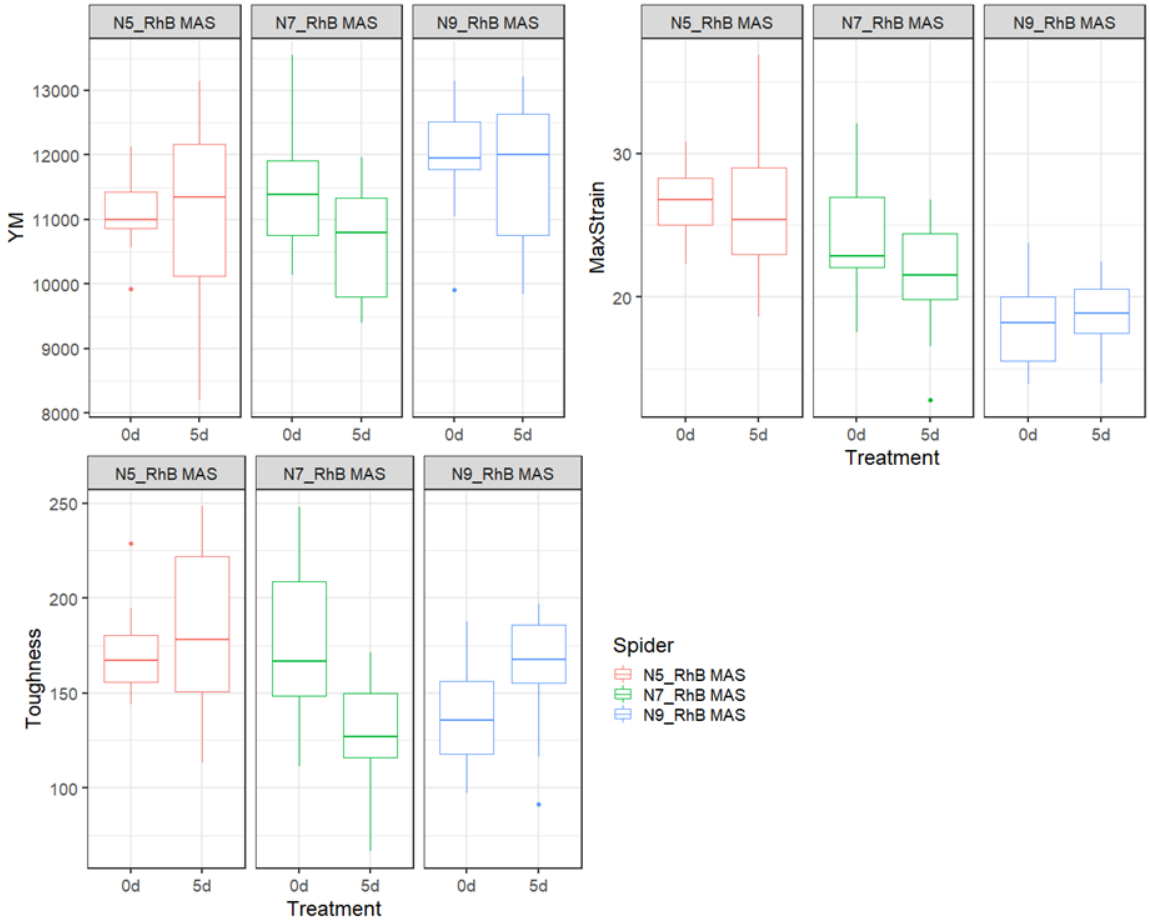

Figure 3.20: Results from spiders fed with 0.05% RhB solution. 0d: control samples. 5d: silks collected from spiders fed with RhB after 5 days. The centre line of the box plot represents the median, the bottom and top portions of the box represent data within the first and third quartile respectively, the dots outside the box plot represent outliers.

Treatment	Parameter	Effect size	df	t-value (T)	p-value (P)	Marginal coefficient	Conditional coefficient
0.05% RhB Solution	Young's Modulus (MPa)	-297.133 ± 223.805	78	-1.328	0.188	0.01996589	0.1012014
0.05% RhB Solution	Maximum Strain (%)	-0.6651 ± 0.8304	78	-0.801	0.4256	0.004681717	0.4226606
0.05% RhB Solution	Toughness (MJ/m^3)	-3.289 ± 8.500	78	-0.387	0.700	0.001766254	0.06304716

Table 3.5: Results from the Mixed-effects model analysis for samples from spiders fed with 0.05% RhB Solution.

The results suggest no significant changes in the three mechanical property parameters examined. In addition, there are no trends in improvement or degradation of the three

parameters that were examined. As with the previous results, the marginal and conditional coefficient values indicate that the fixed effect accounts for a miniscule amount of the variation seen in the dataset. Thus, it is highly unlikely that an inclusion of RhB at this concentration elicits any effect on the mechanical properties of spider silks.

Given that – at the concentrations of RhB used – there was seemingly no concentration-based effects on the mechanical properties of silks; I decided to pool the data from all the spiders together to analyse if there is any effect of RhB in general – within the concentration range used – on the mechanical properties of silks. Although this may seem redundant at first glance, there are advantages to pooling the datasets together. Namely, an increase in confidence and robustness in our results, and a greater statistical power to detect differences within the dataset. Table 3.6 displays the result for the mixed-effect model when applied to the pooled dataset.

Treatment	Parameter	Effect size	df	t-value (T)	p-value (P)	Marginal coefficient	Conditional coefficient
0.01 - 0.05% RhB Solution	Young's Modulus (MPa)	-174.99 ± 146.92	185	-1.191	0.235	0.001933215	0.7383399
0.01 - 0.05% RhB Solution	Maximum Strain (%)	1.1145 ± 0.6975	185	1.598	0.112	0.00362829	0.7271384
0.01 - 0.05% RhB Solution	Toughness (MJ/m^3)	8.215 ± 7.299	185	1.125	0.262	0.003662881	0.4446189

Table 3.6: Results from the Mixed-effects model analysis for samples from spiders fed with 0.01 – 0.05% RhB Solution.

The results suggest no significant changes in the three mechanical property parameters examined. In addition, there are no trends in improvement or degradation of the three parameters that were examined. Once again, the marginal and conditional coefficients indicate that only an infinitesimal proportion of the variation present within the dataset is

explained by the fixed effect. Thus, it is highly unlikely that an inclusion of RhB at this concentration range elicits any effect on the mechanical properties of spider silks.

Overall, the results above would indicate that – for spiders fed up to the 0.05% RhB solution – the inclusion of RhB into silks elicit no effect on their mechanical properties. This is interesting given the fact that my other results show that RhB seems to be interacting with the motifs within spider silks, indicated by the spectral shift in the RhB spectra as well as the polarisation results. The implications of this would be that spider silks – either by virtue of the spinning process that occurs within the silk glands and spinnerets, the molecular structure and motifs within silks, or a combination of both – are able to compensate for small perturbations in their structure due to inclusion of small molecules such as fluorescent dyes; a testament to silks being a high-performing and highly adaptable material in nature.

3.7 Wide-field deconvolution and Zeiss airy scan

We performed wide-field deconvolution imaging experiments as well as Zeiss airy scan experiments to see if further information regarding the binding or distribution of the RhB dye could be gathered from RhB fed spider silks. The results of the experiments are shown in Figure 3.21 and 3.22.

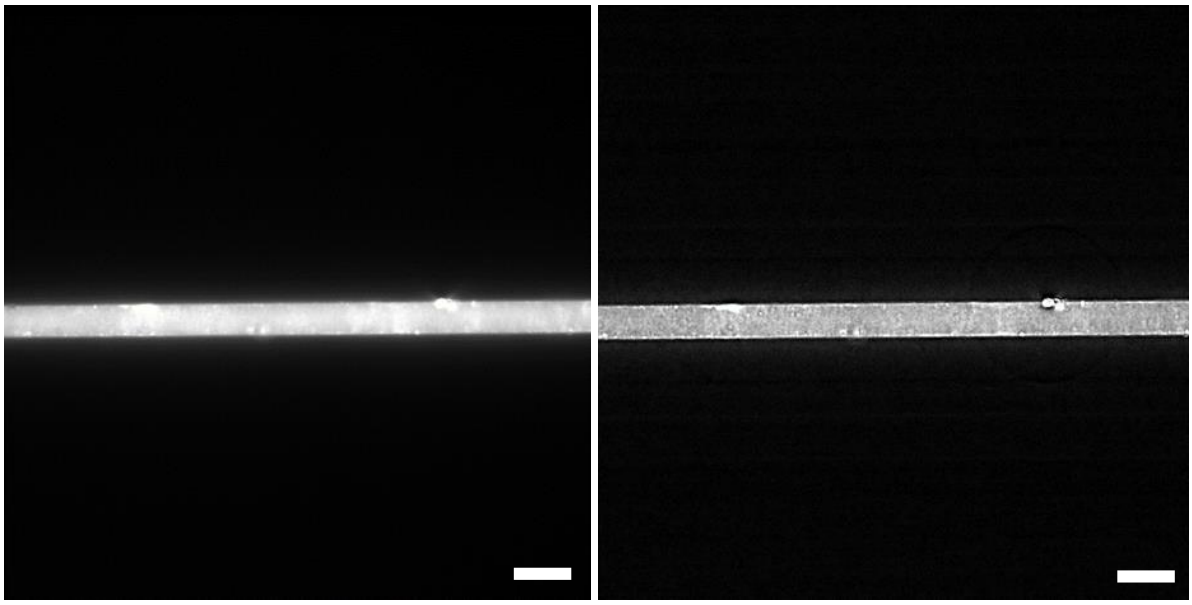

Figure 3.21: (A) Fluorescence image of RhB fed spider silks under standard fluorescence imaging. (B) Fluorescence image of RhB fed spider silk after application of wide-field deconvolution. Scale bar = 5µm.

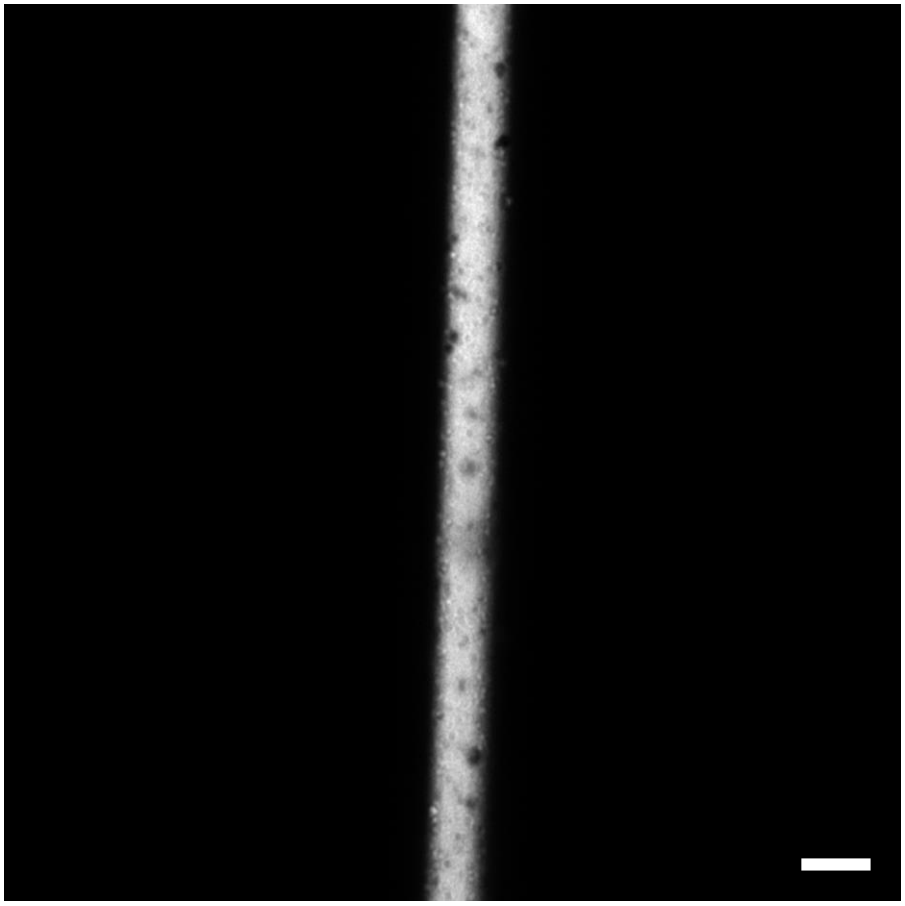

Figure 3.22: Representative fluorescence image of RhB fed spider silks obtained from a Zeiss airy scan. Scale bar = 5µm.

From Figures 3.21 and 3.22, we were not able to discern any appreciable difference between standard confocal fluorescence and the wide-field deconvoluted or Zeiss airy scanned counterparts.

3.8 Trials with ATTO488-COOH and Alexa488

Unlike RhB, ATTO488 and Alexa488 are fluorescence dyes that are suited for super-resolution fluorescence imaging. Given the results we obtained from the RhB fed spider silks, we decided to try feeding spiders super-resolution dyes to see if they enter silks and if we are able to discern any form of distribution within the silks that may help us infer the structure of spider silks.

Unfortunately, none of these dyes seem to incorporate within the silks when fed to the spiders. The few excretions collected from these spiders do fluoresce strongly within the expected fluorescence emission range of these dyes, indicating that the dyes simply enter the spider and are excreted out.

4. Discussion

The results in this chapter indicate that it is possible to insert fluorophores or molecular labels into silks via direct feeding to the organism, with minimal effect on the behaviour of the animal – if the dosage is sufficiently low – as well as the mechanical properties of the silks. The dye used – Rhodamine B – seems to have been incorporated in a non-random manner, suggesting preferable interaction with certain spaces or motifs within the silks. It may be possible to make use of these non-random interactions to further discern structures within silks.

One thing to note is that while it seems that a low concentration of dye within silks do not seem to affect the mechanical properties of the solid spun fibre, some preliminary rheological experiments (data unfortunately not shown here) suggest that the dyed silkworm dope does react differently under shear; it seems that the RhB doped silks are less shear sensitive as the shear transition occurs at higher frequencies. If proven to be true, this suggests that small perturbations due to insertion of dyes/molecules in the silkworm dope may affect the protein folding and reorganisation process during spinning, but ultimately not affect the mechanical properties of the finished fibre.

This is an encouraging prospect because it implies that certain dyes or molecular labels can act as inert reporters of silk state and structure when incorporated in this manner; by inert I mean not adversely affecting the mechanical properties of silks, which is often an issue with dying or labelling silks since they tend to be sensitive to external perturbations. This in turn may lead to future avenues for studying the structure and molecular dynamics of silks by using such labelling methods.

In particular, this work suggests some potential for the inclusion of super-resolution fluorescent dyes which would be of much interest as it would be a spatially resolved technique with potentially sufficient resolution for discerning structures within silks. This is

of great interest because many techniques used to study silks in the past are bulk-averaging; a high-resolution (potentially nanoscale) spatially-resolved technique might give us new insight into specific regions or structures of silks depending on the spaces the fluorophores reside in. Consequently, this would allow researchers to probe and visualise the structures of silks – in particular the non-crystalline regions of silks should the fluorophores localise in that region – in ways not done before. Coupled with real-time imaging and induced stress, it may even be possible to monitor the dynamics of the different motifs in silks as the silk fibres are stretched.

However, this prospective technique is not without its challenges as alluded to in my attempts to include the Alexa488 and ATTO488 super-resolution fluorescent dyes into silks. It seems that dye selection is crucial; we suspect that the reason the aforementioned dyes failed to be incorporated within the silks is due to their high hydrophilicity. This may prevent the dyes from shedding their water shell and thus prevent their interaction with silk motifs within the fibres or indeed the silk dope. The work done by Tansil et.al[168] eluded to this fact as they tried several types of Rhodamine dyes and found that they incorporate at different concentrations within the silk fibres depending on their hydrophilicity. RhB might be unique due to its ability to form dimers under certain conditions and thus potentially modulate their hydrophilicity[168].

Unfortunately, many super-resolution dyes readily available in the market are highly hydrophilic, which presents an additional challenge. One potential workaround might be to chemically modify the side-chains of super-resolution fluorophores of interest to include a hydrophobic tail, thus creating an amphipathic molecule which may have a higher probability of being incorporated within silk fibres.

In some ways, this chapter also serves as a homage to how well adapted and evolved silks are to maintain their robustness of mechanical properties despite minor perturbations due to fluorophore incorporation. This robustness is in-built in both the molecular structure of the silk proteins, as well as the spinning process of silks.

There was mention of producing artificial fibres from NSF, as well as the preparation of cocoon samples for mechanical testing. Unfortunately, I didn't have time to perform those experiments due to lab disruptions and the Covid-19 pandemic.

Acknowledgements

I thank Jonathan Brewer (University of Southern Denmark, Odense) for performing some preliminary fluorescence imaging experiments on the RhB silks, for performing the two-photon excitation polarisation experiments, and for a thorough discussion and collaborative analysis of the resulting fluorescence spectra and polarisation results.

Chapter 4: SHG/FLIM imaging as a novel spatially-resolved method for investigating the structure of silks

1. Introduction

Semicrystalline polymers have been theorized to behave as multi-phase composites for decades[177]. This understanding has been applied to the study of many materials, both synthetic and natural polymers[178,179]. However, there tend to be differences in these two sources depending on origin and process history. The crystallographic orientations of polymers can have a major impact on their performance[180,181]. Natural materials such as wood and silk tend to be anisotropic, while many commodity semicrystalline polymers can be isotropic[182]. Looking at natural polymers, silk is of particular interest for its dynamic nature and variety of manifestations depending on the organism producing it[183]. As Vollrath et al has shown, *Bombyx mori* silk can be fabricated to possess enhanced anisotropic properties depending on processing history[184,185]. As for spider silks, it's been shown that the degree of order and crystallinity of the fibres can be altered based on the speed in which the spiders are reeled at[41,169,186]. This material is ideal for the study of crystallographic orientations and their impact on physical properties. To this end, several studies have been conducted to understand the composition and microstructure of silk from various sources ranging from worms to spiders[187]. Often, techniques such as FTIR, X-Ray diffraction and Neutron Scattering are used to try and understand the structure of silks.

Despite the wealth of knowledge obtained from the aforementioned techniques, they do have their limitations. One of the biggest challenges that silk researchers face is that such commonly used techniques are often bulk-averaging. Whilst they have been pivotal for identifying the structural motifs that exist within silk fibres, they are less suited for spatially resolving structures within a given space, especially for resolving structures at a nanoscale.

Being composed of protein, silk proteins (spidroins and fibroins) are known to have a beta sheet morphology originating from the packing of protein sequences comprised of three amino acids, glycine, alanine, and serine[17,188]. These crystalline domains are non-centrosymmetric, as a result, second harmonic generation (SHG) has been used to visualize the crystalline domains in fibroin and spider silk[111]. However, fibroins and spidroins contain several other amino acids that are present in amorphous regions. Of particular interest are the amino acids known to be fluorescent such as tryptophan, tyrosine, and phenylalanine, with tryptophan being the most responsive[189]. Using time correlated single photon counting fluorescence lifetime imaging (FLIM), the nanosecond timescale dynamics can be captured. This is due to the time a fluorescent center spends in the excited state before emitting a photon is directly related to the local dynamics, which takes place at the order of nanoseconds[190]. The more degrees of freedom available to chain motion, the faster a photon is given off. Consequently, more tightly bound domains will take longer to fluoresce, while more mobile regions will take less time to fluoresce. In combination with SHG, FLIM can render a comprehensive 3-dimensional map of crystalline and amorphous domains with relative nanosecond dynamics in the amorphous regions.

In this work, the fibroin from three layers of cocoon from the *Bombyx mori* worms were imaged using simultaneous SHG and FLIM. Major Ampullate spider silks reeled at different speeds (20mm s^{-1}, 80mm s^{-1}) – as well as supercontracted silks – were also imaged using simultaneous SHG and FLIM. The mechanical properties of the spider silks were also tested to see if the mechanical properties of the silks corroborate the spectral data.

2. Materials and Methods

2.1 Culturing of silkworms

Bombyx mori silkworms in their V^{th} instar were obtained from a supplier (CREA-API Unità di Ricerca di Apicoltura e Bachicoltura) and cultured on normal silkworm feed.

2.2 Sample collection and processing

Cocoons spun by the silkworms were collected and kept in a freezer at -4°C until analysis. Cocoons were divided into three layers: an outer layer, a middle layer and an inner layer. This was done by carefully separating the cocoon layers with tweezers.

2.3 Degumming of Silk Fibroin

The silk cocoons were degummed using the protocol from (T. Gheysens et. al, 2011)[191].

2.4 Handling of spiders and silk collection

Nephila edulis were used as the organism of choice due to their availability and ease of handling their silks. Individual spiders were placed on polystyrene platforms and held in place with a mesh, which contained a hole where the spinnerets of the spiders were exposed. The spiders were then examined under a dissection microscope to identify the location of the different spinnerets. Individual silk fibres – identified by the spinneret they were extracted from as well as their capability to supercontract – were then pulled from the Major Ampullate spinneret onto a calibrated motorized spool.

Major Ampullate Silk (MAS) was reeled as single fibres at a rate of 20mm s^{-1}, and 80mm s^{-1} for tensile testing; the reeling speed of 20mm s^{-1} conforms to the natural reeling speed of spiders in natural conditions [169,170]. The temperature and humidity of the reeling conditions were recorded for each reeling session. Silk at the very start of the reeling procedure was not

used as the mounting procedure likely means that silks collected here are not reeled at a consistent speed. Collected samples were stored on spool segments under lab conditions (20°C, 40% RH).

Supercontracted silks were prepared by first mounting silks spun at 20 mm s^{-1} onto retractable compasses. The silks were then immersed in Type 1 water and allowed to contract until some slack was seen in the fibres. The fibres were then left overnight to remove excess water on their surface.

In theory, silks that are reeled at a high speed should have a larger proportion of β-sheets, as well as a larger degree of order within the silk fibres[147,192]. On the other hand, supercontracted fibres should have a lower degree of crystallinity as water molecules break the β-sheet structures within MAS and disrupts the ordering of the remaining β-sheets[35,193]. These effects should be reflected in the results from the mechanical tests as well as the SHG/FLIM imaging.

Individual silk fibres were mounted onto rectangular cardboard frames with an aperture of 10.4 x 5mm (for tensile testing and CSA measurements) or 5 x 5mm (for DMTA testing). Table 4.1 contains details regarding spider identity and reeling speeds used.

Spider	Reeling speed (mm s^{-1})
N1_Spd	20, 80
N2_Spd	20, 80
N3_Spd	20, 80
N4_Spd	20, 80
N5_Spd	20, 80

Table 4.1: List of spiders and the respective treatments. All silks were MAS.

2.5 Cross-sectional Area Measurement

CSA information is necessary to calculate the mechanical property parameters of interest from spider silks. Cardboard frames containing single MAS fibres were mounted onto SEM stubs with conductive tape. Samples were then sputter coated with gold/palladium metal for 150 seconds at 18 mA, giving the samples a coating of 12.5nm (Quorum Technologies SC7620). Samples were then viewed using a Jeol Neoscope JCM-5000 SEM. Images of the fibres were taken using the SEM, which were then subsequently analysed using ImageJ to obtain the diameters of the fibres. For each treatment group (including supercontracted fibres post-supercontraction), 6 fibres were measured, with 3 measurements made per fibre. The results were then averaged to obtain an average diameter. Individual MAS fibres were observed to be cylindrical and the cross-sectional area was calculated using the formula:

$$A = \pi \left(\frac{d}{2}\right)^2$$

2.6 Tensile Testing & Statistical testing

As in Chapter 3, Section 2.8.[35]

2.7 DMA measurements

All measurements were performed using a TA Instruments Q800 Dynamic Mechanical Analyser. The samples were measured in tension mode using the Tension clamp configuration. The Mass calibration of the drive clamp was determined with a one half of the cardboard frame in place in the clamp to simulate actual measuring conditions. In order to perform the measurements in an inert atmosphere, compressed Nitrogen (high purity) was connected to the DMA and used to activate the drive system. Because the gas that floats the drive system is forced into the furnace chamber, this is the most efficient and effective way of measuring

samples in an inert atmosphere. It was required to perform measurements in an inert atmosphere so that oxidation of the fibres at elevated temperatures was prevented.

The following measuring conditions were used:

Clamping configuration:	Tension
Heating rate:	3C per minute
Temperature range:	Ambient to 275C
Pre-Load (Static force)	0.003 Newtons (0.002 Newtons for SC fibres).
Strain:	0.1%
Sample length:	Approx. 5 mm
No of Strands per frame:	Single strand

5mm wide cardboard inserts were fitted into the rectangular cardboard frames (with an aperture of 10.4 x 5mm) on which the fibres were mounted to reduce the free sample length to 5mm. This was required because the initial samples prepared at 10mm length were found to have insufficient stiffness to be measured by the DMA. One side of the frame was cut away before being mounted into the tension clamps. Care was taken in aligning the frames in the clamps, and fine adjustments were made to the angle of loading such that the fibres were positioned vertically between the fixed and drive clamp.

Once the frames had been loaded, the remaining cardboard edge was cut with scissors. This was done with the drive system locked. After entering the correct fibre dimensions into the DMA instrument control software, the “measure” button was pressed. This gave an indication of the stability of the fibre in the clamp. It was found that for the reeled fibres, a static load of 0.003 Newtons gave a stable response, with no creep observed for the sample at room

temperature. For the Super-contracted samples, this static force had to be reduced to 0.002 Newtons to prevent creep whilst under load.

Table 4.2 includes the sample identity, their respective average diameter and the number of specimens tested (measured using SEM):

Sample Identity	**Mean diameter/ µm**	**No of Specimens tested**
N4 Reeled at 20mm s^{-1}	5.02	5
N4 Reeled at 80mm s^{-1}	4.91	4
N5 Reeled at 20mm s^{-1}	4.04	4
N5 Reeled at 80mm s^{-1}	3.49	5
N4 SC	5.67	3
N5 SC	4.42	3

Table 4.2: Calculated averaged diameters of the tested silk samples. SC samples were made from samples initially reeled at 20mm s^{-1}

It was found that at a reduced sample length of 5mm the stiffness of the samples increased significantly compared to samples prepared at 10mm length. Samples of 10mm length gave a Loss Modulus and Tan Delta response that bounced between positive and negative values during measurement (essentially registering zero) in the early stages. Peaks were observed in Loss Modulus and Tan Delta as the Glass transition of the silk fibres was transcended. Better results could be obtained by having double or even treble threads prepared in each frame. This would significantly increase stiffness which would in turn improve strain control. The signals

are noisy for the sample measurements and this is because the strain control was not ideal due to the low stiffness of the single thread prepared samples.

2.8 Fluorescence Lifetime Image (FLIM) and Second Harmonic Generation (SHG)

Fluorescence microscopy has been well-established in detecting biological and chemical processes well below the detection limits of traditional measurement techniques. Its unique ability to inform on local environment using fluorescence lifetime within a target sample makes it a suitable platform for detecting unique changes within a confined region in the sample. Here, optical measurements were performed using a custom-built two-photon fluorescence microscope at the National Institute of Standards and Technology (NIST). Silk fibres are excited using a Ti-Sapphire laser (Chameleon Ti:Sapphire, Coherent Inc.) operated at 810nm with a pulse width of 140fs. For B*ombyx mori* silkworm fibres, average laser power was 1mW. For MAS, average power was set to 2mW. Samples were raster scanned through the laser focus using an X-Y piezo scan stage to construct the image. The resultant beam was spectrally separated using dichroic beam splitters into two time-resolved photon counting modules. The first channel captures the auto fluorescence and fluorescence lifetime of the silk (420nm – 500nm bandpass filter). A notch filter was used to remove excitation light. The second channel captures the second harmonic generation (SHG) (400nm to 410nm) that results from the asymmetries of the beta sheet structures within the silk fibre. The intensities from each channel is recorded and outputted into separate images.

For fluorescence lifetime, the images were then analysed using SPCImage NG software package. The decay curves were fit using an algorithmically estimated IRF and fit to each pixel. Phasors were generated using the time domain methodology with equations 1 and 2

where g(ω) and s(ω) are x and y coordinates of a cartesian plot. The phasors were then exported and replotted in Origin Pro 2019.

Equation 1: $S_i(\omega) = \frac{\int_0^{\infty} I(t)\sin(n\omega t)dt}{\int_0^{\infty} I(t)dt}$ **Equation 2:** $G_i(\omega) = \frac{\int_0^{\infty} I(t)\cos(n\omega t)dt}{\int_0^{\infty} I(t)dt}$

Where ω is the angular repetition frequency of the excitation source; n is the harmonic frequency, I(t) the decay at each time in each pixel.

2.9 Image Processing

The volume fraction of SHG versus FLIM was conducted using ImageJ and custom MATLAB scripts (written and provided by NIST). The images were binarized with the SHG or FLIM containing pixels set as white. Background noise was removed by either setting the image threshold function in ImageJ to 5, or by subtracting the average background intensity from the image in MATLAB. The white pixels were then counted to determine the area or number of white pixels per optical slice. The z-stacks were then summed up and a percent crystallinity was determined by the number of SHG pixels divided by the number of SHG plus the number of FLIM pixels. This was done with the assumption that either signal (SHG and FLIM) can occupy the same pixel.

3. Results

3.1 SHG/FLIM imaging of *Bombyx mori* cocoon layers

The primary structure of silk fibroin proteins has been well documented[5,43,188,194–198]. Given that the beta sheets that comprise the crystalline domains are composed of fluorescent inactive moieties, any fluorescent amino acids will be located in the amorphous region. Figure 4.1 displays SHG/FLIM images obtained from silkworm fibres of different cocoon layers. Figure 4.2 represent phasor plots which give further detail on the fluorescence lifetimes (FL) of motifs in different regions of silks. Figure 4.3 gives a graph where we try to correlate the SHG/FLIM ratios obtained from our samples from different cocoon layers to the mechanical data of silkworm silks of different cocoon layers in the literature.

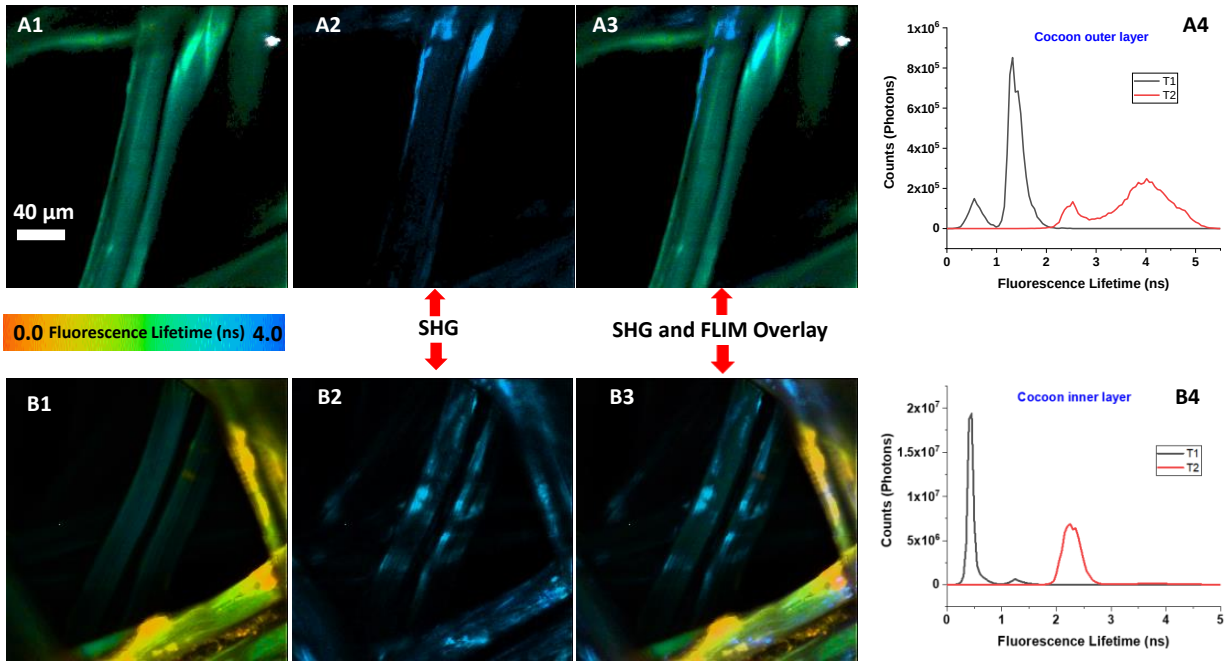

Figure 4.1. False colour images of the outer (B) and inner layer of a cocoon from *Bombyx mori*. False Color images of the amino acid fluorescence lifetimes (A1 and B1). Crystalline domains as shown by SHG for the outer (A2) and inner layer (B2) of the cocoon. (A3 and B3) composite images of the SHG and FLIM. (A4 and B4) Plots of the fluorescence lifetime distributions for the outer (A4) and inner layer(B4). T1: Fluorescence lifetime (FL) for regions around the crystalline domains. T2: FL for regions in the amorphous phase.

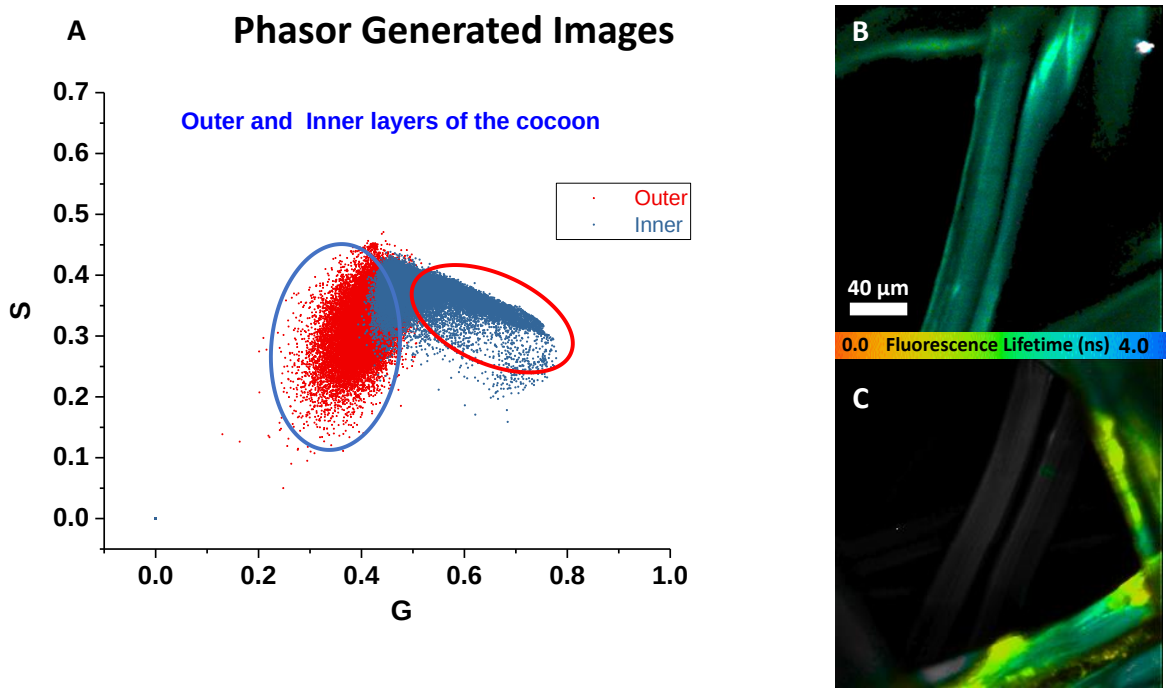

Figure 4.2. (A) Plot of phasors for the outer and inner layer of a cocoon from *Bombyx mori*. Phasors towards larger G indicate a shorter lifetime, while plots to higher S indicate a longer lifetime. Both indicate dominance of two different lifetimes. Corresponding false color images of fibroin fibers from the outer (B) and inner (C) layers of the cocoon. Images processed with the same color scale to show differences in mobility about the fibers.

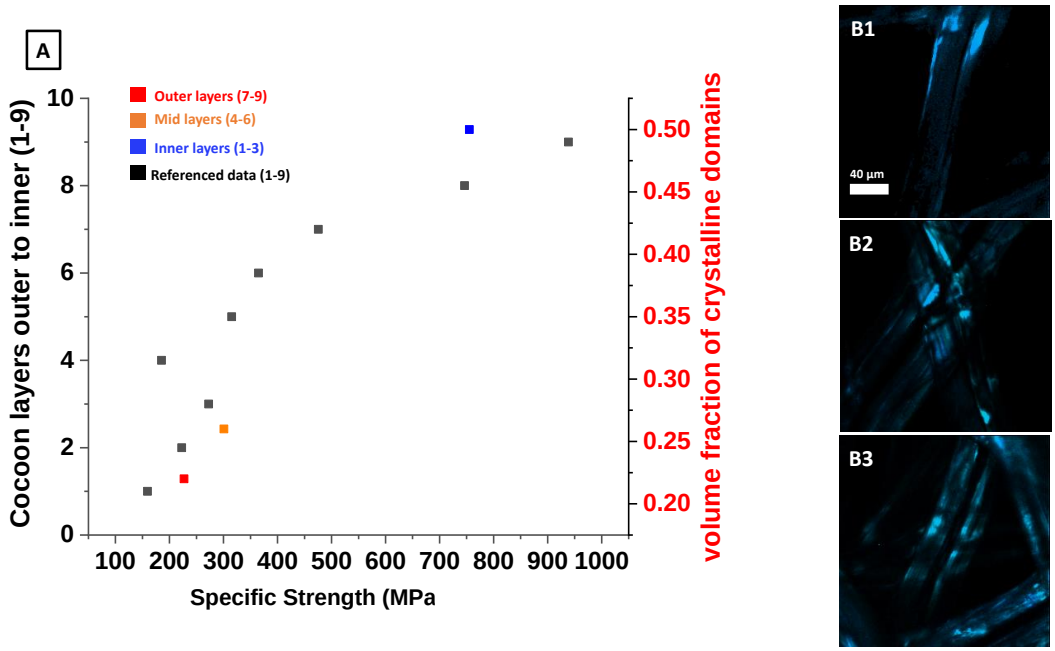

Figure 4.3. A. Compound plot of silk fibroin specific strength as a function of cocoon layer and volume fraction of crystalline domains as a function of layer strength average. The specific strength for the crystalline domains were plotted as an average of three layers. For example, layers 1-3 specific strengths were averaged, and this value was plotted vs the volume fraction of crystalline domains.
B1-B3. Sample optical slices used in the SHG volume fraction determination in descending order. Outer (B1), middle (B2), and Inner layer (B3). Referenced data was obtained from (Chen F, *et al*, 2012)[199]

From the SHG/FLIM images, we confirm that we were able to obtain distinct regions that produced SHG and fluorescence signals. We also noticed that going from the outer to the inner layer of *B. mori* cocoons, the SHG/FLIM ratio – i.e. the proportion of crystalline to non-crystalline regions – increases (Figure 4.1). As of now, it is not known whether this is a functional evolutionary trait whereby the silkworms actively alter the properties of silks as they spin the cocoons, or if this is simply a side-effect from the spinning process of silkworms. Additionally, we can see from the images that the degumming process was not complete as there is some residual sericin, which may also affect our results and interpretation. However, the mechanical properties of silkworm silks from these different layers seem to align with the change in SHG/FLIM ratio, as seen in Figure 4.3.

Additionally, we find that within fibres of a particular layer the lifetime of fluorescing moieties located close to the crystallites (T2 in Fig 4.1 (A4 and B4)) have shorter lifetimes compared to fluorescing moieties located deeper within the non-crystalline regions (T1 in Fig 4.1 (A4 and B4)). This suggests that the motifs containing these fluorescing moieties are less mobile and thus less likely to disperse their energy as fluorescence when located closer to the crystallites, when compared to motifs deeper within the non-crystalline regions. This result is shown in more detail in the Phasor plots as in Figure 4.2.

3.2 SHG/FLIM imaging of *Major Ampullate Silk (MAS)*

We compared the SHG signal to the fluorescence signal to determine the effect of reeling speed on the crystalline phase within the silk fibres. The captured images (128 x 128 pixels, 20um x 20um) were post-processed and binarized with a custom script. The SHG/FLIM signals are compared per pixel to qualitatively determine the amount of crystalline phase within the fibre.

Figure 4.4 below shows the (A/D) FLIM and (B/E) SHG image of MAS reeled at 20 mm/s and 80 mm/s. Background noise is more pronounced in the SHG image for the standard rate (20mm/s) reeled fibres due to the lower crystalline content. When overlaid, fibres reeled at faster rates yielded stronger SHG signal, suggesting the presence of higher crystalline content within the fibre. It is worthwhile to note that for supercontracted samples, the SHG signal is considerably lower than those of the standard and fast reeled samples (Figure 4.5), which is indicative that the SC process disrupting the crystallization process of the fibre.

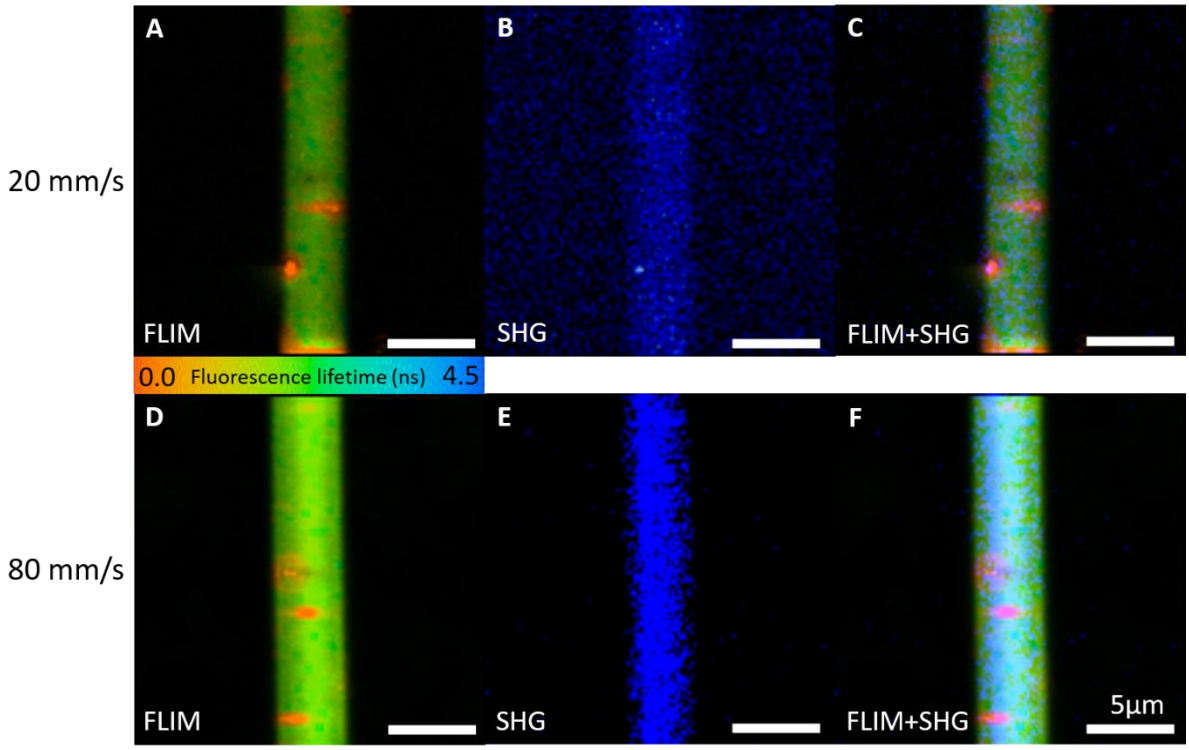

Figure 4.4. FLIM, SHG, and FLIM+SHG images for MAS reeled at 20 mm/s and 80 mm/s. Fibres reeled at higher speeds resulted in stronger SHG signals, suggesting greater crystallinity within the fibre. **GET SC DATA**

The results of the SHG and FLIM ratios are summarized in Table 4.3 and Figure 4.5. For all MAS tested across three spiders and three treatments, the qualitative trend is consistent: fibres reeled at higher (80mm/s) speeds resulted in moderate increase in the SHG signal and therefore crystallinity. For supercontracted fibres, however, a significant drop in the SHG signal can be observed.

Spider	Treatment	SHG/FLIM+SHG Ratio
N1_spd	20 mm/s	0.566 ± 0.010
	80 mm/s	0.627 ± 0.227
	SC	0.025 ± 0.002
N2_spd	20 mm/s	0.423 ± 0.014
	80 mm/s	0.617 ± 0.440
	SC	0.130 ± 0.102
N3_spd	20 mm/s	0.375 ± 0.028
	80 mm/s	0.408 ± 0.061
	SC	0.025 ± 0.011

Table 4.3: SHG/FLIM ratio of the various treatment of the samples.

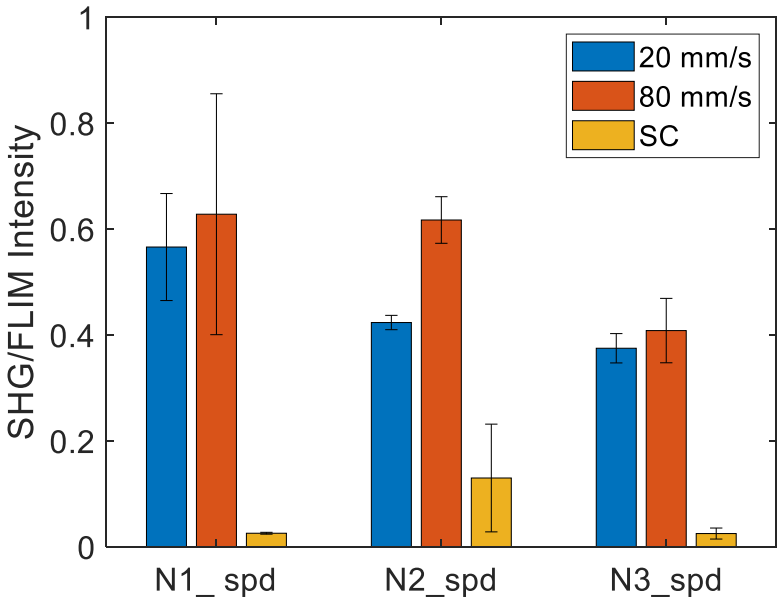

Figure 4.5: SHG/FLIM ratio of imaged MAS fibres.

3.3 Tensile tests

Zwick tensile testing was done to ensure that the effect of reeling speeds on spider silk mechanical properties lines up with what is known in the literature[145,192] as well as our hypothesis. Whilst not a direct reflection of crystallinity within the silks, it is a useful proxy and a simple enough experiment to carry out as a preliminary screening.

Figure 4.6 displays representative stress-strain graphs for the tested samples from N1-N3_Spd. Figure 4.7 and Table 4.4 depict the results obtained from the Zwick tensile tests (N = 3-5 per treatment group per spider).

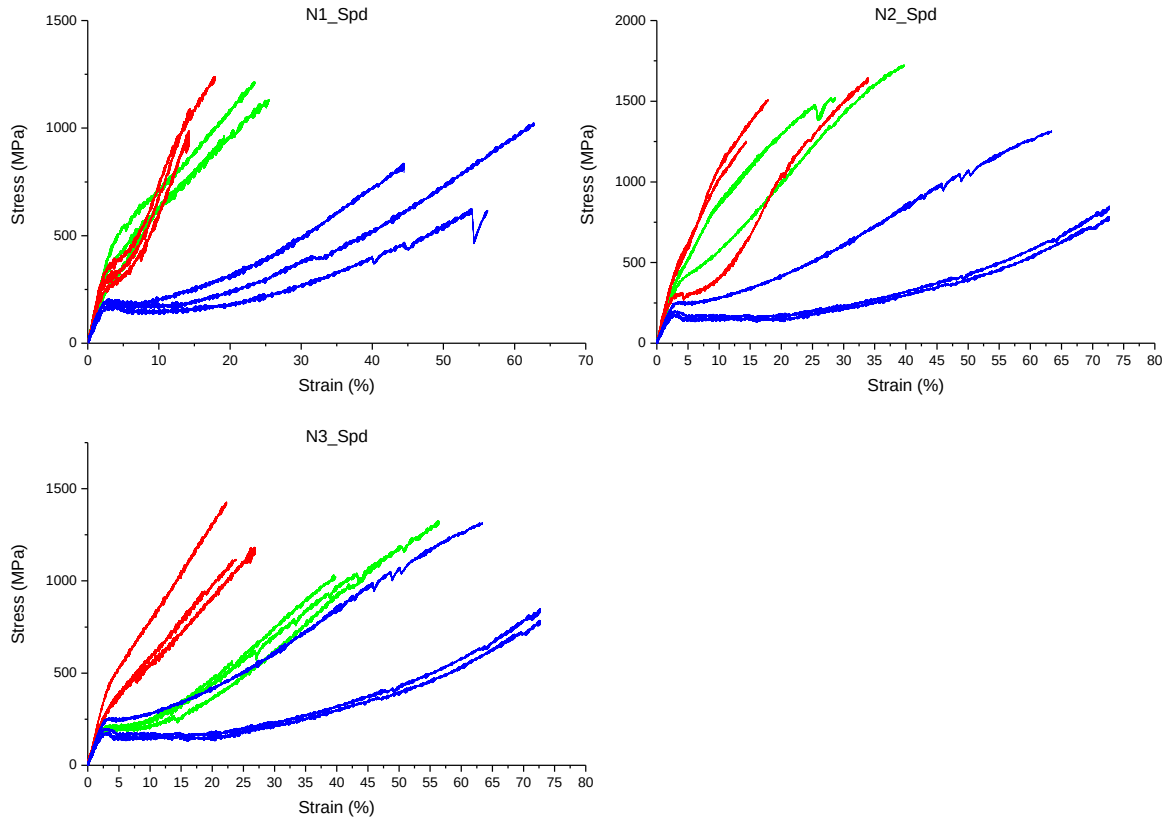

Figure 4.6: Representative stress-strain graphs for N1, N2 and N3_Spd. Green lines: samples reeled at 20mm s^{-1}. Red lines: Samples reeled at 80mm s^{-1}. Blue lines: Supercontracted samples produced from samples reeled at 20mm s^{-1}.

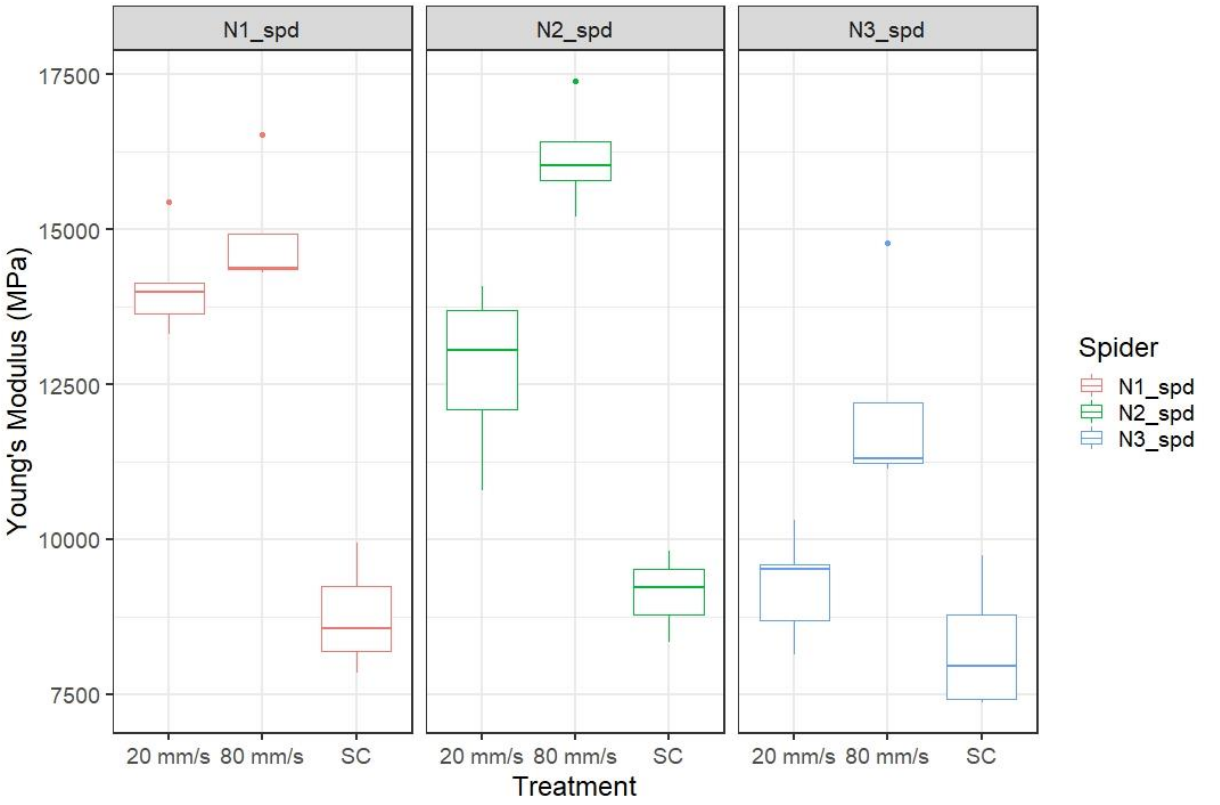
N1_spd
N2_spd
N3_spd
Young's Modulus (MPa)
17500
15000
12500
10000
7500
20 mm/s
80 mm/s
SC
Treatment
Spider
N1_spd
N2_spd
N3_spd

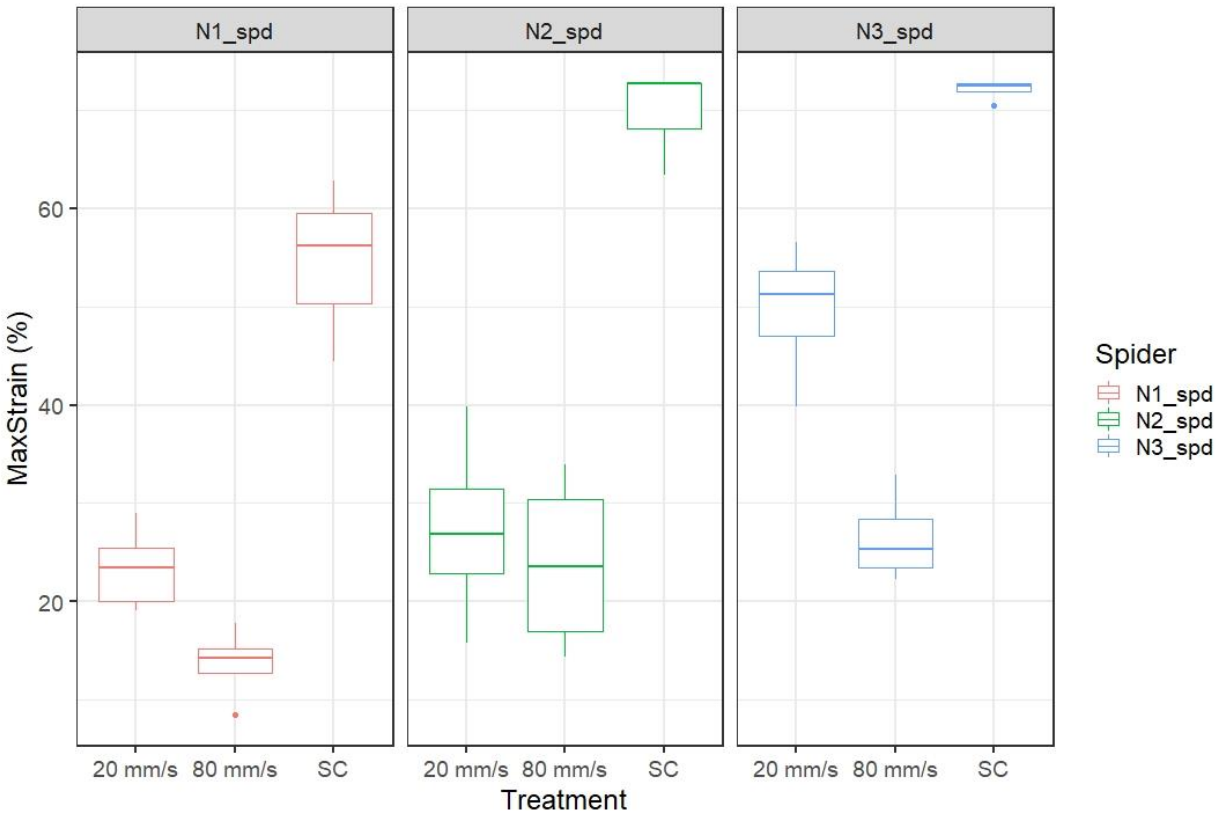
N1_spd
N2_spd
N3_spd
MaxStrain (%)
60
40
20
20 mm/s
80 mm/s
SC
Treatment
Spider
N1_spd
N2_spd
N3_spd

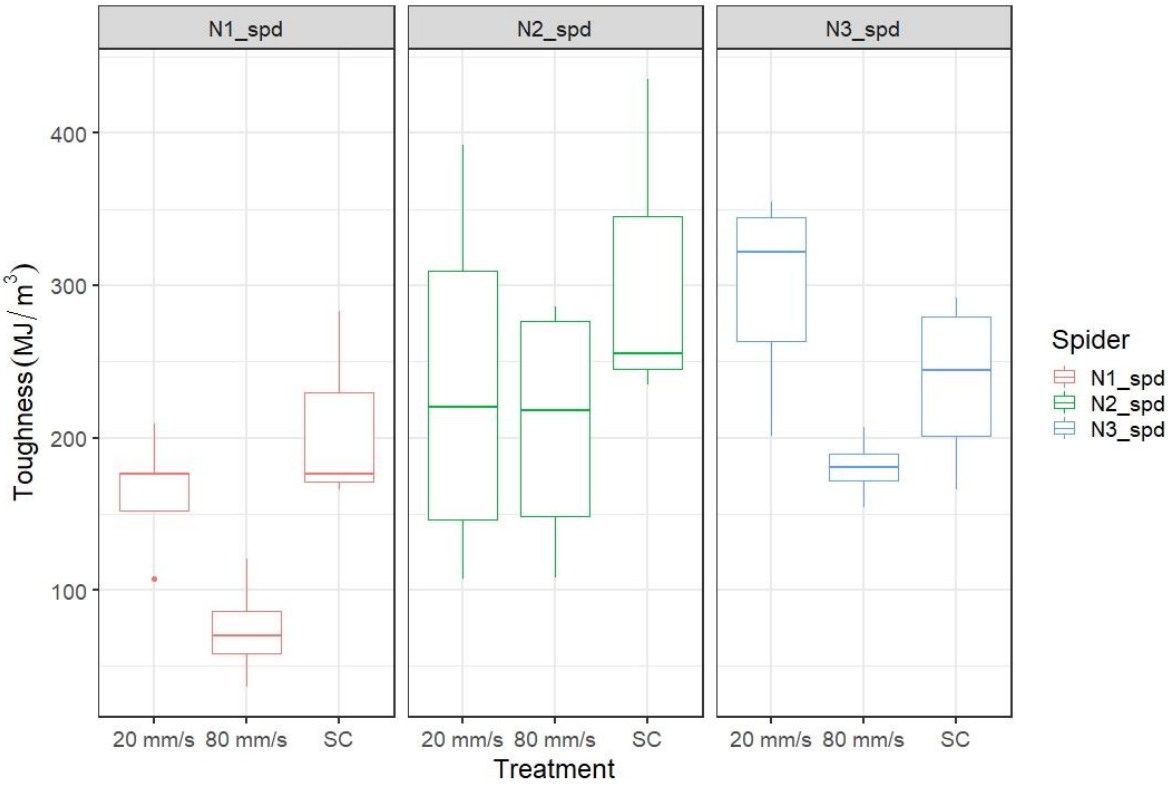

Figure 4.7: Visualisation of stress-strain data obtained from spider silks reeled at different speeds.

Spider	Treatment	Max Force at break	Max Stress at break	Young's Modulus	Max Strain at break	Toughness
N1_spd	20 mm/s	0.010044 ± 0.000896	1137.742 ± 101.4556	14100.28 ± 814.0227	23.44538 ± 4.036964	164.5506 ± 37.72782
N1_spd	80 mm/s	0.007567 ± 0.001353	1029.616 ± 184.1471	14899.87 ± 1090.467	13.72916 ± 3.837077	74.45361 ± 34.91626
N1_spd	SC	0.00924 ± 0.002219	0.00924 ± 0.002219	8780.238 ± 1069.455	54.47146 ± 9.255652	208.4662 ± 64.86584
N2_spd	20 mm/s	0.013769 ± 0.0035	1341.542 ± 340.9762	12744.96 ± 1454.157	27.36088 ± 9.898223	235.1792 ± 127.6145
N2_spd	80 mm/s	0.013818 ± 0.001676	1512.104 ± 183.3749	16172.73 ± 910.1811	23.82746 ± 9.227214	207.5623 ± 86.45735
N2_spd	SC	0.012517 ± 0.003677	983.6763 ± 288.9674	9125.497 ± 736.4379	69.59205 ± 5.371707	308.3963 ± 110.5656
N3_spd	20 mm/s	0.011121 ± 0.001084	1190.144 ± 116.0092	9249.796 ± 842.6008	49.64916 ± 6.497993	297.1742 ± 64.43849
N3_spd	80 mm/s	0.008597 ± 0.000925	1242.306 ± 133.6274	12129.32 ± 1767.434	26.48693 ± 4.695314	180.7043 ± 21.80405
N3_spd	SC	0.008165 ± 0.002156	736.7128 ± 194.547	8257.105 ± 1106.423	72.02468 ± 1.034594	236.4298 ± 58.04542

Table 4.4: Summaries for the different parameters obtained from the stress-strain samples. Values represented are (Mean ± Standard deviation of the sampling distribution).

The values obtained from the tests are as expected from our hypothesis and is not out of the ordinary compared to values of similarly tested spider silks in the literature[169,200–202]. The trends we see are as expected as well; the silks reeled at a high speed have a higher modulus and a lower flexibility. This result is reversed for the supercontracted silks.

A mixed-effect model was applied to the data to test for statistical significance between the different treatments. The model pools data from all three spiders and takes into account intraspecific variability when calculating statistical difference. The results are summarised in Table 4.5.

Treatment	Parameter	Effect size	df	t-value (T)	p-value (P)	Marginal coefficient	Conditional coefficient
80 mm/s	Young's Modulus (MPa)	2356.31 ± 530.71	33	4.440	< 0.001	0.5708682	0.7838187
80 mm/s	Maximum Strain (%)	-12.558 ± 2.826	33	-4.443	< 0.001	0.739402	0.8777621
80 mm/s	Toughness (MJ/m^3)	-79.916 ± 27.825	33	-2.872	< 0.01	0.2014179	0.4062915
Supercontracted	Young's Modulus (MPa)	-3188.15 ± 558.72	33	-5.706	< 0.001	0.5708682	0.7838187
Supercontracted	Maximum Strain (%)	31.209 ± 2.976	33	10.488	< 0.001	0.739402	0.8777621
Supercontracted	Toughness (MJ/m^3)	13.099 ± 29.292	33	0.447	0.658	0.2014179	0.4062915

Table 4.5: Results for the mixed-effect model applied to analyse the mechanical data. The 20 mm/s samples were considered the control group, thus the values seen are comparisons of the 80mm/s and supercontracted samples against the 20 mm/s treatment group. Values in the 'Effect size' column represent (Mean ± Standard deviation).

From the mixed effect model, we see that compared to 'standard (20mm/s)' silks, there is a significant difference in Young's Modulus (stiffness) and maximum strain at breakage (flexibility), with faster reeled samples having a higher stiffness and lower flexibility and vice versa for supercontracted samples. Again, this lines up with our expectations.

With regards to the Toughness parameter, we see a significant reduction in toughness for fast reeled spider silks compared to standard silks, which again is expected[170,203]. However, we see no significant difference in the toughness of SC fibres compared to standard fibres. This result could simply be due to insufficient sample size; further testing would be required to confirm this.

The marginal and conditional coefficients for the Young's Modulus and Maximum strain parameters suggests that a large proportion of the variation within the dataset can be

explained by the fixed effect. This is not the case however for the Supercontracted samples, which might further explain the result observed above.

3.4 DMTA results

DMTA testing will provide information regarding the crystallinity and proportion of non-crystalline regions within silks. It will also provide information regarding the glass transitions of the tested silk samples. The results for fibres from each treatment group were repeatable and consistent. Thus, representative DMTA results for each treatment is displayed in Figure 4.8. A comparison of Tan delta curves is shown in Figure 4.10. The data from other tested samples can be found in the Supplementary Information.

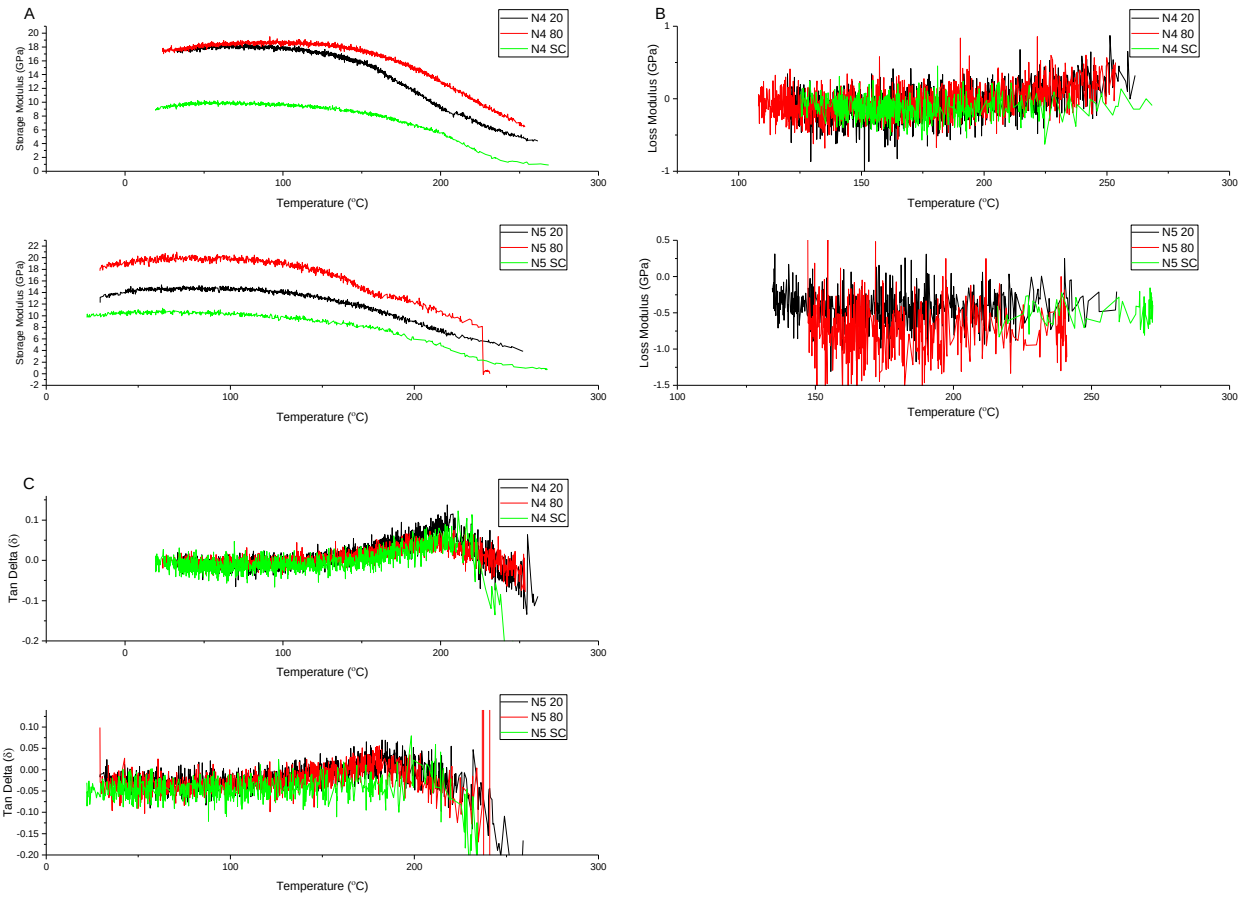

Figure 4.8: Comparison of DMTA results for silks from different treatment groups, taken from representative samples. (A) Storage modulus of tested MAS. (B) Loss modulus of tested MAS. (C) Tan delta of tested MAS.

From the results, we can see that the silks reeled at 80mm/s have a higher storage modulus than silks reeled at 20mm/s, and that the opposite is true for SC samples. This is further confirmed by the application of a Mixed-effect model on the results for the storage modulus measured at 50°C (Figure 4.9 and Table 4.6). These results are consistent with the SHG/FLIM imaging results. It is as expected, the lower ordering of the beta structures within the fibres resulted in lower modulus. Through the SC process, the chains within the fibre become increasingly mobile, and the fibres achieve higher strain at failure under tensile loading.

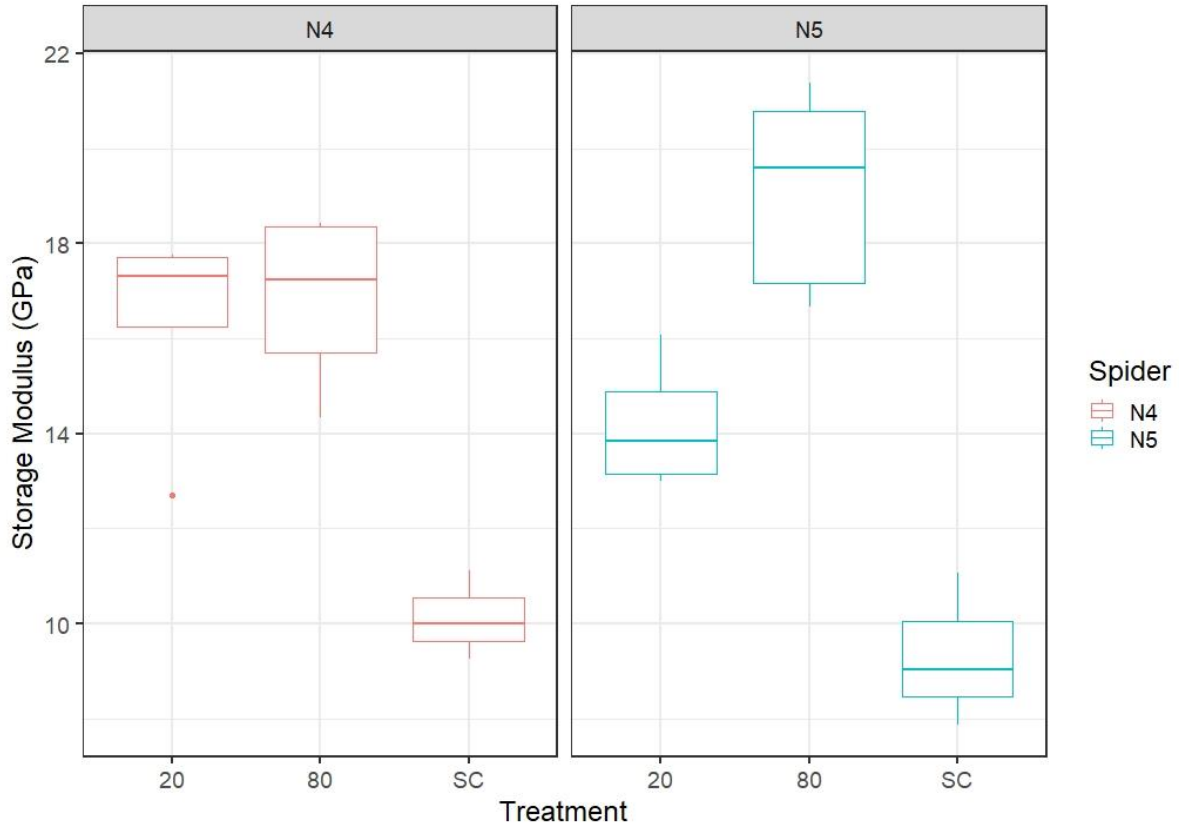

Figure 4.9: Visualisation comparison of storage modulus between differently treated silk samples

Treatment	Parameter	Effect size	df	t-value (T)	p-value (P)	Marginal coefficient	Conditional coefficient
80 mm/s	Storage Modulus (GPa)	2.7022 ± 0.8791	24	3.074	< 0.01	0.7605909	0.7605909
Supercontracted	Storage Modulus (GPa)	-5.6608 ± 0.9829	24	0.447	< 0.001	0.7605909	0.7605909

Table 4.6: Results for the mixed-effect model applied to analyse the Storage Modulus. The 20 mm/s samples were considered the control group, thus the values seen are comparisons of the 80mm/s and supercontracted samples against the 20 mm/s treatment group. Values in the 'Effect size' column represent (Mean ± Standard deviation).

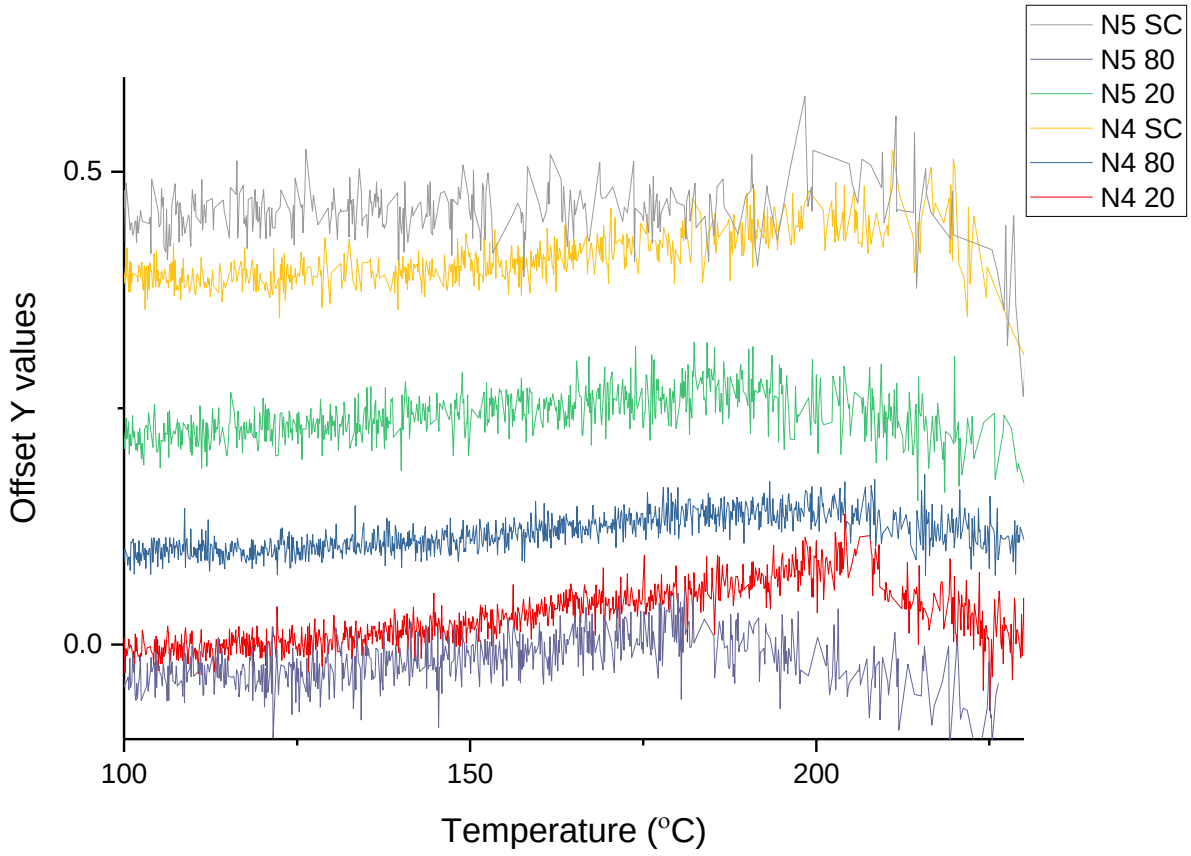

Figure 4.10: Selected Tan delta curves for the tested silk samples.

In Fig 4.8(B), we observe that the loss modulus hovers between 1 and -1 GPa, with a high amount of noise within the dataset. We theorise that this is because the stiffness obtained from the tested samples are at the lower limit of what the machine can tolerate; preliminary tests with samples with a free-length of 10mm – as opposed to 5mm – yielded even noisier

results. In the future, it would be beneficial to prepare the samples as a double strand within the cardboard frame used to hold the silk samples.

Despite the noisy signal obtained from the loss modulus results, we were still able to obtain usable tan(δ) curves for the different treatments. From these results, we were able to estimate the glass transition temperature (T_g) of the different samples. As seen from Fig 4.8 (C), Fig 4.10 and S1, we note that the T_g of silks reeled at 20mm/s and 80mm/s seems to be in between 190°C and 205°C; the expected T_g from *N. edulis* MAS reeled at 20mm/s is 194°C [204].

Unfortunately, the tan(δ) curves are too noisy to accurately resolve any differences in T_g between the three different silk types. In theory, we would expect a decrease in T_g going from silks reeled at 80mm/s, to silks reeled at 20mm/s and finally supercontracted silks, as the mobility and fraction of non-crystalline regions of silks increase. This experiment will be repeated in the future using double stranded samples to investigate the issue further.

4. Conclusions

We've shown that we were able to obtain discernible SHG and FLIM signals from both spider and silkworm silks. We were able to use the ratio of SHG/FLIM to qualitatively characterise the crystallinity of the silks and provide useful insights on the effect of crystalline domains present in the fibre. In the case of silkworm silks, we were able to take this further by identifying different FLs for fluorescing motifs in different regions of silks and create a high-resolution, spatially resolved image of crystalline vs non-crystalline domains.

Additionally, we found that the imaging data corroborates the mechanical data for both spider silks reeled at different speeds and silkworm silks from different cocoon layers – the data for the latter obtained from a literature search. I believe this further supports our argument for SHG/FLIM imaging being an informative and useful technique for spatially resolving the structure of silks.

5. Discussion

We managed to develop a novel multi-spectral imaging technique that is able to spatially-resolve crystalline and non-crystalline structures within silks at the micro-scale. In addition, we are able to quantify the fluorescence lifetimes of said structures. These findings are useful for a myriad of reasons: it is a relatively non-invasive technique that can help explain the mechanical properties of tested materials by relating the properties to the proportion of crystalline vs. non-crystalline motifs, as well as by resolving the proportions of the two regions, and by quantifying the degree of mobility of structural motifs within the material. This makes the technique useful not just for studying silks, but for any material of a viscoelastic nature. The technique may also help explain why certain materials display mechanical variation despite being produced from the same feedstock, thereby linking the effects of environmental factors and variation in the spinning process to a tangible structural difference in the material.

Specifically for silks, the technique may also help explain protein dynamics that occur in the amorphous regions. This is because fluorescence lifetime is a useful indicator for determining they type of environment an imaged motif of interest is in. Couple with data from DMTA, a tangible link between mechanical properties – such as T_g – can be explained by FL data and the spatial relationship between crystalline and non-crystalline motifs.

6. Future work

Despite the success we achieved from the work on this chapter, there are several unanswered questions and gaps in our knowledge. Firstly, we were not able to accurately resolve the T_g for silks reeled at different speeds. It is possible that the fluorescence lifetime data for spider silks from the different treatment groups may shed more light on this matter, as a significant shift in the SHG/FLIM ratio, as well as a shift in FLs would help explain and corroborate data obtained from any T_g shift obtained.

Speaking of which, we have yet to perform a detailed analysis of the FL data obtained from our imaging experiments on spider silks. This data has been collected, however due to the Covid-19 pandemic which led to delays on multiple ends, we did not have time to analyse and incorporate this data at the time of writing.

Additionally, there is still additional work that can be done with regards to the DMA experiments. Certainly, additional repeats using double stranded samples would greatly increase the stiffness of the tested samples and reduce the ambiguity of the loss modulus and the tan delta signals. Porter's Group Interaction Modelling can be applied to the T_g data in conjunction with peptide group contributions to calculate the degree of structural disorder[204] for the differently treated silks.

Another interesting experiment would be to perform forced reeling of silkworms[205] and follow up with the aforementioned SHG/FLIM analysis. This would potentially allow us to

control for the unpredictability of silkworm spinning behaviour during the spinning process and focus on fixed effects of interest such as spinning speed or humidity during spinning.

Lastly, it would be interesting to perform SHG/FLIM measurement on MAS from different species of spiders, or even different silk-types from the same spiders. Ideally this would be corroborated with mechanical and proteomic data to find relationships between primary structure, conditions during spinning and the spatial-relationship of crystalline and non-crystalline regions.

Acknowledgements

I thank Jeremiah Woodcock and Shawn Chen from NIST for performing the SHG/FLIM imaging on silkworm silks and spider silks respectively, for writing the MATLAB script necessary for performing the SHG/FLIM calculations, as well as the follow-up discussion and analysis of the data obtained. I also thank Nicholas Hawkins for performing the DMTA measurements on the spider silks. Finally, I thank Juan Guan for her expert input related to the DMA results obtained, as well as suggestions for increasing the fidelity of future DMTA measurements.

Supporting information

S4.1: Collated results from DMA tests

N4 Reeled at 20 (Five runs overlaid)

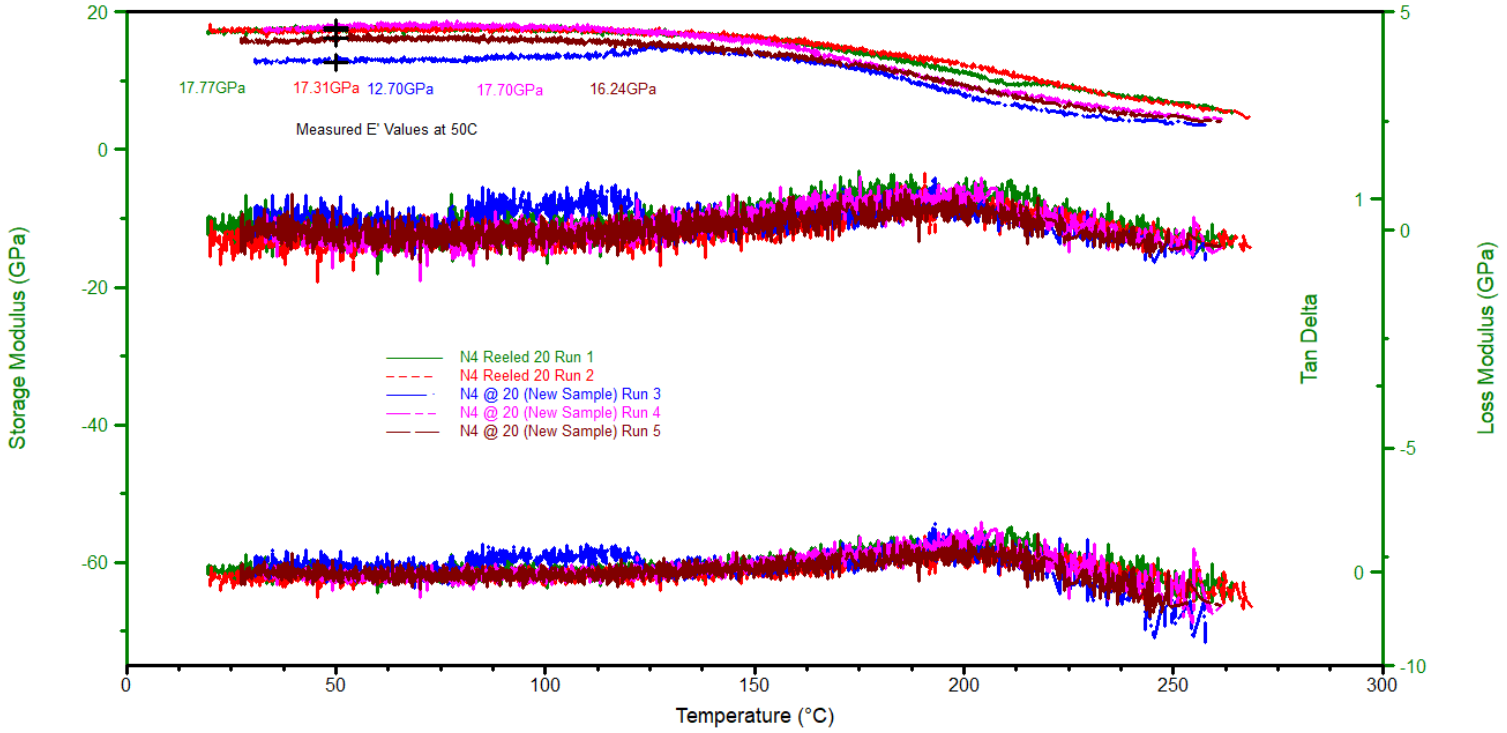

N4 Reeled at 80 (Four Runs Overlaid)

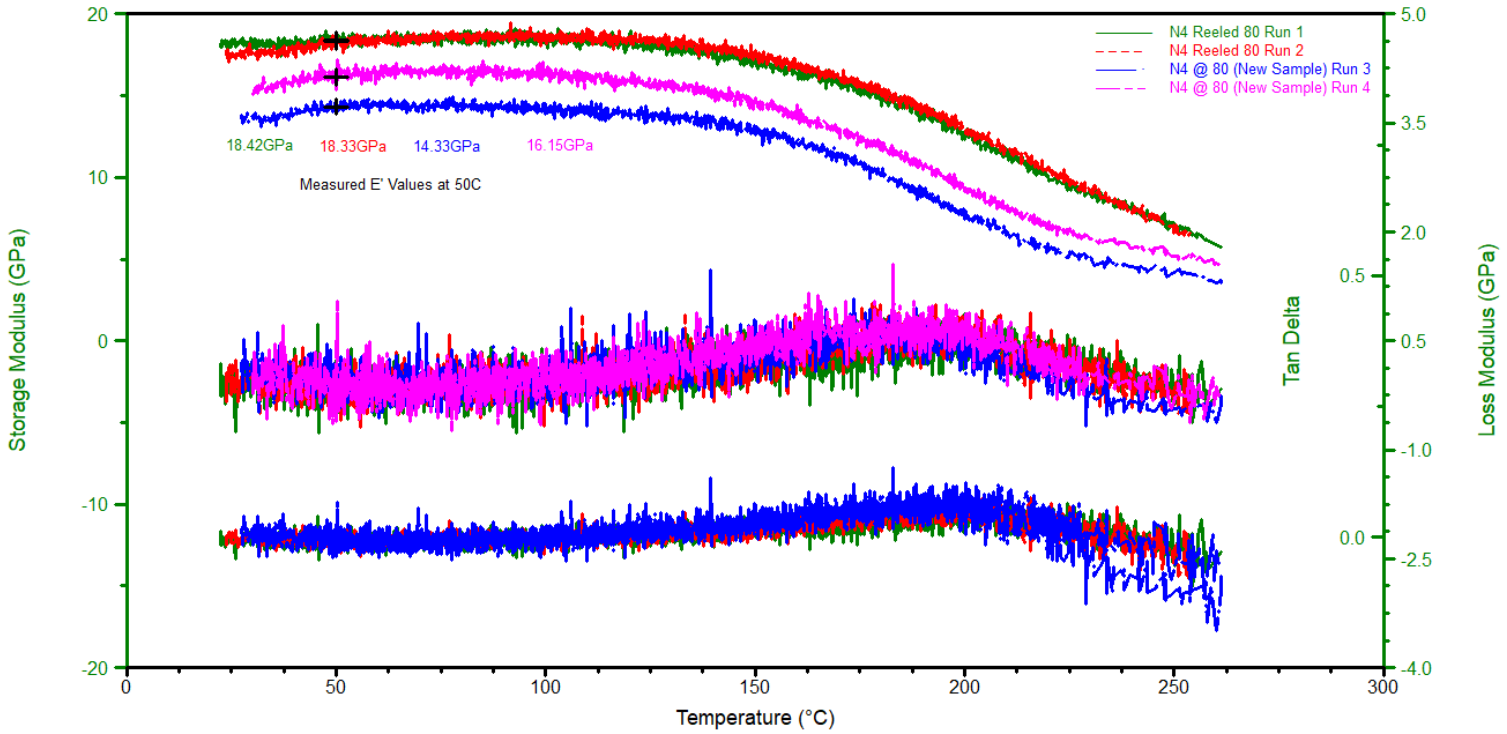

N5 Reeled at 20 (Four runs overlaid)

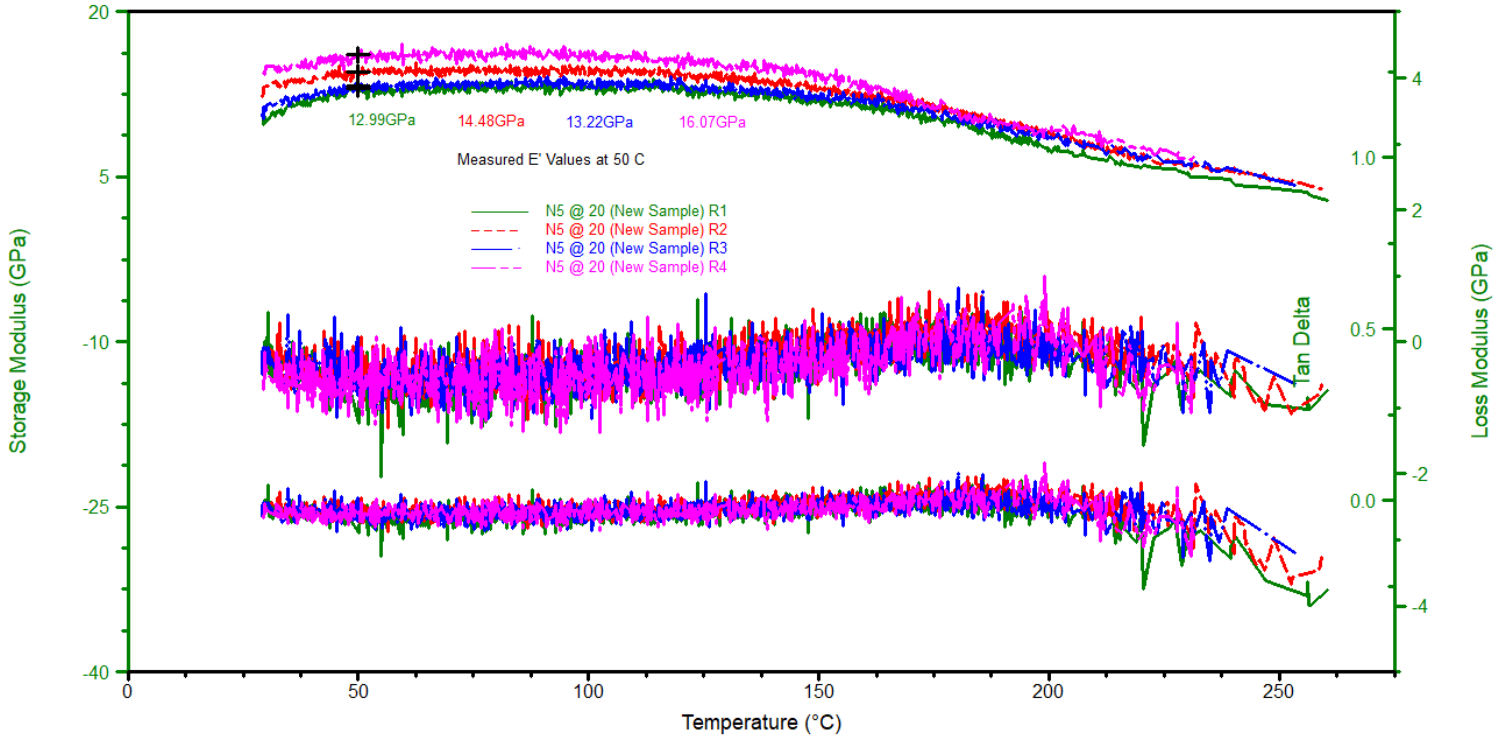

N5 Reeled at 80 (Five runs overlaid. Note Run 1 broke early into the measurement)

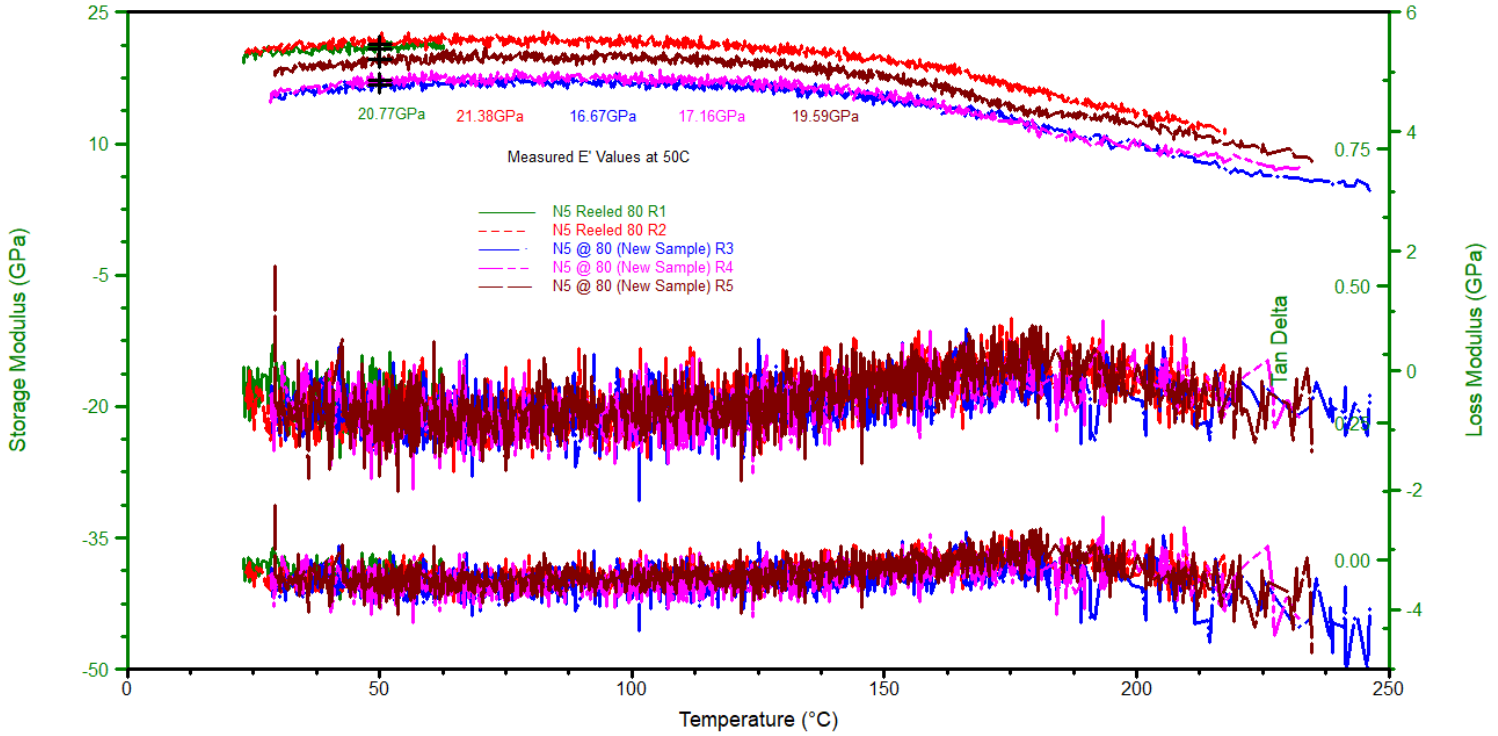

N4 Super-contracted (Three runs overlaid)

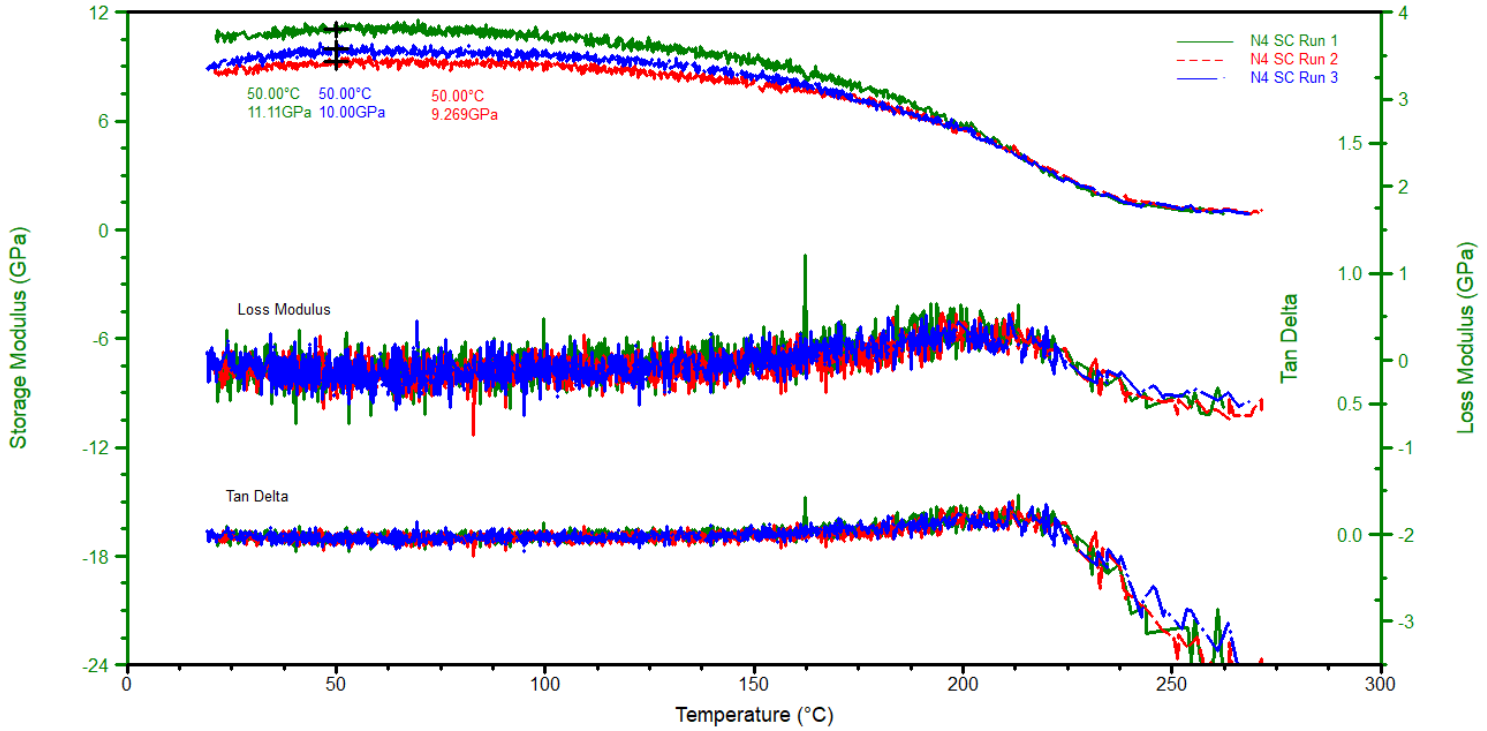

N5 Super-contracted (Three runs overlaid)

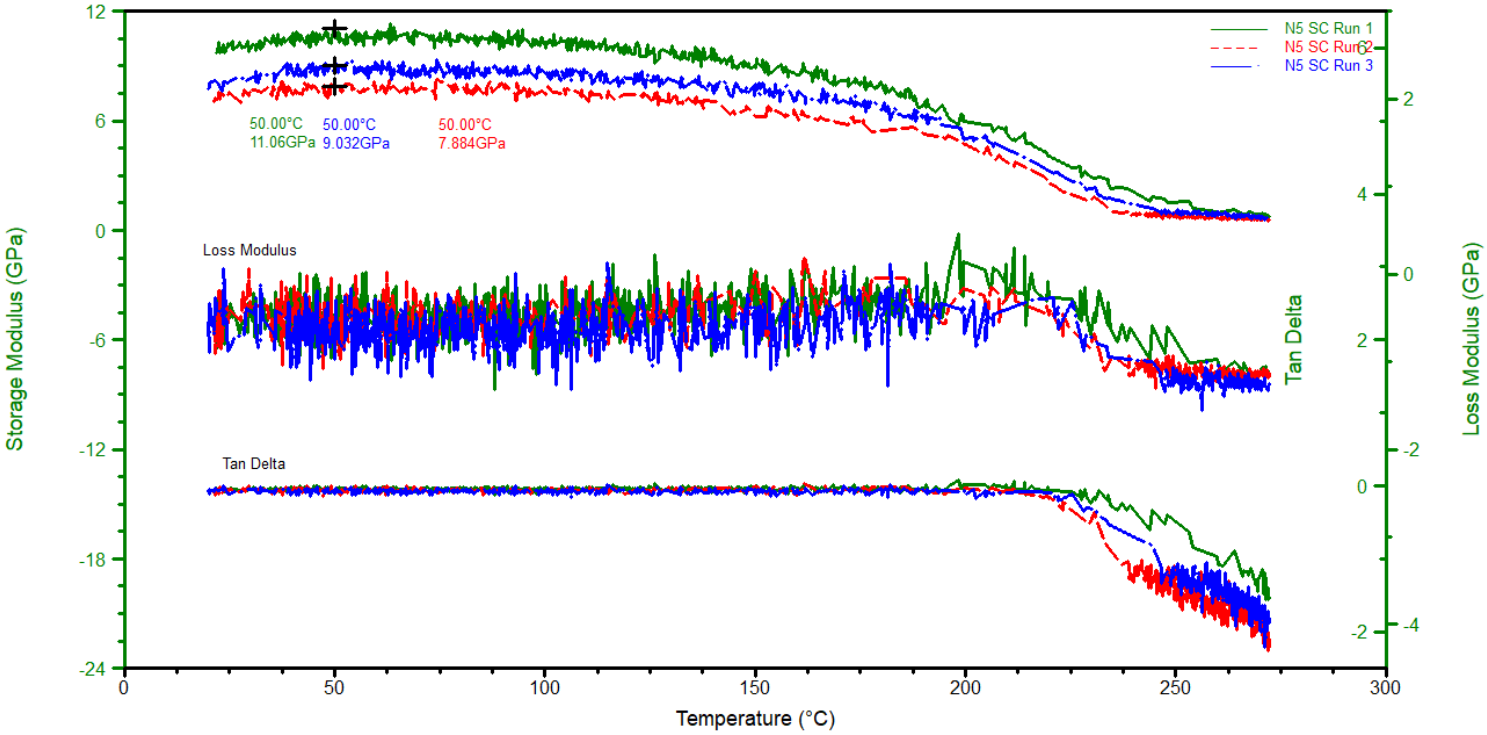

Chapter 5: An investigation into the feasibility of incorporating nanoparticles into spider silks via direct feeding.

1. Introduction

A myriad of biomaterials exist in our world, many of which serve important mechanical functions for the organisms that produce them. Examples include wood, sea shells, glass sponge skeletons and silks[206,207]. These materials often possess a combination of strength, toughness or flexibility that allow them to fulfill their function. In some cases – silks for example – the combination of mechanical properties found in biomaterials surpasses that of man-made polymers [4,43]. What's more remarkable about this feat is that Nature does so using a limited array of starting materials that on their own are inherently weak or brittle: cellulose for wood, calcium carbonate for sea shells, glass for sea sponge skeletons, and proteins for silks. Nature solves this issue by constructing materials with structural hierarchy across multiple length scales [145,208,209].

Of late, there is increasing interest in creating composite materials by combining biomaterials with man-made nanoparticles; the objective being to create new materials with novel properties, or to enhance the properties that exist within one of the materials. Recent examples include compositing biomaterials such as cellulose or silk proteins with nanoparticles [210–214]. One group of man-made materials that have been receiving a lot of research and industrial attention are carbon-based nanoparticles which include carbon nanotubes, graphene, and carbon nanodots. The combination of their small size, chemical inertness, conductivity, and high stiffness has allowed researchers to use them for a myriad of applications including the production of high-modulus materials, novel sensors, conductors, bioencapsulation, photocatalysts, and targeted drug-delivery mechanisms[215–224]. Unsurprisingly, they've also been used to produce bio-composites.

There is a caveat often associated with this process: the biomaterial needs to be broken down into its constituent components before it can be mixed with the nanoparticle of choice. This in turn usually destroys the structural hierarchy that confers the biomaterial's favorable properties.

A potential solution to this conundrum would be to feed organisms of interest nanoparticles; the idea being that the organisms will ingest the nanoparticles and incorporate them within the biomaterials of interest. Several groups purportedly achieved this feat in spiders[114] and silkworm silks [113,164], with claims of improving the mechanical properties of the silks with little to no effect on the organism of interest. However, there are several critiques to be found with regards to the methodology used in the studies. Some of the studies fed the spiders and silkworms by spraying dispersions of nanoparticle solutions into the environment of the organisms, which is also the environment that they produced silks in[113,114]. This greatly increases the likelihood of contamination of samples by nanoparticles from the environment, making positive results for detection of these nanoparticles in silks via surface-dependent techniques such as Raman Spectroscopy questionable. Closer inspection of tensile test results from one of the papers[114] reveals that only a very small subset of spiders (2 of 15) displayed improvements in the mechanical properties of their silks post-feeding. Additionally, the collection and testing procedure of the spider silks was not done in a controlled manner; spider silks are highly sensitive to changes in reeling conditions and sample preparation and improper handling of samples can lead to erroneous conclusions from tensile tests. The combination of these two factors means that there is no guarantee that nanoparticles improve the mechanical properties of spider silks should they go in, and indeed we cannot use improvements in mechanical properties as a proxy for nanoparticles being incorporated into spider silks.

Clearly, there is a need for replicating such works with more stringent methodology to validate the claims of carbon-based nanoparticles entering and improving the mechanical properties of silks, especially since evidence for carbon-based nanoparticles trespassing biological barriers such as the barriers within the gastrointestinal tract (GIT) remain contentious at best [225,226]. In this chapter, I will explore the feasibility of incorporating nanoparticles into spider silks via ingestion using feeding and silk collection methods that minimize the risk of contamination from the environment. In addition to the nanoparticles that have been claimed to be incorporated in the past (graphene and carbon nanotubes), I will also use Graphene Quantum Dots as another candidate. Graphene Quantum Dots are much smaller in size compared to graphene and carbon nanotubes so represent the most likely candidate for nanoparticle incorporation. These quantum dots also fluoresce, which will provide another method for their detection within silks should they be incorporated.

2. Materials and Methods

2.1 Nanoparticle Solutions

Graphene Oxide (GO), Single Walled Carbon Nanotubes (SWNT), 1mg/mL Blue Fluorescent Graphene Dot Solution (GbQD) and 1mg/mL Green Fluorescent Graphene Dot Solution (GgQD) were obtained from Sigma-Aldrich. GO and SWNT were weighed and mixed with water in 1.5mL Eppendorf tubes to form 1mg/mL dispersions. To mix and disperse the nanoparticles, the Eppendorf tubes were sealed and ultrasonicated for 20 minutes. The GbQD and GgQD solutions arrived as dispersed 1mg/mL solutions, thus required no further processing. All dispersions were stored in a fridge at 4°C when not in use. I further dispersed the GO and SWNT nanoparticles in solution by sonicating the Eppendorfs containing the nanoparticles for 5 minutes prior to feeding the spiders with the nanoparticle dispersions.

2.2 Spiders

Adult *Nephila edulis* spiders were used for the experiments. To ensure easy identification of spiders, individual spiders were kept in separate labelled frames throughout the duration of the experiment. The bottom of the frames were layered with waxed baking parchment to allow for easy collection of the spider's excretory products.

2.3 Reeling and feeding procedure

Individual spiders were placed on polystyrene platforms and held in place with a mesh, which contained a hole where the spinnerets of the spiders were exposed. The spiders were then examined under a dissection microscope to identify the location of the different spinnerets. Individual silk fibres were then pulled from the Major Ampullate spinneret onto a calibrated motorized spool. Direct reeling in this manner – alongside isolating the reeling process away from the environment that the spiders were kept in – minimizes the likelihood that samples are contaminated by nanoparticles that might be in the environment. Major Ampullate Silk

(MAS) was reeled as single fibres at a rate of 20mm s^{-1} for tensile testing, and as bundles at 40mm s^{-1}. These two reeling speeds are within the natural range for spinning [200]. The temperature and humidity of the reeling conditions were recorded for each reeling session. Silk at the very start of the reeling procedure was not used. Collected samples were stored on spool segments under lab conditions (20°C, 40% RH).

Prior to feeding the spiders with any nanoparticle solution, the spiders were reeled for MAS; this represented the control samples. Subsequently, spiders were fed up to 40µL of nanoparticle solution daily for 5 days. To minimize the likelihood of cross-contamination of silk samples by nanoparticles in the environment, the feeding was done by loading a P200 Gilson pipette with the nanoparticle solution of interest and directly feeding the spider using the pipette, as opposed to spraying the spider with an aerosolized nanoparticle solution. Throughout this duration, spiders were not fed with any other food source. After 5 days, the spiders were reeled once again for MAS. The duration of 5 days was selected to minimize the effects of starvation on the mechanical properties of silks, and to allow sufficient time for molecules/particles to enter silks should they do so [48]. Details of the spider designations and the nanoparticles used are found in Table 5.1.

Spider	Treatment	Daily dosage (µL)
N1_CNT	1mg/mL SWNT solution	40
N2_CNT	1mg/mL SWNT solution	40
N3_CNT	1mg/mL SWNT solution	40
N4_CNT	1mg/mL SWNT solution	40
N5_CNT	1mg/mL SWNT solution	40
N1_GO	1mg/mL GO solution	40
N2_GO	1mg/mL GO solution	40
N3_GO	1mg/mL GO solution	40
N4_GO	1mg/mL GO solution	40
N5_GO	1mg/mL GO solution	40
N1_GbQD	1mg/mL GbQD solution	40
N2_GbQD	1mg/mL GbQD solution	40
N3_GbQD	1mg/mL GbQD solution	40
N4_GbQD	1mg/mL GbQD solution	40
N5_GbQD	1mg/mL GbQD solution	40
N6_GbQD	1mg/mL GbQD solution	40
N1_GgQD	1mg/mL GgQD solution	40
N2_GgQD	1mg/mL GgQD solution	40
N3_GgQD	1mg/mL GgQD solution	40

Table 5.1: List of spider designations and their respective treatments. CNT: Spiders fed with carbon nanotubes. GO: Spiders fed with graphene oxide. GbQD: Spiders fed with blue graphene quantum dots. GgQD: Spiders fed with green graphene quantum dots.

Single fibres or bundles of MAS were mounted onto cardboard frames with an aperture of 10.4mm x 5mm. Fibres mounted in this manner were used for tensile tests and for RAMAN spectroscopy. As for fluorescence imaging, single fibres were directly mounted onto glass coverslips which were 0.08 – 0.10mm in thickness; these were then glued onto glass slides.

2.4 Fibre cross-sectional area (CSA) measurements

As detailed in Chapter 4, Section 2.5.

2.5 Tensile tests

[35]As detailed in Chapter 3, Section 2.8.

2.6 Fluorescence imaging

Fluorescence imaging was used to determine the presence of GbQD and GgQD in silk fibres. Silk fibres that were mounted onto glass slides were imaged using an Olympus FV3000

confocal fluorescence microscope. Fibres were excited using a 405nm laser (for GbQD samples) laser or a 488nm laser (for GgQD samples) and the resulting image was recorded. Laser parameters e.g. laser power, acquisition voltage and detector gain were kept constant between the control and treatment samples per spider. The images were then analysed using ImageJ with an OlympusViewer plugin to obtain the fluorescence spectra of the fibres. *Nephila edulis* MAS silk fibres naturally fluoresce when excited by a 405nm or 488nm laser, so both intensity and emission spectra of the control and treatment groups were compared against each other to determine if there is a significant difference between groups.

The microscope was also equipped with a 405/488nm dichroic mirror, which blocks light in a sharp band around 405nm and 488nm from entering the detector. Whilst this prevents the excitation laser from entering and influencing the spectra, it also results in a sharp decrease in intensity in the region around 470nm-520nm, which is not representative of the true spectra of the samples tested. The microscope did not have a better alternative for this mirror at the time of writing.

2.7 Statistical analysis

Statistical analysis was performed in R to determine if there are significant differences in parameters of interest between the control and treatment groups. A linear mixed-effects model was used to analyse the data; this accounts for the fact that multiple samples from the same spider are more similar than samples across different spiders, thus accounting for the high intraspecific variability of mechanical properties in spider silks to some extent [169]. In this model, the treatment with NP solutions was the fixed effect, whereas individual spiders were considered a random effect. The Welch-Satterthwaite's method was used as a test for statistical significance.

3. Results

3.1 Tensile tests

When analysing the results of the tensile tests, there are a few key points to consider. Firstly, though the results of the analysis may indicate that the treatment has had a significant effect on the mechanical property parameter of interest, the effect size must be taken into consideration because spider silk properties are known to vary with time. In one study, it has been shown that the breaking strain of spider silks can vary up to ± 20%, and the modulus of the silks can vary by up to ± 2GPa, within a time period of 6 days [169]. Consequently, a result may be statistically significant with regards to my sampling distribution but may not be meaningful when accounting for natural temporal variation.

Secondly, changes in Young's modulus tend to be inversely correlated to changes in maximum strain or strain at break. This represents the trade-off between stiffness vs flexibility in silks. The toughness or energy absorbed before breaking should account for this relationship to some degree since toughness is calculated as the area under the stress-strain curve. Consequently, the results that would be of interest – or indicate some effect of the feeding procedure on the mechanical properties of the silks – would be consistent trends in Young's Modulus or Strain at Break of the samples between individual spiders, or an overall increase/decrease in toughness for the entire sample population after treatment.

Figures 5.1-5.3 present summaries of data for mechanical property parameters of interest. Tables 5.2-5.4 display the results for the mixed-effect model on the parameters of interest.

3.1.1 Samples from spiders fed with 1mg/mL GO solution

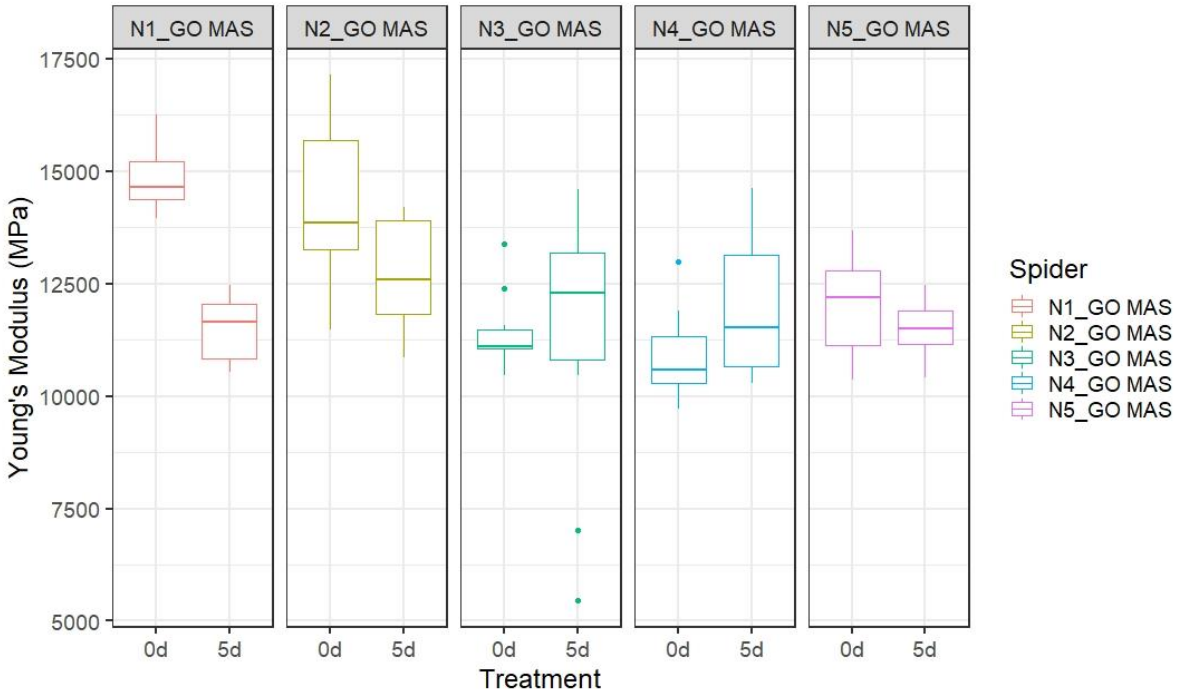

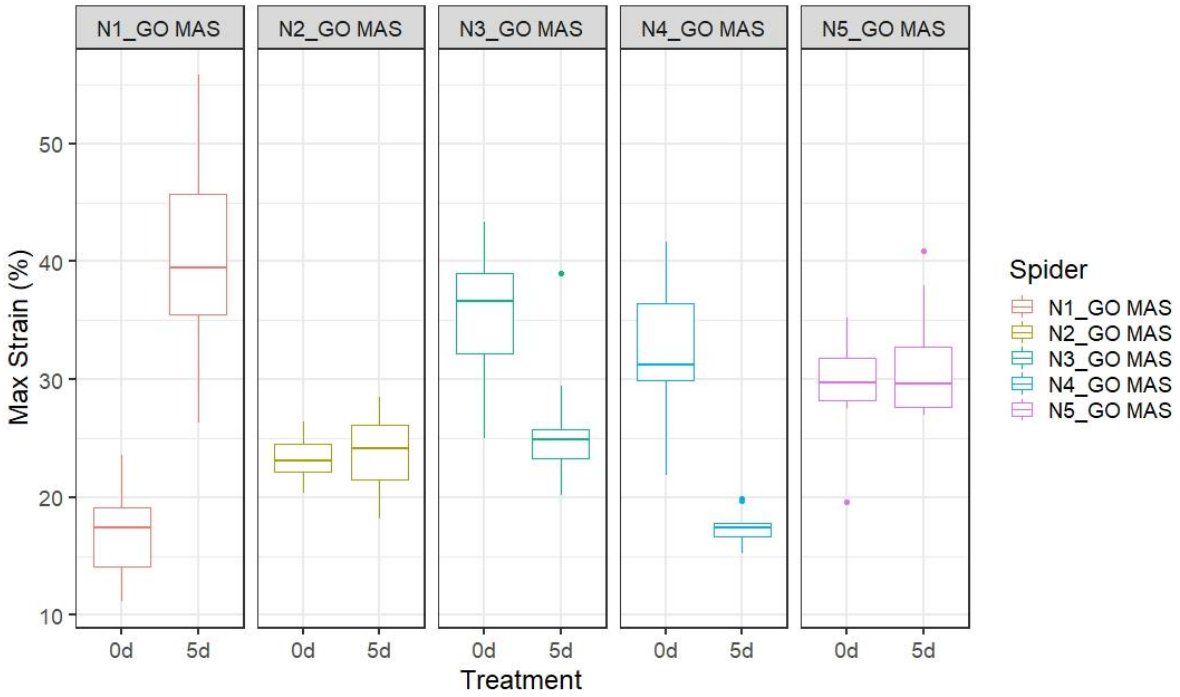

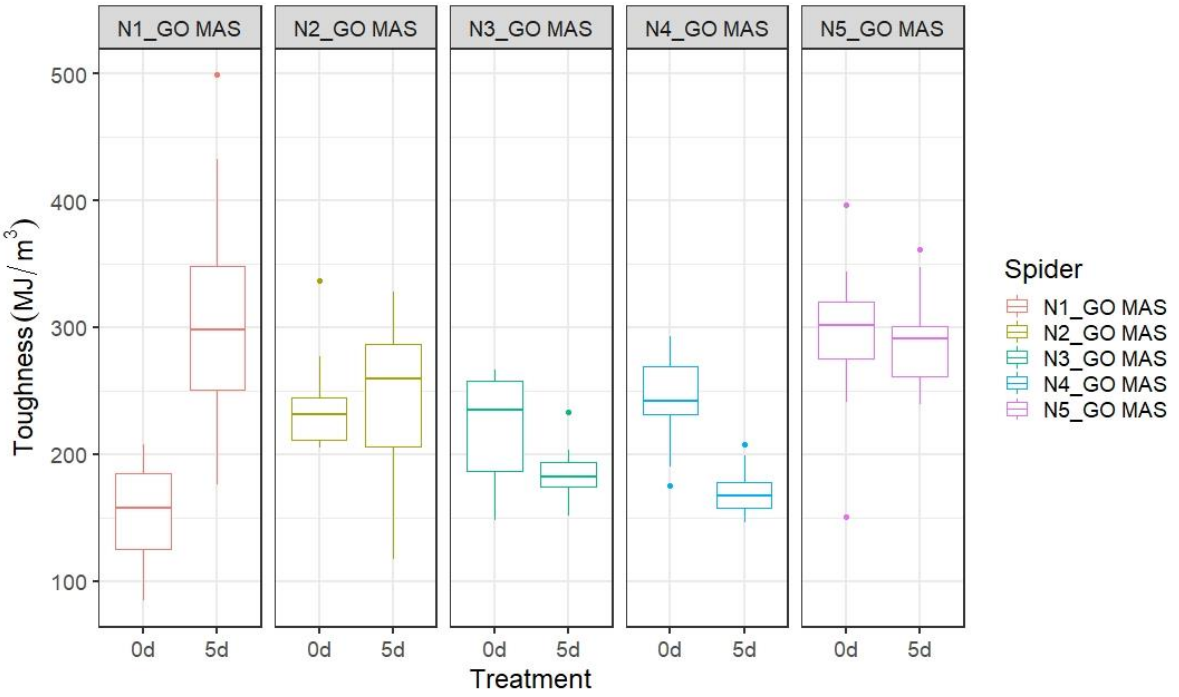

Figure 5.1: Young's Modulus, Maximum strain and Toughness of Major Ampullate silk samples before and after the 1mg/ml GO feeding procedure.

Treatment	Parameter	Effect size	df	t-value (T)	p-value (P)	Marginal coefficient	Conditional coefficient
1mg/ml GO	Young's Modulus (MPa)	-857.943 ± 323.42	95	-2.653	< 0.01	0.0002873695	0.06617239
1mg/ml GO	Maximum Strain (%)	0.2874 ± 1.647	95	0.175	0.862	0.1659121	0.3466938
1mg/ml GO	Toughness (MJ/m^3)	11.191 ± 13.120	95	0.853	0.396	0.006159957	0.161811

Table 5.2: Results from the Mixed-effects model analysis for samples from spiders fed with 1mg/mL GO solution. Results shown are compared against the control samples.

The results suggest a significant reduction in the Young's Modulus of samples. However, close inspection of the data reveals that the result is largely due to samples from one particular spider: N1_GO. Removal of N1_GO from the model results in an effect size of -228.13 (T_{76} = -0.63, P = 0.53) which is statistically insignificant. Thus, this result should be considered with caution as it's possible that the initial significant result may not be an accurate representation of the true effect of the treatment. Additionally, the significant decrease in Young's Modulus for N1_GO is accompanied by a large increase in Maximum strain which is what one would predict would occur naturally. Furthermore, there is no

significant increase or decrease in Toughness when all samples were taken into consideration and no consistent trends in changes in Young's Modulus or Maximum strain. The marginal and conditional coefficient values also indicate that the amount of variation that can be explained by the fixed effect – and even the variation by both the fixed and random effect – is small. With all these factors considered, it seems unlikely that there was any effect of the treatment on the mechanical properties of silks, beyond that of natural temporal variation.

3.1.2 Samples from spiders fed with 1mg/mL SWNT solution

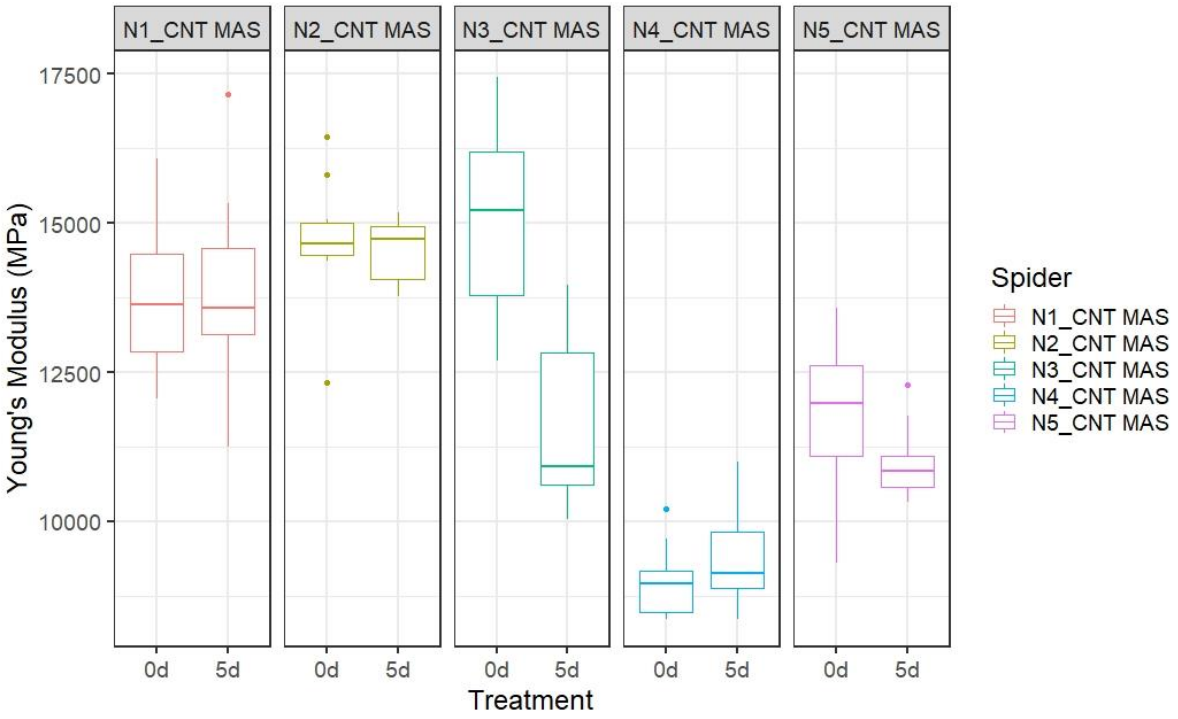

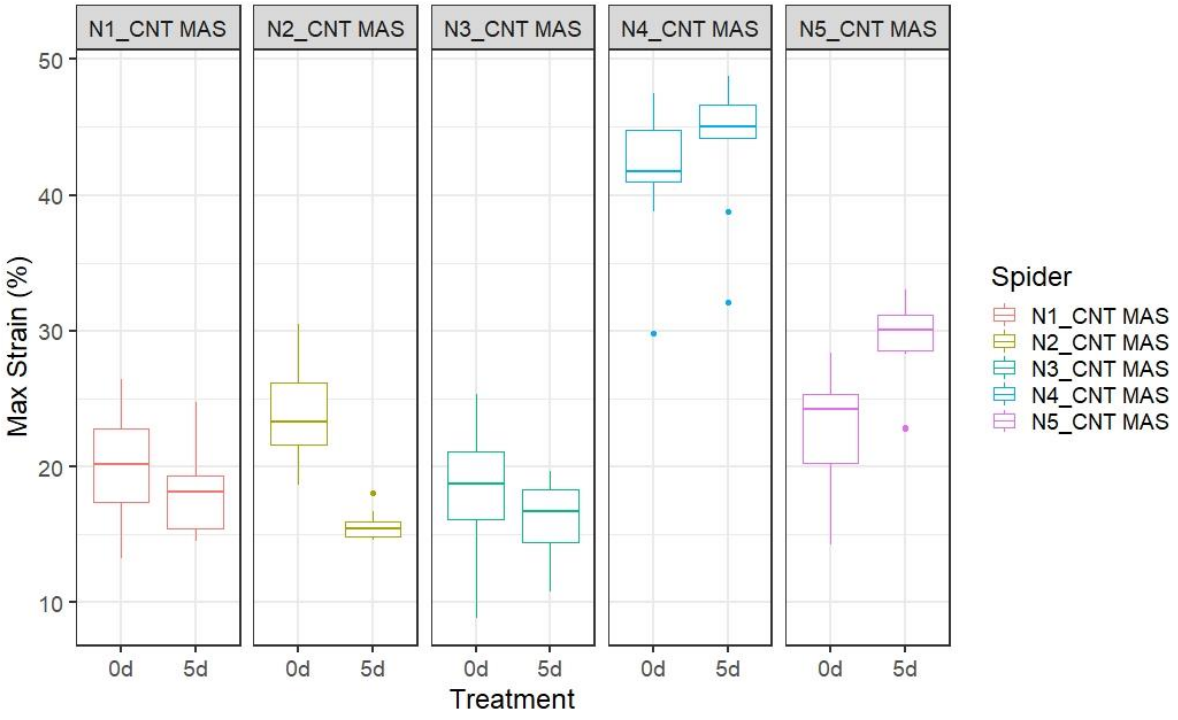

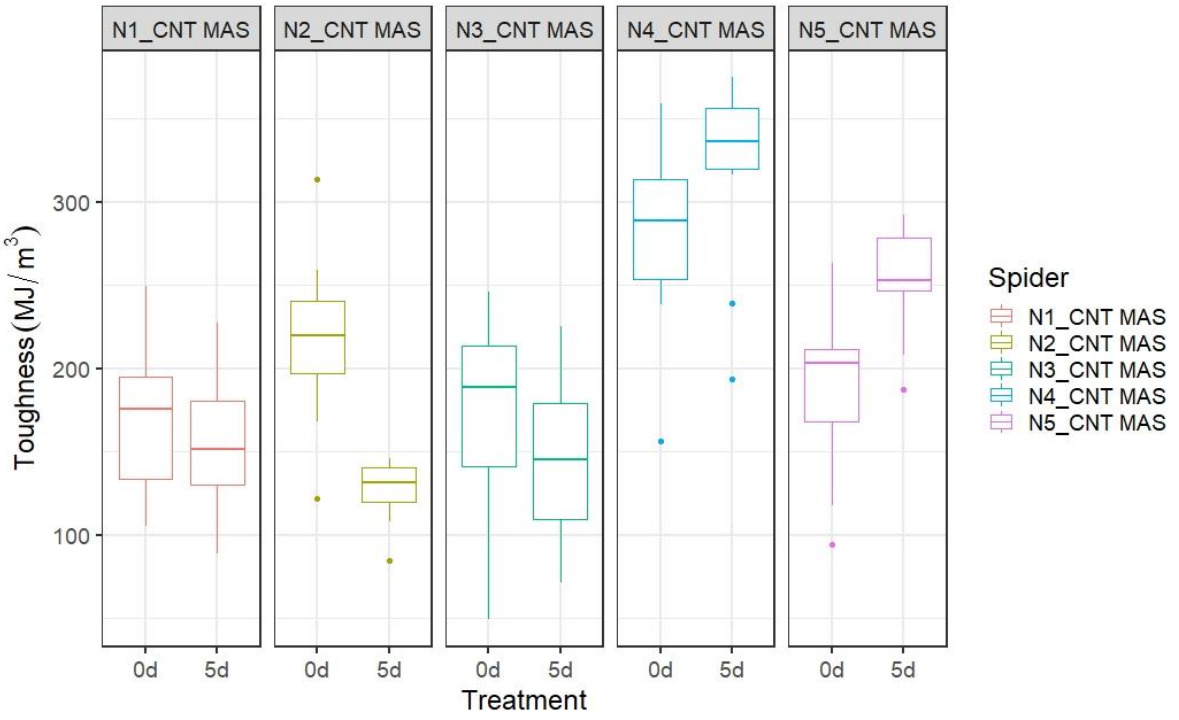

Figure 5.2: Young's Modulus, Maximum strain and Toughness of Major Ampullate silk samples before and after the 1mg/ml SWNT feeding procedure.

Treatment	Parameter	Effect Size	df	t-value	p-value	Marginal coefficient	Conditional coefficient
1mg/ml SWNT	Young's Modulus (MPa)	-767.2854 ± 266.229	95	-2.882	< 0.005	0.02636872	0.6857171
1mg/ml SWNT	Maximum Strain (%)	-0.6938091 ± 0.9087	95	-0.764	0.44704	0.001131842	0.8077911
1mg/ml SWNT	Toughness (MJ/m^3)	-4.75722 ± 10.896	95	-0.437	0.6634	0.00100426	0.4784021

Table 5.3: Results from the Mixed-effects model analysis for samples from spiders fed with 1mg/mL SWNT solution. Results shown are compared against the control samples.

The results suggest a significant reduction in the Young's Modulus of samples. However, close inspection of the data reveals that the result is largely due to samples from one particular spider: N3_CNT. Removal of N3_CNT from the model results in an effect size of -101.52 (T_{76} = -0.42, P = 0.66) which is statistically insignificant. Thus, this result should be considered with caution as it's possible that the initial significant result may not be an accurate representation of the true effect of the treatment. Furthermore, there is no significant increase or decrease in Toughness when all samples were taken into consideration and no consistent trends in changes in Young's Modulus or Maximum strain. The marginal

coefficients indicate that only a very small proportion of the variation in the model is explained by the fixed effect, most of the variation can be explained by the random effect. With all these factors considered, it seems unlikely that there was any effect of the treatment on the mechanical properties of silks, beyond that of natural temporal variation.

3.1.3 Samples from spiders fed with 1mg/mL QD solution

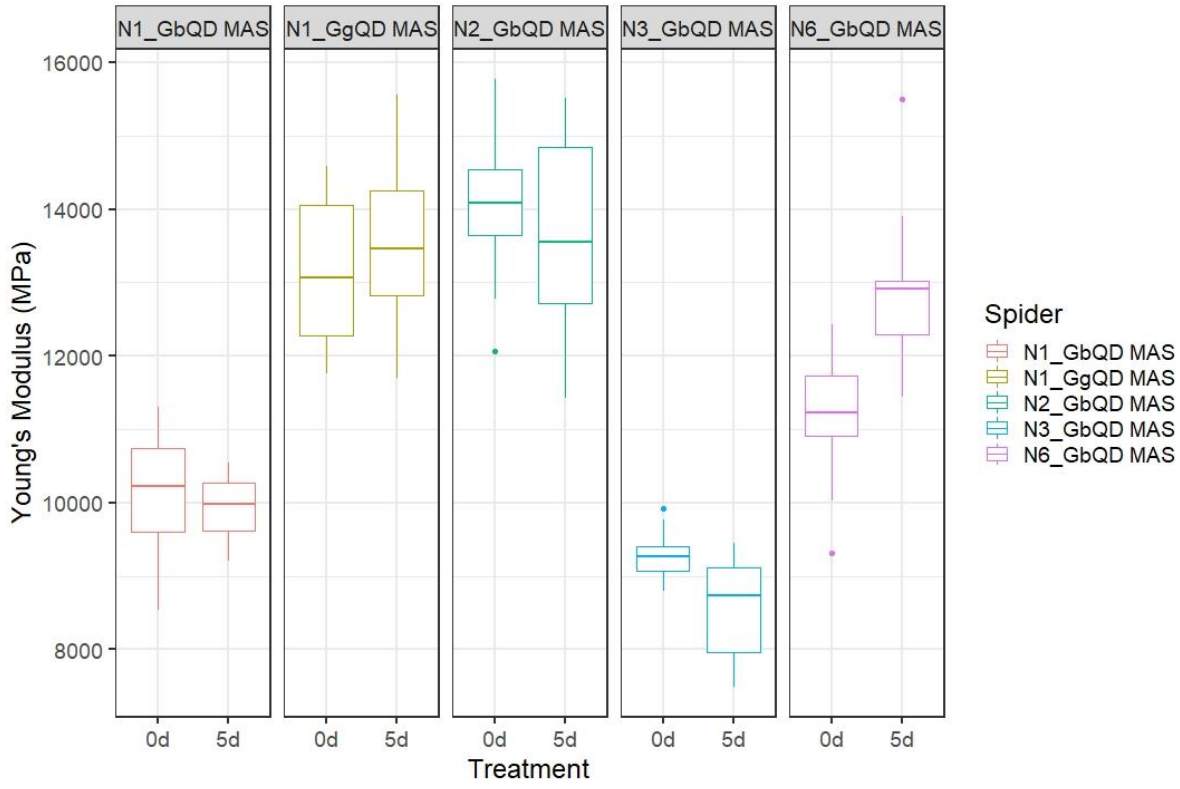

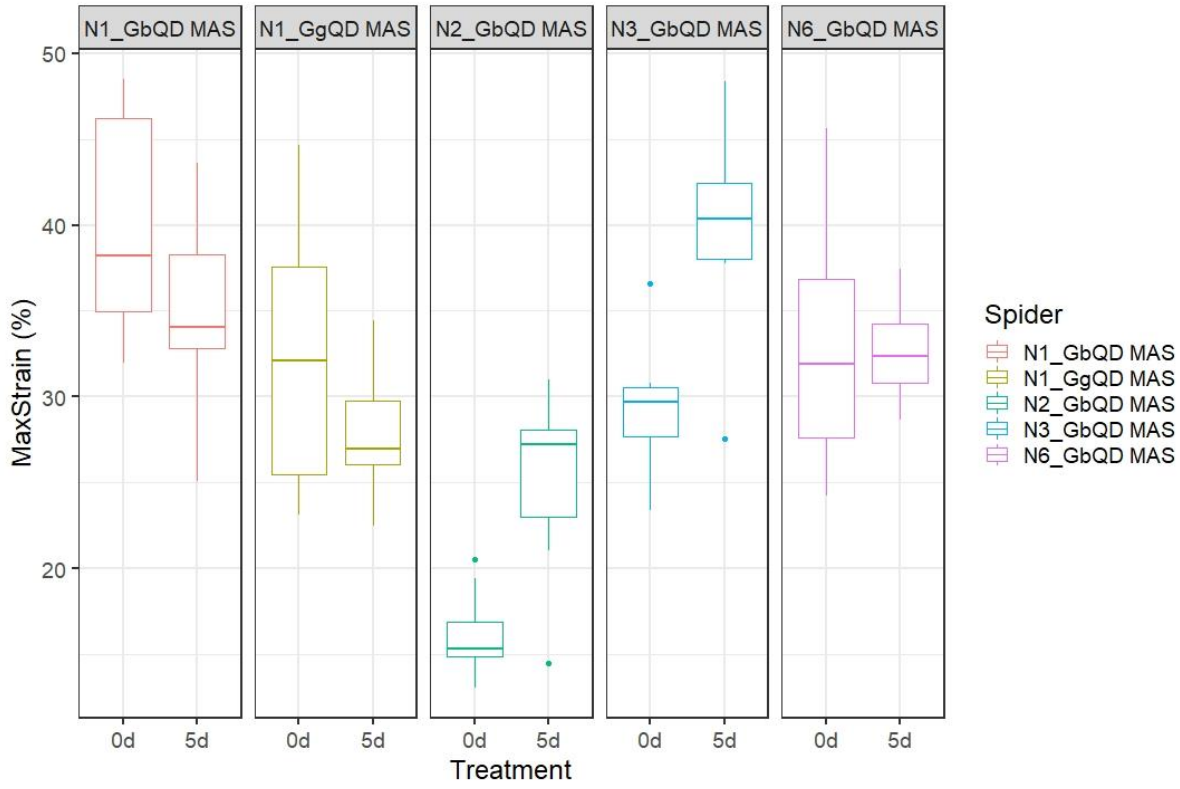

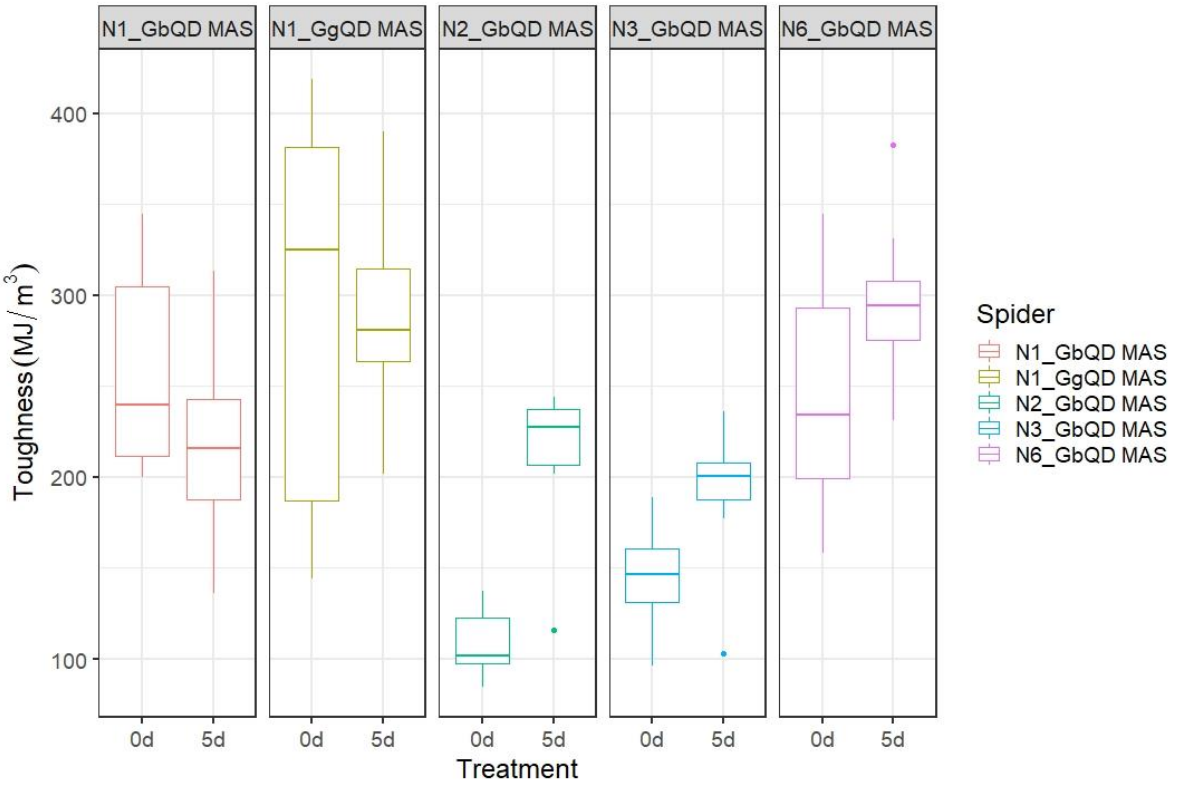

Figure 5.3: Young's Modulus, Maximum strain and Toughness of Major Ampullate silk samples before and after the 1mg/ml QD feeding procedure.

Treatment	Parameter	Effect Size	df	t-value	p-value	Marginal coefficient	Conditional coefficient
1mg/ml NP	Young's Modulus (MPa)	191.363 ± 208.980	95	0.916	0.362	0.002007924	0.7629318
1mg/ml NP	Maximum Strain (%)	1.954 ± 1.261	95	1.549	0.125	0.01349671	0.4432598
1mg/ml NP	Toughness (MJ/m^3)	31.094 ± 11.994	95	2.592	< 0.05	0.03795797	0.4408243

Table 5.4: Results from the Mixed-effects model analysis for samples from spiders fed with 1mg/mL NP solution. Results shown are compared against the control samples.

The results suggest a statistically significant increase in the Toughness of samples, and no statistical difference in the Young's Modulus or Strain at break. However, close inspection of the data reveals that the result is largely due to samples from one particular spider: N2_GbQD. Removal of N2_GbQD from the model results in an effect size of 12.415 (T_{76} = 0.897, P = 0.37) which is statistically insignificant. Thus, this result should be considered with caution as it's possible that the initial significant result may not be an accurate

representation of the true effect of the treatment. The marginal coefficients indicate that only a miniscule proportion of the variation within the model is explained by the fixed effect, with the random effect and error (temporal variation) explaining the majority of the variation within the dataset. As before, there is no convincing evidence for any effect of the treatment on the mechanical properties of silks, beyond that of natural temporal variation.

3.2 Fluorescence imaging

Below are the fluorescence spectra for the samples tested from spiders fed with either 1mg/mL GbQD solution or 1mg/mL GgQD solution, as well as the fluorescence spectra of the QD solutions themselves.

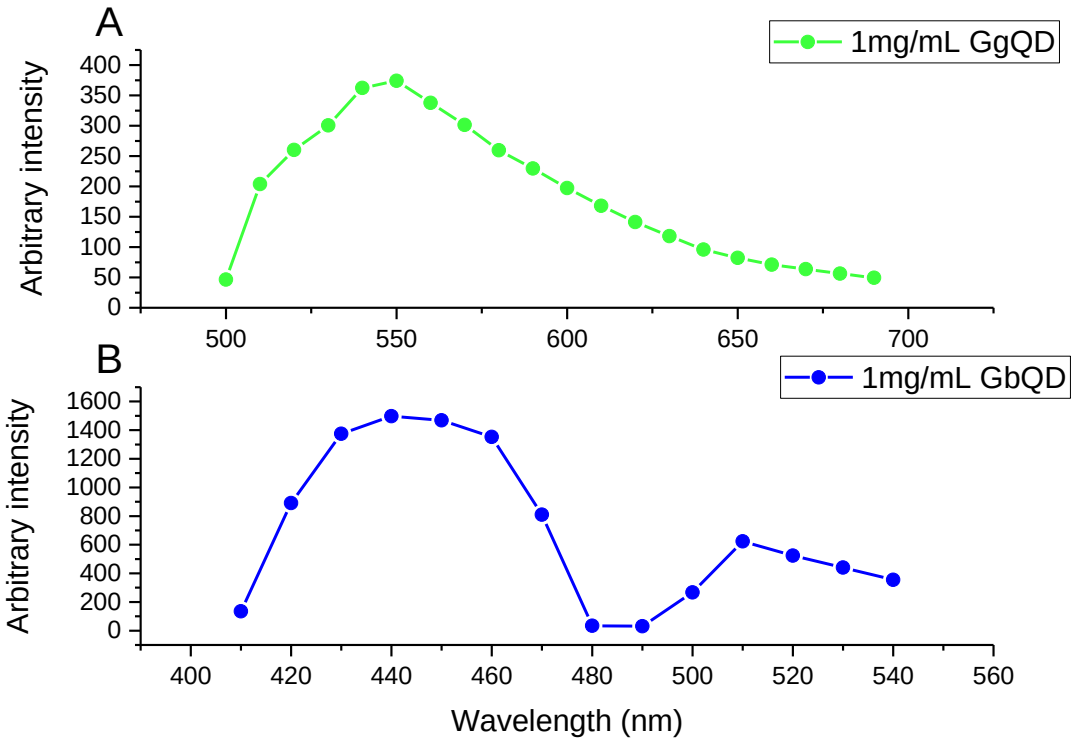

Figure 5.4: (A) Spectral graph of 1mg/mL Graphene green Quantum Dot solution using a 488nm excitation laser. The spectra displays a peak at around 550nm. (B) Spectral graph of 1mg/mL Graphene blue Quantum Dot solution using a 405nm excitation laser. The spectra displays a peak around 430-450nm. Note that the sharp drop between 470-500nm is not a true result; the lightpath of the microscope contained a 405/488nm Dichromatic Mirror which blocks light at a sharp band around 405nm and 488nm.

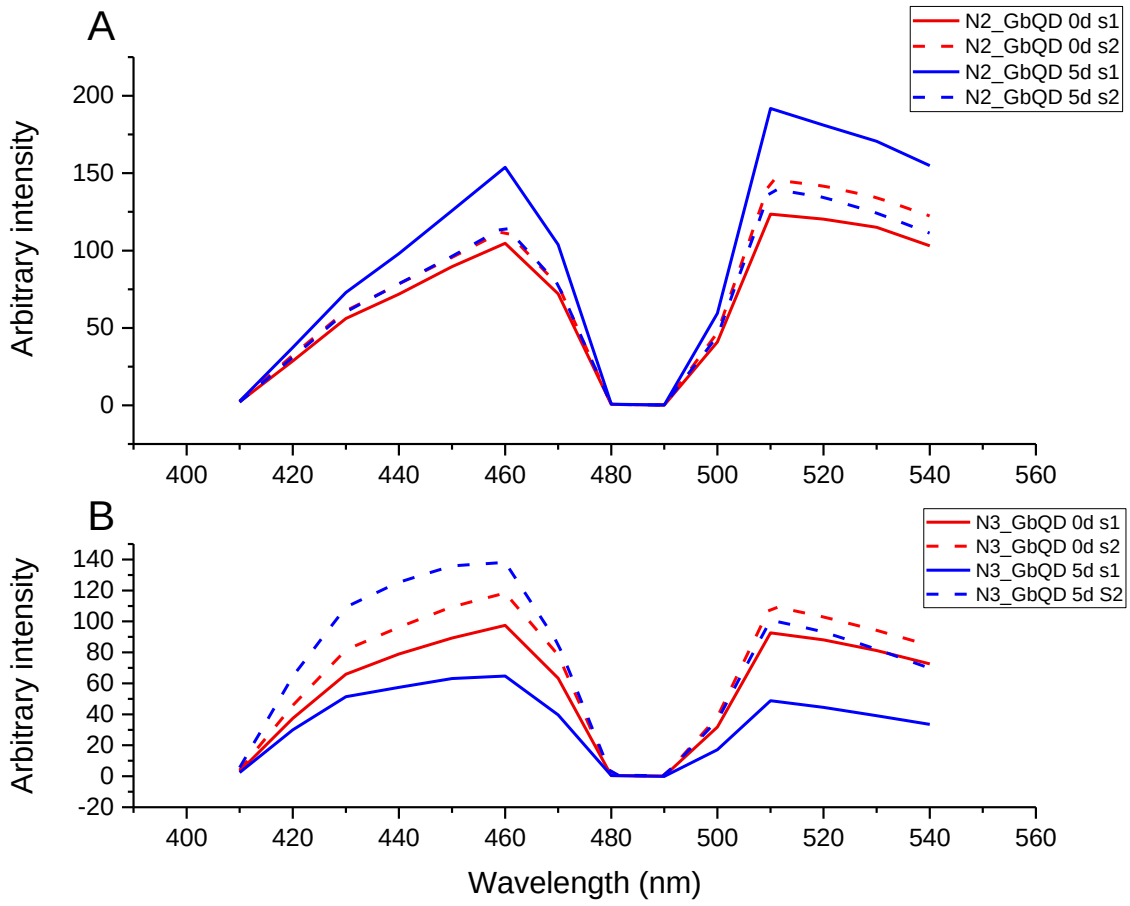

Figure 5.5: Results for silks collected from spiders fed with blue graphene quantum dots. Spectral graphs for samples collected from N2_GbQD (A) and N3_GbQD (B). Red lines represent control samples (0d), blue lines represent samples collected after feeding spiders with the QD solution.

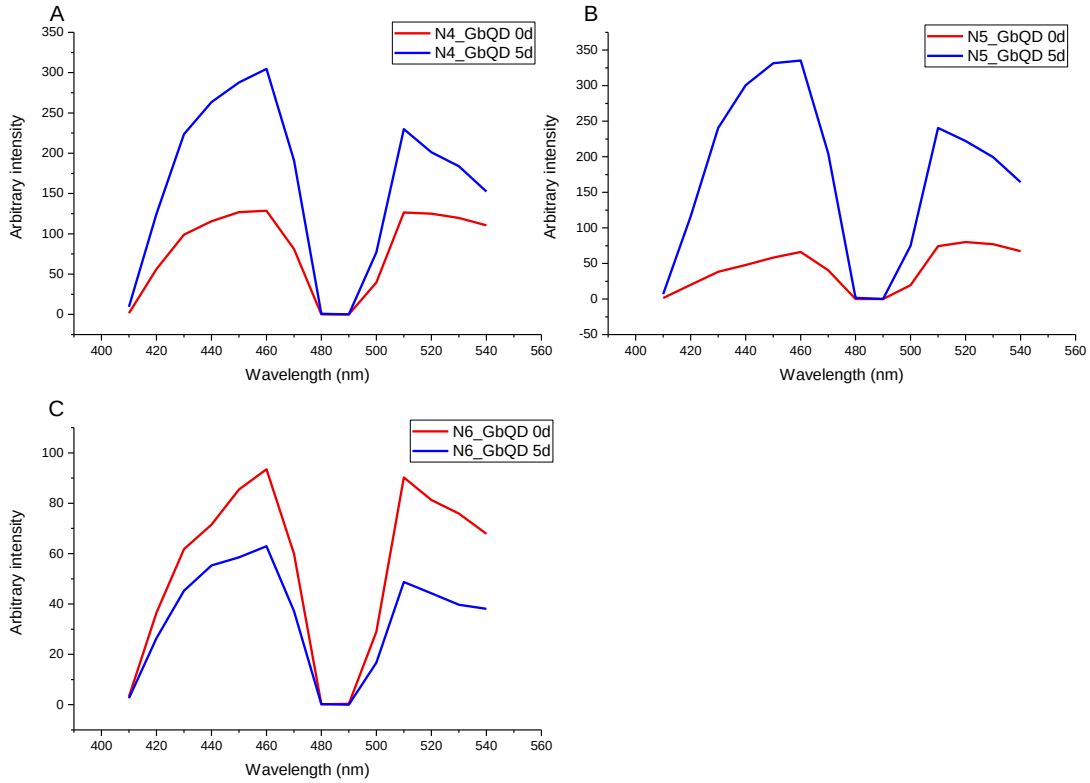

Figure 5.6: Results for silks collected from spiders fed with blue graphene quantum dots. Spectral graphs for samples collected from N4_GbQD (A), N5_GbQD (B) and N6_GbQD (C). Red lines represent control samples (0d), blue lines represent samples collected after feeding spiders with the QD solution.

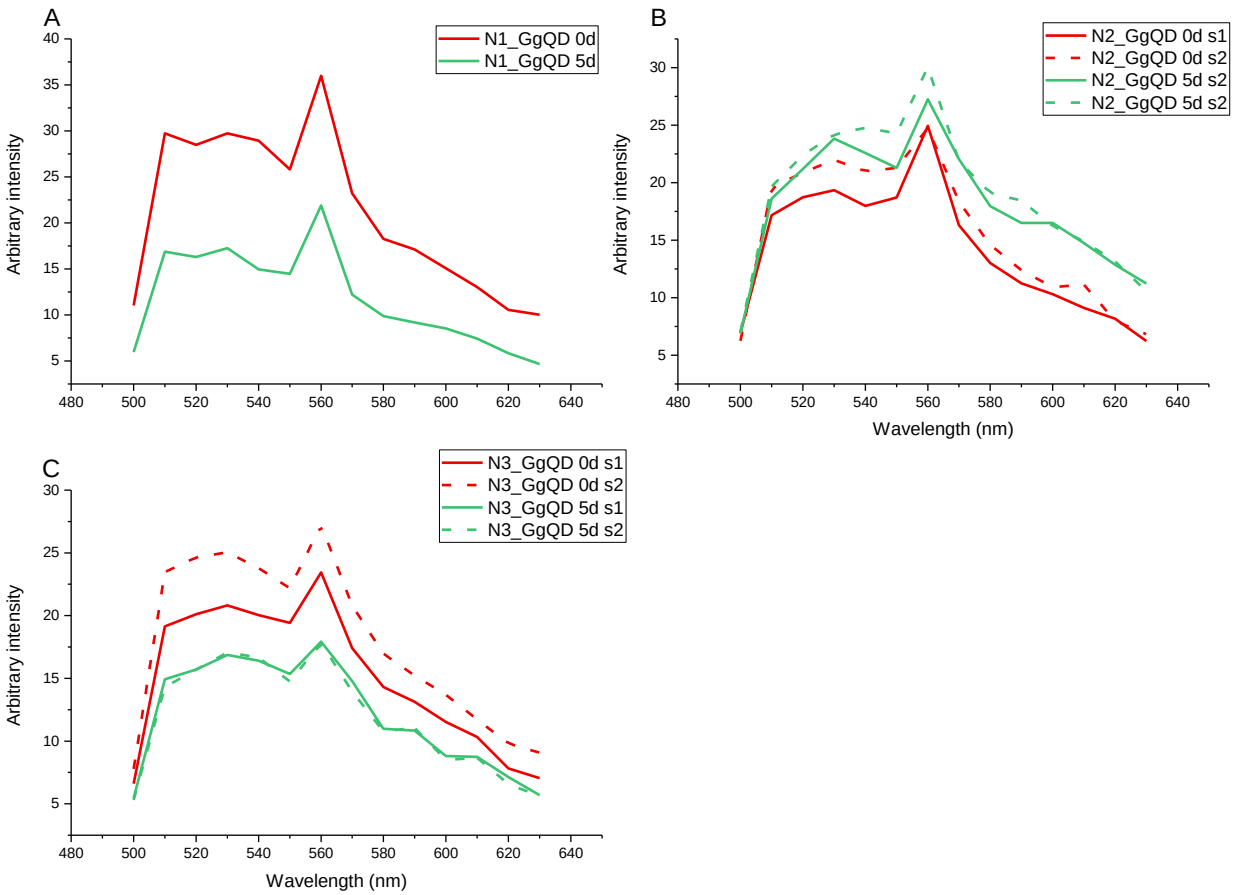

Figure 5.7: Results for silks collected from spiders fed with green graphene quantum dots. Spectral graphs for samples collected from N1_GgQD (A), N2_GgQD (B) and N3_GgQD (C). Red lines represent control samples (0d), green lines represent samples collected after feeding spiders with the QD solution.

From the results, it's clear that using intensity alone is insufficient to infer whether QDs successfully enter spider silks via ingestion; there are instances where the overall intensity of control silks are higher than silks collected after the feeding period, and vice versa.

Based on the results from the GgQD samples, it seems unlikely that GgQDs enter silks via ingestion or that they have no influence on the fluorescence spectra of silks if they do. The spectral graphs for both control and treatment groups are similar in shape. Furthermore, based on the spectra of the 1mg/mL GgQD solution, we would expect a peak around 550nm in the spectra of the treatment group, which we do not see here.

As for the results from the GgQD samples, there is no difference in the fluorescence spectra for samples from N2_GbQD. However, there does seem to be a subtle difference in the spectra for N3, N4, N5 and N6_GbQD; the spectral region between 420-460nm display a higher arbitrary intensity compared to the region from 510-540nm for samples collected after the feeding period. The control samples do not seem to display this property; the peaks in arbitrary intensity between the two regions seem similar. This may be consistent with the idea that the GbQDs entered the silks and caused an increase in fluorescence around the 420-460nm region. However, there is also a possibility that this phenomenon may be present in naturally occurring silks as well, and that my sample size is not big enough to encapsulate this.

Furthermore, I compared the mechanical data obtained from N2_GbQD, N3_GbQD, N6_GbQD and N1_GbQD and their respective fluorescence spectra. If Quantum Dots do enter silks via ingestion and improve the mechanical properties of silks as proposed by previous studies, we should expect to see an increase in the fluorescence intensity to correlate with an increase in overall toughness of the silks. However, from my observations there seem to be no correlation between the intensity of the fluorescence and the toughness of the silks

tested, which further derails the argument that nanoparticles can be incorporated into spider silks via direct feeding.

3.3 Conclusions

Overall, results suggest that the feeding of nanoparticles do not lead to consistent significant improvements in mechanical properties of spider silks, certainly not in the magnitude claimed to be observed in previous literature[114,227].

Discussion

The work in this chapter highlights the difficulty in analysing data from experiments on spider silks with a time delay and emphasizes the importance of considering four crucial factors before drawing conclusions from said data: large intraspecific variation, large temporal variation, effect size of treatment, and sample size.

Due to the large intraspecific variation of silk mechanical properties, there is a need to distinguish samples from individual spiders as separate blocking groups. Without this distinction, the effect of a treatment may be masked due to the randomness created by the intraspecific variation. Worse still, one may obtain false positives and subsequently draw the wrong conclusions from the dataset if the sample size is not sufficiently large. The work in the chapter considers this variation by using mixed-effect models and considering individual spiders as random effects within them.

Large temporal variations affect the dataset in a similar manner to large intraspecific variation; it tends to either mask true treatment effects if the effect size is small, or it can create false positives. Both these cases happen if the sample size is not sufficiently large. Unfortunately, this is a much harder factor to circumvent and the best way to solve for this issue would be to have a large sample size.

As eluded to from the previous arguments, a large enough sample size would indeed aid in minimizing the effect of said predicaments. However, just how many spiders are required for a ‘sufficiently large’ sample size. We can try to estimate the number of spiders required by

using a power calculation. I will use strain at break as an example: let the population mean be 35% and let us use a semi-conservative value of 15% for the standard deviation of the maximum strain. Let us then assume that the treatment will elicit an increase of 5% to the maximum strain of silks. If we let $\alpha = 0.05$, $\beta = 0.2$, and a power of 0.8, the value for N – and thus our recommended sample size – is N = 71. Given the time and labour required to handle the spiders; carefully reel, store and tests silks; obtain multiple repeats per spider; and the time required to carry out any long-term feeding or tests, this sample size would be incredibly laborious. The sample size required would be even larger if the expected effect size is less than 5%, and vice versa.

Returning to the data within this chapter, it remains incredibly hard to ascertain whether nanoparticles do enter via ingestion and if they elicit any effect on the mechanical properties of spider silks. Even if they do elicit some form of effect, the effect size – if any – must be smaller than the natural variation in silks simply due to time. There certainly doesn't seem to be any consistent trend in the change in mechanical properties of the silks, nor are there any huge mechanical improvements that various authors [113,114] claim to have observed. The fluorescence spectra from the tested samples tell a similar story: they suggest minimal to no effect and any indication of an effect by the GbQDs on the fluorescence spectra on silks are vague at best. One could of course argue that the sample sizes for my experiments are too small, hence my inability to discern an effect. However, this same argument can be applied to works from other authors who use similar sample sizes yet make conclusive remarks about the results they obtained.

There are a few experiments that can be carried out in the future to further investigate the question at hand. It would be useful to carry out TEM experiments to obtain cross-sections on the fibres obtained from spiders fed with the nanoparticle solutions to see whether nanoparticles can be found within the fibres. If nanoparticles are present, one could then

calculate the density of nanoparticles per unit area or volume of the fibre and try to corroborate that information with the mechanical data collected. I would not use RAMAN as a technique for confirming the presence of nanoparticles within silk fibres since RAMAN is a surface-based technique and detection of nanoparticles might simply be due to cross-contamination. Furthermore, one would not expect a drastic effect of nanoparticles on the mechanical properties of fibres if it was just on the surface of the fibres. Of course, the issues encountered in my work – necessity for large sample size, high intraspecific and temporal variability – still apply.

Theoretically, the best way to test the effect of nanoparticle inclusion into silk fibres would be to make up a silk feedstock containing nanoparticles of interest, then artificially spin the feedstock into fibres and compare their mechanical properties to a control. This would eliminate the issue of having to deal with the large intraspecific and temporal variation seen in naturally spun silks. I would imagine that incorporating nanoparticles into silks via this method would have more real-world applications as well since it is likely less laborious, and variable compared to obtaining fibres spun by the animals themselves. Indeed, several authors have attempted such research and produced carbon-silk bio-composites[228–230].

Chapter 6: Further thoughts and future work

The work in this thesis probed the viability of modifying silks through manipulation of the spider's and silkworm's diet. Three avenues were explored: the incorporation of unnatural amino acids within their protein backbone (Chapter 2), incorporating fluorophores within the silk structure (Chapter 3), and the viability of incorporating nanoparticles into silks (Chapter 5). We also explored using a multi-spectral technique for studying silks; the techniques (SHG and FLIM) are suited for studying different regions of silks (crystalline vs non-crystalline) so combining them seemed to be the next logical step for developing an informative, high-resolution spatially-resolved method for imaging silks.

The reason for attempting modifications through diet – as opposed to modifying silks post-spinning – is to try and keep the silks in their 'native' state as much as possible. Modifications post-spinning – which require more exposure to chemicals, solvents and environmental changes compared to a feeding regime – is likely to perturb the original structure of silks somewhat since the structure and mechanical properties of silks are affected by water and solvent exposure[35,186,231,232]. Depending on the purpose of the modified silk, this may not matter. However, my interests lie in understanding the structure of silks with as little perturbation to their structure as possible, hence my approach to modifying silks via diet. A dietary approach to modifying silks circumvent the aforementioned issues, which allow us to find stronger relationships between any chemical or mechanical changes with any successful modifications.

The data presented in this thesis showed that it is indeed possible to modify silks by incorporating UAAs containing both structural and chemical modification (Chapter 2), and that it was possible to insert fluorophore dyes with specific solvation properties into silks without significant perturbation to their mechanical properties (Chapter 3). I was unable to

detect any successful incorporation of nanoparticles into silks, nor was there any indication of improvement in mechanical properties of silks (Chapter 5).

Additionally, I showed that there are spectral properties of silks that can be exploited to elucidate the structure of silks; by utilising SHG/FLIM imaging, we were able to exploit the fluorescence properties and Second Harmonic Generated signals from silks, enabling us to obtain spatially-resolved images of silks at the sub-micron level that reflected their structural state as well (Chapter 4).

Overall, the work in my thesis shows that there are still new methods to be found for unravelling the enigma that is the structure of silks and silk processing. Advances in chemical methods, imaging technology, genetics, and most importantly integrating these advances with a core understanding of evolution and the biology of spiders is key in developing novel methods for future studies on silks. I believe the data outlined in my data chapters serve as a stepping stone for future silk research and in the rest of this chapter, I reiterate a few important conclusions and future prospects of the work in this thesis, as well as a few further thoughts and ideas.

New toolkits for studying the protein structure and dynamics of silks

Successful UAA incorporation into silks means the potential for new molecular labels and contrast agents for studying silks, which in turn allow for techniques such as F-NMR[92,93], bio-orthogonal noncanonical amino acid tagging (BONCAT)[127,233], quantitative noncanonical amino acid tagging (QuaNCAT)[83] to be used for silk studies. The absence of such labels in the natural world would result in a very high signal-to-noise ratio and no false positives, assuming a decent amount of label is incorporated. Of particular interest in this regard is the incorporation of ^{13}C- fluorinated UAAs as this opens up the potential for deciphering protein

structures around the targeted UAA. Spectral details due to the Fluorine-Carbon correlation should allow researchers to decipher the structure and chemical environment around the targeted UAA as well as open the potential for monitoring dynamic structural changes within the protein by making use of the Nuclear Overhauser effect and by performing LIDOR experiments[92,93,135].This in conjunction with real-time temperature ramped F-NMR experiments would allow researchers to monitor the protein dynamics and interactions during the transition from the liquid dope to the solid silk state at a molecular level. I believe such data – combined with the power of proteomics and tandem mass spectrometry – will prove invaluable for helping researcher further probe the protein dynamics and structures that exist within silk at different stages of silk production.

In Chapter 2, I focused on methionine as a target for replacement with UAAs; the reason for this is the elevated flexibility of the aaRS system involved in methionine incorporation into peptides[66,69]. This is particularly important for UAAs with structural and chemical changes such as azidohomoalanine but might not be as important for UAAs with only chemical changes such as trifluorinated UAAs. Potential experiments to perform in the future would be to try feeding trifluorinated UAAs in other sites; a potential candidate could be alanine as it is one of the most abundant amino acids in silks. It might even be possible to target amino acids known to reside within the non-crystalline regions of silks (potentially the amino acids Q, Y, L, R)[28,53,194] as it might allow researchers to resolve the protein motifs within that region. Coupling these experiments with verification using proteomics (to identify peptides containing such modifications) would be a powerful toolkit for studying regions of silks around such targeted amino acids that were not possible in the past.

The potential of fluorophore dyes as an inert reporter

My work in Chapter 2 shows that spider silks are robust to perturbations and interactions by certain fluorescent dyes when incorporated via feeding to the spider. We also note that the dyes are not randomly distributed within the silks; they seem to interact with motifs within silks and their properties change within silks. Trying to understand the fundamental reasons for the change in these dye properties may allow researchers to infer silk structure around the target dye, based on the chemical groups found on the dye, the polarity and hydrophilicity of the dye.

This work – as well as the work of others[100,168] – also show that not all dyes interact in the same way, which is not surprising since factors such as hydrophilicity, stearic considerations and side moieties likely play a role in how well dyes interact with silk proteins[162,168,234]. Exploring different dye options to test if they interact differently with different regions of silks could be of great interest; especially if these dyes are also suitable for super-resolution fluorescence microscopy as it may allow the resolution of the protein structures – both crystalline and non-crystalline depending on where the dye attaches to – at nanoscale levels of resolution.

Intraspecific and temporal variation: A cautionary tale and a unique opportunity

My work in Chapter 3 and Chapter 5 highlights the difficulty in performing experiments on spider silks collected from spiders at different timepoints. This isn't new information: the high temporal and intraspecific variation of spider silks is well documented186 however this variation is sometimes unaccounted for in literature that looks at the effect of a particular treatment on the mechanical properties of silks. My work shows that there is a need for

stringent methodology and appropriate sample sizes to be used when such experiments are conducted.

Though frustrating at first glance, this high temporal variation might offer a unique opportunity for probing the chemistry and structure of silks. We have some idea for why the variation occurs[203,235] but not the whole story. Could it be due to a change in the primary structure of the silks, change in the isoform ratio of spidroins used on a particular day, a change in the spinning process internal to the spider? Proteomic studies on silks collected from the same spider under a controlled diet on different days, coupled with appropriate mechanical testing could provide an answer for the source of this variation.

Nanoparticles and silks

In the past decade, there has been a fair amount of hype and interest around incorporating carbon nanoparticles – such as nanotubes, graphene sheets and graphene quantum dots – into silks through feeding the spider or silkworm with a NP solution[112,114,164]. My work in Chapter 5 shows that achieving such incorporation and mechanical improvements in spider silks by simply feeding spiders various NP solutions is not as easy as these authors make it seem. In fact, from my work I am unable to detect incorporation of any sort, even after using quantum dots which are the smallest and easiest to detect.

There are still a few gaps in my work that should be filled before coming to any strong conclusions. Ideally, one would test the excrements collected from the spiders before and after the feeding regime to test for the presence of nanoparticles. I would also have liked to perform transmission electron microscopy (TEM) experiments on the spider silk samples that I collected to confirm the presence or absence of NPs within the structure of spider silks, since this technique allows us to see within silks and since carbon nanoparticles display

signals on TEM images. This was initially the plan however the Covid-19 pandemic meant I could not carry out these experiments before the hand in deadline.

I also do not know whether the findings in Chapter 5 translate to silkworms. It is possible that silkworms have a less selective gastrointestinal tract which may allow nanoparticles to get into the silk glands and subsequently into the silks. Once again, this work will need to be repeated with stringent measures to prevent cross-contamination of NPs from the environment, and with consideration for temporal and intraspecific variation of mechanical properties of silks. Coupled with TEM, this work would allow us to determine whether NPs enter silks via ingestion.

The benefit of two-photon techniques

Due to their miniscule size and hierarchy from the nanoscale, many conventional single-photon imaging and spectroscopic techniques used on silks require the use of high-power beams and lasers with very short wavelengths in order to obtain a high signal-to-noise ratio and a high enough resolution to discern the structures within silks. This often leads to issues like photobleaching and damage to the samples[101,157,236].

Two-photon techniques circumvent this issue due to the up-conversion that occurs from the non-linear optical processes that these techniques exploit. As a result, high-resolution images can be achieved without the need for high power lasers. Additionally, the signals that arise from this process tend to be specific to the molecular orientation and structure of the moieties involved, making it possible for one to distinguish various regions and structures within silks using the same technique. I used SHG for this purpose in Chapter 4, but other techniques such as Coherent Anti-Stokes Raman (CARS)[157,158] exist and should be applicable for the study of silk structure as well, since such techniques can distinguish different regions and motifs of silks.

Going beyond nature?

The ultimate mechanical properties of silks are a result of the primary structure of silk proteins (the feedstock), and the silk spinning methodology responsible for the appropriate folding, formation and orientation of structural motifs that arise from the primary structure of silks. Given silk proteins have evolved over the course of 300 million years, we can assume that the primary structure of silks is quite well suited for their purpose of forming a multi-purpose fibre that is both strong yet flexible, and we'd be hard-pressed to come up with something better from scratch. The fact that most companies and researchers who have tried making artificial silk proteins from scratch have yet to discover something that comes close to the natural protein supports this argument[237].

However, natural selection is restricted to the ecological context that the target resides in. In other words, evolution is restricted by the natural materials available around the target and is energetically restrictive. What if we as humans don't care about such energetic restrictions and have access to materials not available to nature? I've shown in Chapter 2 that it is possible to modify silk proteins by incorporating azide-bearing UAAs. UAA incorporation via site- or residue-specific modification is not the only method for introducing azides or alkynes into proteins; various methods exist for selectively introducing azides on lysine or cysteine residues[66,238]. Perhaps through such incorporation and further functionalisation via click-chemistry, we may be able to achieve silk properties that surpass those of natural silks. Introducing cross-links via azide-alkyne linkages to toughen silks or perhaps increasing extensibility by covalent attachment of extensible materials such as elastane are a few ideas that come to mind.

References

1. Craig, C. L. Evolution of Arthropod Silks. *Annual Review of Entomology* **42**, 231–267 (1997).

2. Garrison, N. L. *et al.* Spider phylogenomics: untangling the Spider Tree of Life. *PeerJ* **4**, e1719 (2016).

3. Eisoldt, L., Smith, A. & Scheibel, T. Decoding the secrets of spider silk. *Materials Today* **14**, 80–86 (2011).

4. Porter, D. & Vollrath, F. Silk as a biomimetic ideal for structural polymers. *Advanced Materials* **21**, 487–492 (2009).

5. Vollrath, F. & Knight, D. P. Liquid crystalline spinning of spider silk. *Nature* **410**, 541–8 (2001).

6. Porter, D. & Vollrath, F. The role of kinetics of water and amide bonding in protein stability. *Soft Matter* **4**, 328 (2008).

7. Holland, C., Vollrath, F., Ryan, A. J. & Mykhaylyk, O. O. Silk and synthetic polymers: Reconciling 100 degrees of separation. *Advanced Materials* **24**, 105–109 (2012).

8. Knight, D. P., Knight, M. M. & Vollrath, F. Beta transition and stress-induced phase separation in the spinning of spider dragline silk. *International Journal of Biological Macromolecules* **27**, 205–210 (2000).

9. Boulet-Audet, M., Terry, A. E., Vollrath, F. & Holland, C. Silk protein aggregation kinetics revealed by Rheo-IR. *Acta Biomaterialia* **10**, 776–784 (2014).

10. Holland, C., Porter, D. & Vollrath, F. Comparing the rheology of mulberry and “wild” silkworm spinning dopes. *Biopolymers* **97**, 362–367 (2012).

11. Holland, C., Urbach, J. S. & Blair, D. L. Direct visualization of shear dependent silk fibrillogenesis. *Soft Matter* **8**, 2590–2594 (2012).

12. Dicko, C., Kenney, J. M., Knight, D. & Vollrath, F. Transition to a beta-sheet-rich structure in spidroin in vitro: the effects of pH and cations. *Biochemistry* **43**, 14080–14087 (2004).

13. Dicko, C., Vollrath, F. & Kenney, J. M. Spider silk protein refolding is controlled by changing pH. *Biomacromolecules* **5**, 704–710 (2004).

14. Laity, P. R., Gilks, S. E. & Holland, C. Rheological behaviour of native silk feedstocks. *Polymer (United Kingdom)* **67**, 28–39 (2015).

15. Chen, X., Knight, D. P., Shao, Z. & Vollrath, F. Conformation transition in silk protein films monitored by time-resolved fourier transform infrared spectroscopy: Effect of potassium ions on Nephila spidroin films. *Biochemistry* **41**, 14944–14950 (2002).

16. Mortimer, B., Guan, J., Holland, C., Porter, D. & Vollrath, F. Linking naturally and unnaturally spun silks through the forced reeling of Bombyx mori. *Acta Biomaterialia* **11**, 247–255 (2015).

17. Sutherland, T. D., Young, J. H., Weisman, S., Hayashi, C. Y. & Merritt, D. J. Insect Silk: One Name, Many Materials. *Annual Review of Entomology* **55**, 171–188 (2010).

18. Kronenberger, K., Dicko, C. & Vollrath, F. A novel marine silk. *Naturwissenschaften* **99**, 3–10 (2012).

19. Craig, C. L. & Riekel, C. Comparative architecture of silks, fibrous proteins and their encoding genes in insects and spiders. *Comparative Biochemistry and Physiology - B Biochemistry and Molecular Biology* **133**, 493–507 (2002).

20. Terry, A. E., Knight, D. P., Porter, D. & Vollrath, F. pH induced changes in the rheology of silk fibroin solution from the middle division of Bombyx mori silkworm. *Biomacromolecules* **5**, 768–772 (2004).

21. Vollrath, F. Biology of spider silk. *International Journal of Biological Macromolecules* **24**, 81–88 (1999).

22. Vollrath, F., Porter, D. & Holland, C. There are many more lessons still to be learned from spider silks. *Soft Matter* **7**, (2011).

23. Sponner, A. *et al.* Characterization of the protein components of Nephila clavipes dragline silk. *Biochemistry* **44**, 4727–4736 (2005).

24. Hinman, M. B. & Lewis, R. V. Isolation of a clone encoding a second dragline silk fibroin. *J. Biol. Chem.* **267**, 19320–19324 (1992).

25. Colgin, M. A. & Lewis, R. V. Spider minor ampullate silk proteins contain new repetitive sequences and highly conserved non-silk-like “spacer regions.” *Protein Sci.* **7**, 667–672 (1998).

26. Inoue, S. *et al.* Silk fibroin of Bombyx mori is secreted, assembling a high molecular mass elementary unit consisting of H-chain, L-chain, and P25, with a 6:6:1 molar ratio. *Journal of Biological Chemistry* **275**, 40517–40528 (2000).

27. Santos-Pinto, J. R. A. dos, Arcuri, H. A., Lubec, G. & Palma, M. S. Structural characterization of the major ampullate silk spidroin-2 protein produced by the spider Nephila clavipes. *Biochimica et Biophysica Acta (BBA) - Proteins and Proteomics* **1864**, 1444–1454 (2016).

28. Lefèvre, T., Rousseau, M.-E. & Pézolet, M. Protein secondary structure and orientation in silk as revealed by Raman spectromicroscopy. *Biophys. J* . **92**, 2885–2895 (2007).

29. Hayashi, C. Y., Shipley, N. H. & Lewis, R. V. Hypotheses that correlate the sequence, structure, and mechanical properties of spider silk proteins. *International Journal of Biological Macromolecules* **24**, 271–275 (1999).

30. Asakura, T., Okushita, K. & Williamson, M. P. Analysis of the structure of Bombyx mori silk fibroin by NMR. *Macromolecules* **48**, 2345–2357 (2015).

31. Schwarze, S., Zwettler, F. U., Johnson, C. M. & Neuweiler, H. The N-terminal domains of spider silk proteins assemble ultrafast and protected from charge screening. *Nature Communications* **4**, 1–7 (2013).

32. Rising, A. & Johansson, J. Toward spinning artificial spider silk. *Nature chemical biology* **11**, 309–15 (2015).

33. Hagn, F. *et al.* A conserved spider silk domain acts as a molecular switch that controls fibre assembly. *Nature* **465**, 239–42 (2010).

34. Gao, Z. *et al.* Structural Characterization of Minor Ampullate Spidroin Domains and Their Distinct Roles in Fibroin Solubility and Fiber Formation. *PLoS ONE* **8**, (2013).

35. Guan, J., Vollrath, F. & Porter, D. Two mechanisms for supercontraction in Nephila spider dragline silk. *Biomacromolecules* **12**, 4030–4035 (2011).

36. Gaines IV, W. A.; Marcotte Jr, W. R. Identification and Characterization of Multiple Spidroin 1 Genes Encoding Major Ampullate Silk Proteins in Nephila clavipes. **17**, 465–474 (2010).

37. Motriuk-Smith, D., Smith, A., Hayashi, C. Y. & Lewis, R. V. Analysis of the conserved N-terminal domains in major ampullate spider silk proteins. *Biomacromolecules* **6**, 3152–3159 (2005).

38. Liu, Y., Sponner, A., Porter, D. & Vollrath, F. Proline and processing of spider silks. *Biomacromolecules* **9**, 116–121 (2008).

39. Guinea, G. V. *et al.* Minor ampullate silks from Nephila and Argiope spiders: Tensile properties and microstructural characterization. *Biomacromolecules* **13**, 2087–2098 (2012).

40. Grzelak, K. Control of expression of silk protein genes. *Comparative Biochemistry and Physiology* **110**, 671–681 (1995).

41. Vollrath, F., Holtet, T., Thogersen, H. C. & Frische, S. Structural organization of spider silk. *Proceedings of the Royal Society of London Series B-Biological Sciences* **263**, 147–151 (1996).

42. Vollrath, F. & Porter, D. Spider silk as a model biomaterial. *Applied Physics A: Materials Science and Processing* **82**, 205–212 (2006).

43. Vollrath, F., Porter, D. & Holland, C. The science of silks. *MRS Bulletin* **38**, 73–80 (2013).

44. Termonia, Y. Molecular Modeling of Spider Silk Elasticity. *Macromolecules* **27**, 7378–7381 (1994).

45. Vollrath, F. & Porter, D. Silks as ancient models for modern polymers. *Polymer* **50**, 5623–5632 (2009).

46. Thiel, B. L., Guess, K. B. & Viney, C. Non-periodic lattice crystals in the hierarchical microstructure of spider (major ampullate) silk. *Biopolymers* **41**, 703–719 (1997).

47. Asakura, T. *et al.* Silk structure studied with nuclear magnetic resonance. *Progress in Nuclear Magnetic Resonance Spectroscopy* **69**, 23–68 (2013).

48. Jenkins, J. E., Holland, G. P. & Yarger, J. L. High resolution magic angle spinning NMR investigation of silk protein structure within major ampullate glands of orb weaving spiders. *Soft Matter* **8**, 1947–1954 (2012).

49. Holland, G. P., Jenkins, J. E., Creager, M. S., Lewis, R. V & Yarger, J. L. Solid-State NMR Investigation of Major and Minor Ampullate Spider Silk in the Native and Hydrated States Solid-State NMR Investigation of Major and Minor Ampullate Spider Silk in the Native and Hydrated States. *Society* 651–657 (2008) doi:10.1021/bm700950u.

50. Yao, J., Nakazawa, Y. & Asakura, T. Structures of Bombyx mori and Samia cynthia ricini silk fibroins studied with solid-state NMR. *Biomacromolecules* **5**, 680–688 (2004).

51. Asakura, T., Ito, T., Okudaira, M. & Kameda, T. Structure of Alanine and Glycine Residues of *Samia c ynthia r icini* Silk Fibers Studied with Solid-State ^{15} N and ^{13} C NMR. *Macromolecules* **32**, 4940–4946 (1999).

52. Hronska, M., van Beek, J. D., Williamson, P. T. F., Vollrath, F. & Meier, B. H. NMR characterization of native liquid spider dragline silk from Nephila edulis. *Biomacromolecules* **5**, 834–839 (2004).

53. van Beek, J. D., Hess, S., Vollrath, F. & Meier, B. H. The molecular structure of spider dragline silk: folding and orientation of the protein backbone. *Proceedings of the National Academy of Sciences* **99**, 10266–10271 (2002).

54. Hijirida, D. H. *et al.* 13C NMR of Nephila clavipes major ampullate silk gland. *Biophysical Journal* **71**, 3442–3447 (1996).

55. Asakura, T., Kuzuhara, A., Tabeta, R. & Saito, H. Conformation Characterization of Bombyx mori Silk Fibroin in the Solid State by High-Frequency 13C Cross Polarization-Magic Angle Spinning NMR, X-ray Diffraction, and Infrared Spectroscopy. *Macromolecules* **18**, 1841–1845 (1985).

56. Asakura, T., Suzuki, Y., Nakazawa, Y., Holland, G. P. & Yarger, J. L. Elucidating silk structure using solid-state NMR. *Soft Matter* **9**, 11440–11450 (2013).

57. Asakura, T. *et al.* NMR study of silk I structure of Bombyx mori silk fibroin with N-15- and C-13-NMR chemical shift contour plots. *Biopolymers* **41**, 193–203 (1997).

58. Asakura, T., Yoshimizu, H. & Yoshizawa, F. NMR of Silk Fibroin. 9. Sequence and Conformation Analyses of the Silk Fibroins from Bombyx mori and Philosamia cynthia ricini by 15N NMR Spectroscopy. *Macromolecules* **21**, 2038–2041 (1988).

59. Asakura, T., Endo, M., Tasei, Y., Ohkubo, T. & Hiraoki, T. Hydration of Bombyx mori silk cocoon, silk sericin and silk fibroin and their interactions with water as studied by 13C NMR and 2H NMR relaxation. *Journal of Materials Chemistry B* **5**, 1624–1632 (2017).

60. Asakura, T. & Murakami, T. NMR of Silk Fibroin. 4. Temperature-and Urea-Induced Helix-Coil Transitions of the-(Ala)n-Sequence in Philosamia cynthia ricini Silk

Fibroin Protein Monitored by 13C NMR Spectroscopy. *Macromolecules* **18**, 2614–2619 (1985).

61. Asakura, T. & Yao, J. 13C CP/MAS NMR study on structural heterogeneity in Bombyx mori silk fiber and their generation by stretching. *Protein Science* **11**, 2706–2713 (2009).

62. Eles, P. T. & Michal, C. A. A DECODER NMR study of backbone orientation in Nephila clavipes dragline silk under varying strain and draw rate. *Biomacromolecules* **5**, 661–665 (2004).

63. Suzuki, Y., Yamazaki, T., Aoki, A., Shindo, H. & Asakura, T. NMR study of the structures of repeated sequences, GAGXGA (X = S, Y, V), in bombyx mori liquid silk. *Biomacromolecules* **15**, 104–112 (2014).

64. Xu, D., Yarger, J. L. & Holland, G. P. Exploring the backbone dynamics of native spider silk proteins in Black Widow silk glands with solution-state NMR spectroscopy. *Polymer* **55**, 3879–3885 (2014).

65. Asakura, T. & Demura, M. Structure and dynamics of silk fibroin studied with C-13, N-15 and H-2 solid state NMR. *Macromolecular Symposia* **143**, 1–10 (1999).

66. Sletten, E. M. & Bertozzi, C. R. Bioorthogonal chemistry: Fishing for selectivity in a sea of functionality. *Angewandte Chemie - International Edition* **48**, 6974–6998 (2009).

67. Johnson, J. A., Lu, Y. Y., Van Deventer, J. A. & Tirrell, D. A. Residue-specific incorporation of non-canonical amino acids into proteins: Recent developments and applications. *Current Opinion in Chemical Biology* **14**, 774–780 (2010).

68. Johnson, J. A., Lu, Y. Y., Deventer, J. A. Van & Tirrell, D. A. Into Proteins : Recent Developments and Applications. **14**, 774–780 (2011).

69. Kiick, K. L., Saxon, E., Tirrell, D. A. & Bertozzi, C. R. Incorporation of azides into recombinant proteins for chemoselective modification by the Staudinger ligation. *Proceedings of the National Academy of Sciences* **99**, 19–24 (2002).

70. Link, A. J., Vink, M. K. S. & Tirrell, D. A. Preparation of the functionalizable methionine surrogate azidohomoalanine via copper-catalyzed diazo transfer. *Nature protocols* **2**, 1879–1883 (2007).

71. Teramoto, H. *et al.* Genetic Code Expansion of the Silkworm *Bombyx mori* to Functionalize Silk Fiber. *ACS Synthetic Biology* **7**, 801–806 (2018).

72. Hein, J. E. & Fokin, V. v. Copper-catalyzed azide–alkyne cycloaddition (CuAAC) and beyond: new reactivity of copper(i) acetylides. *Chemical Society Reviews* **39**, 1302 (2010).

73. Kolb, H. C., Finn, M. G. & Sharpless, K. B. Click Chemistry: Diverse Chemical Function from a Few Good Reactions. *Angewandte Chemie - International Edition* **40**, 2004–2021 (2001).

74. Sletten, E. M. & Bertozzi, C. R. From mechanism to mouse: A tale of two bioorthogonal reactions. *Accounts of Chemical Research* **44**, 666–676 (2011).

75. Jewett, J. C. & Bertozzi, C. R. Cu-free click cycloaddition reactions in chemical biology. *Chemical Society Reviews* **39**, 1272 (2010).

76. Ma, Y., Mcclatchy, D. B., Barkallah, S., Wood, W. W. & Yates, J. R. HILAQ: A Novel Strategy for Newly Synthesized Protein Quantification. *Journal of Proteome Research* **16**, 2213–2220 (2017).

77. McClatchy, D. B. *et al.* Pulsed azidohomoalanine labeling in mammals (PALM) detects changes in liver-specific LKB1 knockout mice. *Journal of Proteome Research* **14**, 4815–4822 (2015).

78. Shen, W. *et al.* Acute Synthesis of CPEB Is Required for Plasticity of Visual Avoidance Behavior in Xenopus. *Cell Reports* **6**, 737–747 (2014).

79. Glenn, W. S. *et al.* Bioorthogonal Noncanonical Amino Acid Tagging (BONCAT) Enables Time-Resolved Analysis of Protein Synthesis in Native Plant Tissue. *Plant Physiology* **173**, 1543–1553 (2017).

80. Teramoto, H. & Kojima, K. Incorporation of methionine analogues into Bombyx mori silk fibroin for click modifications. *Macromolecular Bioscience* **15**, 719–727 (2015).

81. Mamidyala, S. K. & Finn, M. G. In situ click chemistry: probing the binding landscapes of biological molecules. *Chemical Society Reviews* **39**, 1252 (2010).

82. Budelier, M. M. *et al.* Ligand Incorporation in Integral Membrane Proteins. **89**, 2636–2644 (2017).

83. Howden, A. J. M. *et al.* QuaNCAT: Quantitating proteome dynamics in primary cells. *Nature Methods* **10**, 343–346 (2013).

84. Chen, P. R. *et al.* A facile system for encoding unnatural amino acids in mammalian cells. *Angewandte Chemie - International Edition* **48**, 4052–4055 (2009).

85. Ullrich, M. *et al.* Bio-orthogonal labeling as a tool to visualize and identify newly synthesized proteins in Caenorhabditis elegans. *Nature Protocols* **9**, 2237–2255 (2014).

86. Hinz, F. I., Dieterich, D. C., Tirrell, D. A. & Schuman, E. M. Noncanonical amino acid labeling in vivo to visualize and affinity purify newly synthesized proteins in larval zebrafish. *ACS Chemical Neuroscience* **3**, 40–49 (2012).

87. Calve, S., Witten, A. J., Ocken, A. R. & Kinzer-Ursem, T. L. Incorporation of non-canonical amino acids into the developing murine proteome. *Scientific Reports* **6**, 1–7 (2016).

88. Teramoto, H. & Kojima, K. Incorporation of methionine analogues into Bombyx mori silk fibroin for click modifications. *Macromolecular Bioscience* **15**, 719–727 (2015).

89. Teramoto, H., Nakajima, K. I. & Kojima, K. Azide-Incorporated Clickable Silk Fibroin Materials with the Ability to Photopattern. *ACS Biomaterial Science and Engineering* **2**, 251–258 (2016).

90. Teramoto, H. & Kojima, K. Production of Bombyx mori silk fibroin incorporated with unnatural amino acids. *Biomacromolecules* **15**, 2682–2690 (2014).

91. Boeszoermenyi, A. *et al.* Aromatic 19 F- 13 C TROSY: a background-free approach to probe biomolecular structure, function, and dynamics. *Nature Methods* **16**, 333–340 (2019).

92. Boeszoermenyi, A., Ogórek, B., Jain, A., Arthanari, H. & Wagner, G. The precious fluorine on the ring: fluorine NMR for biological systems. *Journal of Biomolecular NMR* **74**, 365–379 (2020).

93. Welte, H., Zhou, T., Mihajlenko, X., Mayans, O. & Kovermann, M. What does fluorine do to a protein? Thermodynamic, and highly-resolved structural insights into fluorine-labelled variants of the cold shock protein. *Scientific Reports* **10**, 1–12 (2020).

94. Leung, R. L. C. *et al.* Monitoring the Disassembly of Virus-like Particles by 19F-NMR. *Journal of the American Chemical Society* **139**, 5277–5280 (2017).

95. Shimanovich, U. *et al.* Biophotonics of Native Silk Fibrils. *Macromolecular Bioscience* **1700295**, 1–8 (2018).

96. Datta, R., Heaster, T. M., Sharick, J. T., Gillette, A. A. & Skala, M. C. Fluorescence lifetime imaging microscopy: fundamentals and advances in instrumentation, analysis, and applications. *Journal of Biomedical Optics* **25**, 1 (2020).

97. Shimanovich, U. *et al.* Biophotonics of Native Silk Fibrils. *Macromolecular Bioscience* **1700295**, 1–8 (2018).

98. Becker, W. Fluorescence lifetime imaging – techniques and applications. **247**, 119–136 (2012).

99. Tansil, N. C. *et al.* Intrinsically colored and luminescent silk. *Advanced Materials* **23**, 1463–1466 (2011).

100. Tansil, N. C. *et al.* The use of molecular fluorescent markers to monitor absorption and distribution of xenobiotics in a silkworm model. *Biomaterials* **32**, 9576–9583 (2011).

101. Campagnola, P. J. & Dong, C. Y. Second harmonic generation microscopy: Principles and applications to disease diagnosis. *Laser and Photonics Reviews* **5**, 13–26 (2011).

102. Freund, I., Deutsch, M. & Sprecher, A. Connective tissue polarity. Optical second-harmonic microscopy, crossed-beam summation, and small-angle scattering in rat-tail tendon. *Biophysical Journal* **50**, 693–712 (1986).

103. Pena, A. M. *et al.* Three-dimensional investigation and scoring of extracellular matrix remodeling during lung fibrosis using multiphoton microscopy. *Microscopy Research and Technique* **70**, 162–170 (2007).

104. Zoumi, A., Lu, X., Kassab, G. S. & Tromberg, B. J. Imaging coronary artery microstructure using second-harmonic and two-photon fluorescence microscopy. *Biophysical journal* **87**, 2778–2786 (2004).

105. Stoller, P., Reiser, K. M., Celliers, P. M. & Rubenchik, A. M. Polarization-modulated second harmonic generation in collagen. *Biophysical Journal* **82**, 3330–3342 (2002).

106. Yeh, A. T., Choi, B., Nelson, J. S. & Tromberg, B. J. Reversible Dissociation of Collagen in Tissues. *Journal of Investigative Dermatology* **121**, 1332–1335 (2003).

107. Cox, G. *et al.* 3-Dimensional imaging of collagen using second harmonic generation. *Journal of Structural Biology* **141**, 53–62 (2003).

108. Odin, C., le Grand, Y., Renault, A., Gailhouste, L. & Baffet, G. Orientation fields of nonlinear biological fibrils by second harmonic generation microscopy. *Journal of Microscopy* **229**, 32–38 (2008).

109. Campagnola, P. J. *et al.* Three-dimensional high-resolution second-harmonic generation imaging of endogenous structural proteins in biological tissues. *Biophysical Journal* **82**, 493–508 (2002).

110. Zhao, Y., Hien, K. T. T., Mizutani, G. & Rutt, H. N. Second-Order Nonlinear Optical Microscopy of Spider Silk. 2–9 (2017) doi:10.1007/s00340-017-6766-z.

111. Rice, W., Firdous, S., Gupta, S. & Hunter, M. Non-invasive characterization of structure and morphology of silk fibroin biomaterials using non-linear microscopy. *Biomaterials* **29**, 617–627 (2008).

112. Wang, Q., Wang, C., Zhang, M., Jian, M. & Zhang, Y. Feeding Single-Walled Carbon Nanotubes or Graphene to Silkworms for Reinforced Silk Fibers. *Nano Letters* acs.nanolett.6b03597 (2016) doi:10.1021/acs.nanolett.6b03597.

113. Wu, G. H. *et al.* Robust composite silk fibers pulled out of silkworms directly fed with nanoparticles. *International Journal of Biological Macromolecules* **104**, 533–538 (2017).

114. Lepore, E. *et al.* Spider silk reinforced by graphene or carbon nanotubes. (2017).

115. Blackledge, T. a & Hayashi, C. Y. Silken toolkits: biomechanics of silk fibers spun by the orb web spider Argiope argentata (Fabricius 1775). *The Journal of Experimental biology* **209**, 2452–2461 (2006).

116. Kappe, C. O. & van der Eycken, E. Click chemistry under non-classical reaction conditions. *Chem. Soc. Rev.* **39**, 1280–1290 (2010).

117. Presolski, S. L., Hong, V. P. & Finn, M. G. Copper-Catalyzed Azide-Alkyne Click Chemistry for Bioconjugation. *Current Protocols in Chemical Biology* **3**, 153–162 (2011).

118. Jewett, J. C. & Bertozzi, C. R. Cu-free click cycloaddition reactions in chemical biology. *Nature Reviews Cancer* **13**, 83–96 (2010).

119. Harvey, D., Bardelang, P., Goodacre, S. L., Cockayne, A. & Thomas, N. R. Antibiotic Spider Silk: Site-Specific Functionalization of Recombinant Spider Silk Using “Click” Chemistry. *Advanced Materials* **29**, 1–5 (2017).

120. Santi, S. *et al.* A Bio-inspired Multifunctionalized Silk Fibroin. *ACS Biomaterials Science and Engineering* **7**, 507–516 (2021).

121. Hagn, F. A structural view on spider silk proteins and their role in fiber assembly. *Journal of Peptide Science* **18**, 357–365 (2012).

122. Heiby, J. C., Goretzki, B., Johnson, C. M., Hellmich, U. A. & Neuweiler, H. Methionine in a protein hydrophobic core drives tight interactions required for assembly of spider silk. *Nature Communications* **10**, (2019).

123. Schneider, D., Schneider, T., Rösner, D., Scheffner, M. & Marx, A. Improving bioorthogonal protein ubiquitylation by click reaction. *Bioorganic and Medicinal Chemistry* **21**, 3430–3435 (2013).

124. Taskent-Segin, H. *et al.* Azidohomoalanine: A conformationally Sensitive IR Probe of Protein Folding, Protein Structure, and Electrostatics. **49**, 7473–7475 (2011).

125. Yasui, H., Yamamoto, T., Tokunaga, E. & Shibata, N. Robust synthesis of trifluoromethionine and its derivatives by reductive trifluoromethylation of amino acid disulfides by CF3I/Na/Liq.NH 3 system. *Journal of Fluorine Chemistry* **132**, 186–189 (2011).

126. Andruszkiewicz, R. & Rożkiewicz, D. An Improved Preparation of N^2 - *tert* -Butoxycarbonyl- and N^2 -Benzyloxy-carbonyl-(*S*)-2,4-diaminobutanoic Acids. *Synthetic Communications* **34**, 1049–1056 (2004).

127. Dieterich, D. C., Link, A. J., Graumann, J., Tirrell, D. A. & Schuman, E. M. Selective identification of newly synthesized proteins in mammalian cells using bioorthogonal noncanonical amino acid tagging (BONCAT). *Proceedings of the National Academy of Sciences* **103**, 9482–9487 (2006).

128. Greenstone, M. H. Spider feeding behaviour optimises dietary essential amino acid composition (reply). *Nature* **284**, 578 (1980).

129. Ling, S., Qi, Z., Knight, D. P., Shao, Z. & Chen, X. Synchrotron FTIR microspectroscopy of single natural silk fibers. *Biomacromolecules* **12**, 3344–3349 (2011).

130. Hammes, G. G. *Spectroscopy for the Biological Sciences*. (Wiley- Interscience, 2005). doi:10.1002/0471733555.

131. dos Santos-Pinto, J. R. A. *et al.* Structure and post-translational modifications of the web silk protein spidroin-1 from Nephila spiders. *Journal of Proteomics* **105**, 174–185 (2014).

132. Tillinghast, E. K. & Townley, M. A. Free amino acids in spider hemolymph. *Comparative Biochemistry and Physiology - B Biochemistry and Molecular Biology* **151**, 286–295 (2008).

133. Andersen, S. O. Amino acid composition of spider silks. *Comparative Biochemistry And Physiology* **35**, 705–711 (1970).

134. Work, R. W. & Young, C. T. The Amino Acid Compositions of Major and Minor Ampullate Silks of Certain Orb-Web-Building Spiders (Araneae, Araneidae). *Journal of Arachnology* **15**, 65–80 (1987).

135. Ionin, B. I. & Ershov, B. A. The Fundamentals of NMR Spectroscopy. in *NMR Spectroscopy in Organic Chemistry* 1–59 (Springer US, 1970). doi:10.1007/978-1-4684-1785-2_1.

136. Teramoto, H. *et al.* Genetic Code Expansion of the Silkworm *Bombyx mori* to Functionalize Silk Fiber. *ACS Synthetic Biology* **7**, 801–806 (2018).

137. Amgarten, B. *et al.* Collagen labelling with an azide-proline chemical reporter in live cells. *Chemical communications (Cambridge, England)* **51**, 5250–2 (2015).

138. Holub, J. M. & Kirshenbaum, K. Tricks with clicks: modification of peptidomimetic oligomers via copper-catalyzed azide-alkyne [3 + 2] cycloaddition. *Chemical Society Reviews* **39**, 1325 (2010).

139. Asakura, T. & Murakami, T. NMR of Silk Fibroin. 4. Temperature-and Urea-Induced Helix-Coil Transitions of the-(Ala)n-Sequence in Philosamia cynthia ricini Silk Fibroin Protein Monitored by 13C NMR Spectroscopy. *Macromolecules* **18**, 2614–2619 (1985).

140. Golas, L., Matyjaszewski, K., Wang, C. & Wang, Q. Themed issue : Applications of click chemistry Applications of click chemistry themed issue. **0012**, (2010).

141. Teramoto, H. Intermolecular Crosslinking of Silk Fibroin by Click Chemistry. *J. Silk Sci. Tech. Jpn* **25**, 17–25 (2017).

142. Zhao, H. *et al.* Decoration of silk fibroin by click chemistry for biomedical application. *Journal of Structural Biology* **186**, 420–430 (2014).

143. Amgarten, B. *et al.* Collagen labelling with an azide-proline chemical reporter in live cells. *Chemical communications (Cambridge, England)* **51**, 5250–2 (2015).

144. Vollrath, F. & Knight, D. P. Structure and function of the silk production pathway in the spider Nephila edulis. *International Journal of Biological Macromolecules* **24**, 243–249 (1999).

145. Du, N. *et al.* Design of superior spider silk: From nanostructure to mechanical properties. *Biophysical Journal* **91**, 4528–4535 (2006).

146. Krasnov, I. *et al.* Mechanical properties of silk: Interplay of deformation on macroscopic and molecular length scales. *Physical Review Letters* **100**, 2–5 (2008).

147. Riekel, C., Madsen, B., Knight, D. & Vollrath, F. X-ray diffraction on spider silk during controlled extrusion under a synchrotron radiation X-ray beam. *Biomacromolecules* **1**, 622–626 (2000).

148. Grubb, D. T. & Jelinski, L. W. Fiber Morphology of Spider Silk: The Effects of Tensile Deformation. *Macromolecules* **30**, 2860–2867 (1997).

149. Shao, J., Zheng, J., Liu, J. & Carr, C. M. Fourier transform Raman and Fourier transform infrared spectroscopy studies of silk fibroin. *Journal of Applied Polymer Science* **96**, 1999–2004 (2005).

150. Boulet-Audet, M., Lefèvre, T., Buffeteau, T. & Pézolet, M. Attenuated total reflection infrared spectroscopy: An efficient technique to quantitatively determine the orientation and conformation of proteins in single silk fibers. *Applied Spectroscopy* **62**, 956–962 (2008).

151. Chen, X., Knight, D. P., Shao, Z. & Vollrath, F. Conformation transition in silk protein films monitored by time-resolved fourier transform infrared spectroscopy: Effect of potassium ions on Nephila spidroin films. *Biochemistry* **41**, 14944–14950 (2002).

152. Lefèvre, T., Paquet-Mercier, F., Rioux-Dubé, J. F. & Pézolet, M. Review: Structure of silk by Raman spectromicroscopy: From the spinning glands to the fibers. *Biopolymers* **97**, 322–336 (2012).

153. Shao, Z., Vollrath, F., Sirichaisit, J. & Young, R. J. Analysis of spider silk in native and supercontracted states using Raman spectroscopy. *Polymer* **40**, 2493–2500 (1999).

154. Sapede, D. *et al.* Nanofibrillar structure and molecular mobility in spider dragline silk. *Macromolecules* **38**, 8447–8453 (2005).

155. Renz, M. Fluorescence microscopy-A historical and technical perspective. *Cytometry Part A* **83**, 767–779 (2013).

156. Sahl, S. J., Hell, S. W. & Jakobs, S. Fluorescence nanoscopy in cell biology. *Nature Reviews Molecular Cell Biology* **18**, 685–701 (2017).

157. Renz, M. Fluorescence microscopy-A historical and technical perspective. *Cytometry Part A* **83**, 767–779 (2013).

158. Combs, C. A. Fluorescence microscopy: A concise guide to current imaging methods. *Current Protocols in Neuroscience* 1–19 (2010) doi:10.1002/0471142301.ns0205s00.

159. Jensen, E. C. Types of Imaging, Part 2: An Overview of Fluorescence Microscopy. *Anatomical Record* **295**, 1621–1627 (2012).

160. Georgakoudi, I. *et al.* Intrinsic fluorescence changes associated with the conformational state of silk fibroin in biomaterial matrices. *Optics Express* **15**, 1043–1053 (2007).

161. Shashkova, S. & Leake, M. C. Single-molecule fluorescence microscopy review: Shedding new light on old problems. *Bioscience Reports* **37**, 1–19 (2017).

162. Dempsey, G. T., Vaughan, J. C., Chen, K. H., Bates, M. & Zhuang, X. Evaluation of fluorophores for optimal performance in localization-based super-resolution imaging. *Nature Methods* **8**, 1027–1040 (2011).

163. Iizuka, T. *et al.* Colored fluorescent silk made by transgenic silkworms. *Advanced Functional Materials* **23**, 5232–5239 (2013).

164. Fan, S. *et al.* Super-strong and Intrinsically Fluorescent Silkworm Silk from Carbon Nanodots Feeding. *Nano-Micro Letters* **11**, 1–11 (2019).

165. Guinea, G. v, Elices, M., Pérez-Rigueiro, J. & Plaza, G. R. Stretching of supercontracted fibers: a link between spinning and the variability of spider silk. *The Journal of experimental biology* **208**, 25–30 (2005).

166. Pérez-Rigueiro, J., Elices, M. & Guinea, G. v. Controlled supercontraction tailors the tensile behaviour of spider silk. *Polymer* **44**, 3733–3736 (2003).

167. Elices, M., Plaza, G. R., Pérez-Rigueiro, J. & Guinea, G. v. The hidden link between supercontraction and mechanical behavior of spider silks. *Journal of the Mechanical Behavior of Biomedical Materials* **4**, 658–669 (2011).

168. Tansil, N. C. *et al.* Intrinsically colored and luminescent silk. *Advanced Materials* **23**, 1463–1466 (2011).

169. Madsen, B., Shao, Z. Z. & Vollrath, F. Variability in the mechanical properties of spider silks on three levels: Interspecific, intraspecific and intraindividual. *International Journal of Biological Macromolecules* **24**, 301–306 (1999).

170. Vollrath, F., Madsen, B. & Shao, Z. The effect of spinning conditions on the mechanics of a spider's dragline silk. *The Royal Society* **268**, 2339–2346 (2001).

171. Bernchou, U. *et al.* Texture of lipid bilayer domains. *Journal of the American Chemical Society* **131**, 14130–14131 (2009).

172. Iachina, I. & Brewer, J. R. Strain-Dependent Structural Changes in Major and Minor Ampullate Spider Silk Revealed by Two-Photon Excitation Polarization. *Biomacromolecules* **20**, 2384–2391 (2019).

173. Vollrath, F., Hawkins, N., Porter, D., Holland, C. & Boulet-Audet, M. Differential Scanning Fluorimetry provides high throughput data on silk protein transitions. *Scientific reports* **4**, 5625 (2014).

174. Holland, C. *et al.* Differential Scanning Calorimetry of Native Silk Feedstock. *Macromolecular Bioscience* **19**, 6–11 (2019).

175. Kajiwara, T., Chambers, R. W. & Kearns, D. R. Dimer spectra of rhodamine B. *Chemical Physics Letters* **22**, 37–40 (1973).

176. Ilich, P., Mishra, P. K., Macura, S. & Burghardt, T. P. Direct observation of rhodamine dimer structures in water. *Spectrochimica Acta - Part A Molecular Spectroscopy* **52**, 1323–1330 (1996).

177. Patterson, W. & Force, A. The Halpin-Tsai Equations: A Review. **16**, (1976).

178. Schrauwen, B. A. G., Janssen, R. P. M., Govaert, L. E. & Meijer, H. E. H. Intrinsic deformation behavior of semicrystalline polymers. *Macromolecules* **37**, 6069–6078 (2004).

179. Shen, Y., Johnson, M. A. & Martin, D. C. Microstructural characterization of Bombyx mori silk fibers. *Macromolecules* **31**, 8857–8864 (1998).

180. Zheng, Y. Q. *et al.* Effect of Halogenation in Isoindigo-Based Polymers on the Phase Separation and Molecular Orientation of Bulk Heterojunction Solar Cells. *Macromolecules* **48**, 5570–5577 (2015).

181. Zhu, W. *et al.* Crystallography, Morphology, Electronic Structure, and Transport in Non-Fullerene/Non-Indacenodithienothiophene Polymer:Y6 Solar Cells. *Journal of the American Chemical Society* **142**, 14532–14547 (2020).

182. Bédoui, F., Diani, J., Régnier, G. & Seiler, W. Micromechanical modeling of isotropic elastic behavior of semicrystalline polymers. *Acta Materialia* **54**, 1513–1523 (2006).

183. Ali, A. & Ahmed, S. Natural polymers: An overview. *Natural Polymers: Derivatives, Blends and Composites, Volume I* **1**, 1–22 (2016).

184. Chen, X., Shao, Z., Knight, D. P. & Vollrath, F. Conformation transition kinetics of Bombyx mori silk protein. *Proteins: Structure, Function and Genetics* **68**, 223–231 (2007).

185. Mortimer, B., Holland, C. & Vollrath, F. The forced reeling of Bombyx mori silk: separating behaviour and processing conditions. *Acta Biomaterialia* **Submitted**, (2013).

186. Liu, Y., Shao, Z. & Vollrath, F. Relationships between supercontraction and mechanical properties of spider silk. *Nature materials* **4**, 901–905 (2005).

187. Prez-rigueiro, J., Elices, M. & Plaza, G. R. Similarities and Differences in the Supramolecular Organization of Silkworm and Spider Silk Similarities and Differences in the Supramolecular Organization of Silkworm and Spider Silk. *Organization* 5360–5365 (2007) doi:10.1021/ma070478o.

188. Kaplan, D., Adams, W. W., Farmer, B. & Viney, C. Chapter 1 Silk : Biology , Structure , Properties , and Genetics. 2–16 (1994).

189. Lee, E. H., Pokoo, R., Oh, E., Lim, S. & Lee, C. Y. Fluorescent Properties of the Tryptophan Containing Variants of Leucine-responsive Regulatory Proteins. *Journal of the Korean Chemical Society (JKCS)* **63**, 505–510 (2019).

190. Clegg, R. M., Holub, O. & Gohlke, C. Fluorescence lifetime-resolved imaging: Measuring lifetimes in an image. *Methods in Enzymology* **360**, 509–542 (2003).

191. Gheysens, T., Collins, A., Raina, S., Vollrath, F. & Knight, D. P. Demineralization enables reeling of wild silkmoth cocoons. *Biomacromolecules* **12**, 2257–2266 (2011).

192. Riekel, C. & Vollrath, F. Spider silk fibre extrusion: combined wide- and small-angle X-ray microdiffraction experiments. *International Journal of Biological Macromolecules* **29**, 203–210 (2001).

193. Work, R. W. & Morosoff, N. A Physico-Chemical Study of the Supercontraction of Spider Major Ampullate Silk Fibers. *Textile Research Journal* **52**, 349–356 (1982).

194. Malay, A. D. *et al.* Relationships between physical properties and sequence in silkworm silks. *Nature Publishing Group* **6 VN-re**, 1–11 (2016).

195. Keten, S., Xu, Z., Ihle, B. & Buehler, M. J. Nanoconfinement controls stiffness, strength and mechanical toughness of beta-sheet crystals in silk. *Nature materials* **9**, 359–367 (2010).

196. Römer, L. & Scheibel, T. The elaborate structure of spider silk: structure and function of a natural high performance fiber. *Prion* **2**, 154–161 (2008).

197. Holland, C., Vollrath, F., Ryan, A. J. & Mykhaylyk, O. O. Silk and synthetic polymers: Reconciling 100 degrees of separation. *Advanced Materials* **24**, 105–109 (2012).

198. Ulrich, S., Glišović, A., Salditt, T. & Zippelius, A. Diffraction from the β -sheet crystallites in spider silk. *European Physical Journal E* **27**, 229–242 (2008).

199. Chen, F., Porter, D. & Vollrath, F. Silk cocoon (Bombyx mori): Multi-layer structure and mechanical properties. *Acta Biomaterialia* **8**, 2620–2627 (2012).

200. Vollrath, F., Madsen, B. & Shao, Z. The effect of spinning conditions on the mechanics of a spider's dragline silk. *The Royal Society* **268**, 2339–2346 (2001).

201. Liu, Y., Shao, Z. & Vollrath, F. Elasticity of spider silks. *Biomacromolecules* **9**, 1782–1786 (2008).

202. Porter, D., Guan, J. & Vollrath, F. Spider silk: Super material or thin fibre? *Advanced Materials* **25**, 1275–1279 (2013).

203. Madsen, B., Shao, Z. Z. & Vollrath, F. Variability in the mechanical properties of spider silks on three levels: Interspecific, intraspecific and intraindividual. in *International Journal of Biological Macromolecules* vol. 24 301–306 (1999).

204. Guan, J. *et al.* Glass transitions in native silk fibres studied by dynamic mechanical thermal analysis. *Soft Matter* **12**, 5926–5936 (2016).

205. Mortimer, B., Holland, C. & Vollrath, F. The forced reeling of Bombyx mori silk: separating behaviour and processing conditions. *Acta Biomaterialia*, (2013).

206. Fratzl, P. & Weinkamer, R. Nature's hierarchical materials. *Progress in Materials Science* **52**, 1263–1334 (2007).

207. RS Lokes. Materials with structural hierarchy. *Nature* **361:511–15**, 511–515 (1993).

208. Fratzl, P. & Weinkamer, R. Nature's hierarchical materials. *Progress in Materials Science* (2007) doi:10.1016/j.pmatsci.2007.06.001.

209. Michel, J. A. & Yunker, P. J. Structural hierarchy confers error tolerance in biological materials. *Proceedings of the National Academy of Sciences of the United States of America* **116**, 2875–2880 (2019).

210. Chu, M. *et al.* Functionalization of composite bacterial cellulose with C60 nanoparticles for wound dressing and cancer therapy. *RSC Advances* **8**, 18197–18203 (2018).

211. Limaye, M. V., Gupta, V., Singh, S. B., Paik, G. R. & Singh, P. Antimicrobial Activity of Composite Consisting of Cellulose Nanofibers and Silver Nanoparticles. *ChemistrySelect* **4**, 12164–12169 (2019).

212. Kang, M., Chen, P. & Jin, H. J. Preparation of multiwalled carbon nanotubes incorporated silk fibroin nanofibers by electrospinning. *Current Applied Physics* **9**, S95–S97 (2009).

213. Mohammadi, P. *et al.* Biomimetic composites with enhanced toughening using silk-inspired triblock proteins and aligned nanocellulose reinforcements. *Science Advances* **5**, 1–12 (2019).

214. Hardy, J. G. & Scheibel, T. R. Composite materials based on silk proteins. *Progress in Polymer Science (Oxford)* **35**, 1093–1115 (2010).

215. Allen, M. J., Tung, V. C. & Kaner, R. B. Honeycomb carbon: A review of graphene. *Chemical Reviews* **110**, 132–145 (2010).

216. Moniruzzaman, M. & Winey, K. I. Polymer nanocomposites containing carbon nanotubes. *Macromolecules* **39**, 5194–5205 (2006).

217. Fiedler, B. & Schulte, K. Carbon nanotube-based composites. *Comprehensive Composite Materials II* **6–8**, 201–229 (2018).

218. Li, H., Kang, Z., Liu, Y. & Lee, S. T. Carbon nanodots: Synthesis, properties and applications. *Journal of Materials Chemistry* **22**, 24230–24253 (2012).

219. Xiao, L. & Sun, H. Novel properties and applications of carbon nanodots. *Nanoscale Horizons* **3**, 565–597 (2018).

220. Saifuddin, N., Raziah, A. Z. & Junizah, A. R. Carbon nanotubes: A review on structure and their interaction with proteins. *Journal of Chemistry* **2013**, (2013).

221. Rao, R. *et al.* Carbon Nanotubes and Related Nanomaterials: Critical Advances and Challenges for Synthesis toward Mainstream Commercial Applications. *ACS Nano* **12**, 11756–11784 (2018).

222. Anzar, N., Hasan, R., Tyagi, M., Yadav, N. & Narang, J. Carbon nanotube - A review on Synthesis, Properties and plethora of applications in the field of biomedical science. *Sensors International* **1**, 100003 (2020).

223. Sciortino, A., Cannizzo, A. & Messina, F. Carbon Nanodots: A Review—From the Current Understanding of the Fundamental Photophysics to the Full Control of the Optical Response. *C* **4**, 67 (2018).

224. Tiwari, S. K., Sahoo, S., Wang, N. & Huczko, A. Graphene research and their outputs: Status and prospect. *Journal of Science: Advanced Materials and Devices* **5**, 10–29 (2020).

225. Strugari, A. F. G., Stan, M. S., Gharbia, S., Hermenean, A. & Dinischiotu, A. Characterization of nanoparticle intestinal transport using an in vitro co-culture model. *Nanomaterials* **9**, (2019).

226. Bergin, I. L. & Witzmann, F. A. Nanoparticle toxicity by the gastrointestinal route: evidence and knowledge gaps. *International Journal of Biomedical Nanoscience and Nanotechnology* **3**, 163 (2013).

227. Lepore, E. *et al.* Silk reinforced with graphene or carbon nanotube spun by spiders. *Physiological Research* **64**, 897–905 (2015).

228. Dionigi, C. *et al.* A nanostructured conductive bio-composite of silk fibroin-single walled carbon nanotubes. *Journal of Materials Chemistry B* **2**, 1424–1431 (2014).

229. Cheung, H. Y., Lau, K. T., Tao, X. M. & Hui, D. A potential material for tissue engineering: Silkworm silk/PLA biocomposite. *Composites Part B: Engineering* **39**, 1026–1033 (2008).

230. Wojcieszak, M., Percot, A. & Colomban, P. Regenerated silk matrix composite materials reinforced by silk fibres: Relationship between processing and mechanical properties. *Journal of Composite Materials* **52**, 2301–2311 (2018).

231. Shao, Z. & Vollrath, F. The effect of solvents on the contraction and mechanical properties of spider silk. *Polymer* **40**, 1799–1806 (1999).

232. Wang, Y., Porter, D. & Shao, Z. Using solvents with different molecular sizes to investigate the structure of antheraea pernyi silk. *Biomacromolecules* **14**, 3936–3942 (2013).

233. Sletten, E. M. & Bertozzi, C. R. Bioorthogonal chemistry: Fishing for selectivity in a sea of functionality. *Angewandte Chemie - International Edition* **48**, 6974–6998 (2009).

234. Berrones-Reyes, J. C. *et al.* Fluorescent organotin compounds as dyes in silk fibroin (Bombyx mori): ultrasound-assisted synthesis, chemo-optical characterization, cytotoxicity, and confocal fluorescence microscopy. *New Journal of Chemistry* **43**, 5150–5158 (2019).

235. Blamires, S. J., Wu, C. L. & Tso, I. M. Variation in protein intake induces variation in spider silk expression. *PLoS ONE* **7**, (2012).

236. Bueno, J. M., Avila, F. J. & Artal, P. Second Harmonic Generation Microscopy: A Tool for Quantitative Analysis of Tissues. *Recent Advances in Graphene Research* 257–297 (2016) doi:http://dx.doi.org/10.5772/63493.

237. Koeppel, A. & Holland, C. Progress and Trends in Artificial Silk Spinning: A Systematic Review. *ACS Biomaterials Science and Engineering* **3**, 226–237 (2017).

238. Spicer, C. D. & Davis, B. G. Selective chemical protein modification. *Nature Communications* **5**, (2014).